Methodology for Stored Heat “Heat In Place” (HIP) assessment of geothermal aquifers – Exemplified by a study of the Arnager Greensand in SW Scania

Oskar Sundberg

Dissertations in Geology at Lund University,
Master’s thesis, no 671
(45 hp/ECTS credits)

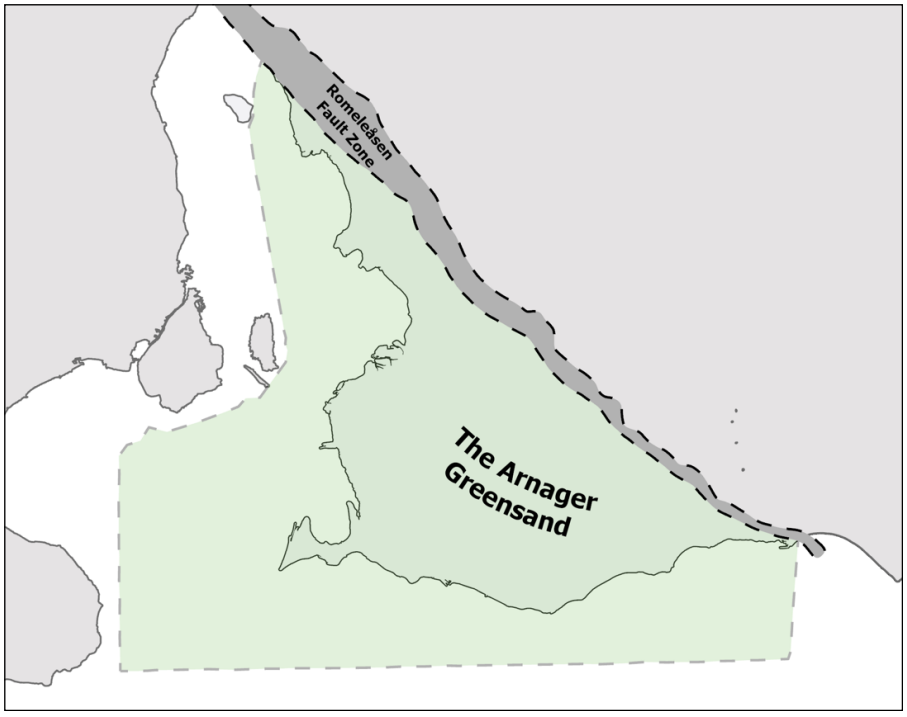

Department of Geology
Lund University
2023

Methodology for Stored Heat “Heat In Place” (HIP) assessment of geothermal aquifers – Exemplified by a study of the Arnager Greensand in SW Scania

Master’s thesis
Oskar Sundberg

Department of Geology
Lund University
2023

Contents

Cover Picture: A schematic seismic data coverage map of the Arnager Greensand over southwest Scania and the adjacent Romeleåsen Fault Zone. Figure illustrated by Oskar Sundberg.

Methodology for Stored Heat “Heat In Place” (HIP) assessment of geothermal aquifers – Exemplified by a study of the Arnager Greensand in SW Scania

Oskar Sundberg

Sundberg, O., 2023: Methodology for Stored Heat “Heat In Place” (HIP) assessment of geothermal aquifers – Exemplified by a study of the Arnager Greensand in SW Scania. *Dissertations in Geology at Lund University*, No. 671, 56 pp. 45 hp (45 ECTS credits).

Abstract: In the sedimentary bedrock of southwest Scania, located in the southernmost part of Sweden, there are several low-enthalpy Mesozoic sandstone aquifers situated at different depths. These aquifers collectively hold the potential for direct-heat geothermal utilization. Given the energy supply challenge across Europe, there is a growing need to characterise the geothermal resources and quantify their energy content. Despite this demand, the assessment of geothermal resources in Sweden has not been performed to any larger extent in comparison to assessment studies of similar geothermal aquifers in Europe. This limitation is concerning, as these aquifers should be acknowledged as national renewable energy assets. This study presents a first-ever geothermal assessment using the stored heat “Heat-In-Place” (HIP) method on the Cretaceous Arnager Greensand over southwest Scania. The results present a set of maps that illustrate the stored heat in the subsurface for the Arnager Greensand, and additional maps detailing the spatial distribution, such as the depth to the formation, thickness, and reservoir temperature. The Arnager Greensand stores a total of 3270 PJ in a range of 1.25 – 4.53 GJ/m^2 over SW Scania. The stored heat values are slightly higher with a total of 3610 PJ in the range of 1.37 – 4.99 GJ/m^2 in the rock matrix and reservoir fluids separately. The produced maps show the regional geothermal signatures of the Arnager Greensand where the stored heat is particularly marked in the southern parts of the region covering the Falsterbo Peninsula. The relatively greater stored heat in this area can be attributed to the greater thickness of the Arnager Greensand formation. The region from the Falsterbo Peninsula to Malmö and Trelleborg demonstrates relatively greater stored heat values, offering potential for further local geothermal investigations. Its proximity to urban and industrial areas significantly enhances the feasibility of integrating a well-doublet system into a district heating system. Due to the absence of borehole data, the assessment of the stored heat over the Skurup Platform is uncertain. This necessitates additional borehole information to improve the geothermal assessment. In a broader regional context, the stored heat findings indicate that the Arnager Greensand has limited potential as a geothermal reservoir as the stored heat values are lower than those of similar geothermal aquifers in comparable geological settings. Taking into account the Lower Cretaceous sandstones beneath the Arnager Greensand as a combined aquifer with a greater cumulative thickness, the geothermal potential increases over the Lower Cretaceous interval in SW Scania.

Keywords: geothermal energy, geothermal resource assessment, geothermal potential, volume method, volumetric method, recovery factor, direct use, direct heat, Mesozoic aquifers

Supervisor(s): Mikael Erlström (LU), Daniel Sopher (SGU), and Jan-Erik Rosberg (LTH)

Subject: Bedrock Geology

Oskar Sundberg, Department of Geology, Lund University, Sölvegatan 12, SE-223 62 Lund, Sweden. E-mail: oskarsundberg96@hotmail.com

Metod för lagrad värme ”Heat In Place” (HIP) bedömning av geotermiska akviferer – Exemplifierad med en studie av Arnagegrönsanden i sydvästra Skåne

Oskar Sundberg

Sundberg, O., 2023: Metod för lagrad värme ”Heat In Place” (HIP) bedömning av geotermiska akviferer – Exemplifierad med en studie av Arnagergrönsanden i sydvästra Skåne. *Examensarbeten i geologi vid Lunds universitet*, Nr. 671, 56 sid. 45 hp.

Sammanfattning: I den sedimentära berggrunden i sydvästra Skåne finns flera mesozoiska sandstensakviferer. Dessa akviferer kännetecknas av låga entalpinivåer och återfinns på olika djup och har en potential att användas för geotermisk värmeutvinning. I samband med den pågående utmaningen att säkerhetsställa Europas energiförsörjning ökar behovet av att karakterisera och kvantifiera de geotermiska resurserna. Trots detta har bedömningen av geotermiska resurser i Sverige inte genomförts i någon större utsträckning jämfört med bedömningar av liknande akviferer i Europa. Denna begränsning är problematisk, särskilt med tanke på att dessa akviferer utgör betydande nationella förnybara energitillgångar inom ramen för den gröna omställningen. Denna studie presenterar en geotermisk energibedömning av den kretaceiska Arnagergrönsanden i sydvästra Skåne. Metoden som har använts heter Stored heat "Heat-In-Place" (HIP) metoden. Studiens resultat redovisas med kartor som visualiserar den lagrade geotermiska energin i Arnagergrönsanden, samt ytterligare kartor som visar djupet till formationen, mäktigheten och reservoartemperaturen. Arnagergrönsanden har en lagrad geotermisk energi på totalt 3270 PJ inom intervallet 1,25 – 4,53 GJ/m^2 över sydvästra Skåne. Den geotermiska energin är något högre med en total på 3610 PJ inom intervallet 1,37 – 4,99 GJ/m^2 om man beräknar energin för bergarten och reservoarvätskorna separat. Kartorna visar Arnagergrönsandens regionala geotermiska signaturer där den geotermiska energin är som störst i de södra delarna av regionen över Falsterbohalvön, vilket beror på att Arnagergrönsanden är som mäktigast i detta område. Från Falsterbohalvön till Malmö och Trelleborg sträcker sig ett område med relativt höga energivärden, vilket öppnar upp möjligheter för framtida lokala geotermiska undersökningar. Områdets närhet till stads- och industriområden förbättrar avsevärt möjligheterna att integrera en geotermianläggning i fjärrvärmenätet. Osäkerheterna i den geotermiska energibedömningen är betydande över Skurupsplatformen på grund av avsaknaden av borrhålsdata. För att förbättra modellen skulle ytterligare djupborrningar vara av stort värde. I en regional kontext visar den geotermiska energibedömningen att Arnagergrönsanden har en begränsad potential att användas som en geotermisk reservoar för värmeutvinning. De resulterande värdena är lägre än de för liknande geotermiska akviferer i jämförbara geologiska miljöer. Om man inkluderar de kretaceiska sandstenarna som är belägna under Arnagergrönsanden som en kombinerad akvifer med en större kumulativ mäktighet ökar den geotermiska potentialen över det nedre kretaceiska intervallet i sydvästra Skåne.

Nyckelord: geotermi, geotermisk energi, geotermisk potential, potentialkartor, geotermisk bedömningsmetod, geotermisk energibedömning, direktanvändning, mesozoiska akviferer

Handledare: Mikael Erlström (LU), Daniel Sopher (SGU), Jan-Erik Rosberg (LTH)

Ämnesinriktning: Berggrundsgeologi

Oskar Sundberg, Geologiska institutionen, Lunds Universitet, Sölvegatan 12, 223 62 Lund, Sverige. E-post: oskarsundberg96@hotmail.com

1 Introduction

The energy supply is a significant challenge facing most European countries today. There is also, according to the EU energy roadmap for the year 2050, a need to increase the amount of renewable energy in the energy mix, such as geothermal energy, to shift away from non-renewables (European Commission, 2011). The fundamental principle behind geothermal energy extraction is to harness the naturally occurring heat in the earth's crust to generate electricity and/or to supply thermal energy for heating. This can be accomplished by accessing relatively high-temperature fluids and steam in the subsurface, located within permeable sedimentary formations or within fractures in crystalline rock. The warm fluids are then brought to the surface using wells (Norden, 2011; Trumpy et al., 2016; Zarrouk & McLean, 2019a; Stober & Bucher, 2021d).

Geothermal aquifers consist of permeable fluid-bearing sedimentary rocks (more commonly porous sandstones) located between depths of a few hundred meters to several kilometres in the subsurface (Norden, 2011; Marrero-Diaz et al., 2015; Limberger et al., 2018). These reservoirs are typically outside of volcanic terrains classified as low – medium enthalpy reservoirs which roughly corresponds to low – medium temperature reservoirs. These reservoirs have been the target of exploration and successfully exploited for direct-heat utilization worldwide over the past decades (Marrero-Diaz et al., 2015; Trumpy et al., 2016).

The terminology direct-use, also frequently referred to as direct utilization or direct heat in the literature, encompasses all forms of geothermal resource utilizations that do not include the generation of electricity. These applications can for example include, space heating and cooling, recreation, greenhouse heating, aquaculture, agricultural drying, and industrial use (Lund, 2009; Zarrouk & McLean, 2019a). A common divider between direct-use and electric power generation is that direct-use applications use geothermal fluids between 30 and 150 °C corresponding to low temperature resources (Lienau et al., 1989; Pahud, 2002; Norden, 2011; Limberger et al., 2018; Zarrouk & McLean, 2019a). The specific temperature utilized will vary based on the geological conditions and the actual geothermal plant design and specific usage. The major advantage of using geothermal energy for direct -use is that geothermal aquifers in the low – intermediate temperature ranges are widespread across the world and can be accessed at economic drilling depths (Lund, 2009).

From a European perspective, the assessment of the geothermal resources is showcased in the Netherlands, where abundant publicly available oil and gas data from previous hydrocarbon campaigns have been used to create subsurface structure models for various sandstone reservoirs situated at depths of 1 – 4 kilometres. These models have in turn been used as a foundation for further regional-scale mapping of geothermal reservoirs (Kramers et al., 2012; Pluymaekers et al., 2012). Sandstones are not the only viable reservoirs for geothermal utilization. Fractured carbonate aquifers also constitute a substantial portion of the geothermal reservoirs that have been identified and exploited. Carbonate aquifers (Karst) often have considerable geothermal potential as the aquifers often have sufficient porosity and natural permeability (Goldscheider et al., 2010). A successful geothermal development of a carbonate aquifer is exemplified by the exploitation of the Dogger limestone aquifers situated at a depth of 1.5 – 2 kilometres in the Paris Basin. The Dogger geothermal project has been operating for more than 40 years, which exemplifies the viability of sustainable geothermal direct-use exploitation (Lopez et al., 2010).

The potential of geothermal energy as an expandable renewable energy resource has become increasingly important worldwide. By the end of 2020, there were 350 direct-use district heating plants in Europe with a total capacity of 6 GW (thermal energy) and 232 new projects were under development (European Geothermal Energy Council, 2022). At the same time by the end of 2020, there were also 139 operational geothermal power plants with a total capacity of 3.5 GW (electric energy) (European Geothermal Energy Council, 2022). To put these numbers into perspective, the worldwide geothermal capacity in 2021 totalled an estimated 35 GW for thermal energy and 14.5 GW for electric energy (Renewable Energy Policy Network, 2022). Although the total contribution of geothermal energy to the worldwide energy pool remains low, it is estimated that the geothermal resource could provide as much as 5.8 EJ annually by 2050 (1600 Terawatt-hours) (International Energy Agency, 2011). The successive review articles by Lund et al. (2011), Lund and Boyd (2016), and Lund & Toth (2021) overviews the current state of global geothermal energy utilization for direct-use applications.

In view of this, there is a growing demand to characterise the geothermal resources and quantify the geothermal energy in the ground that can be utilized for energy purposes. One common way of assessing the geothermal potential in the ground is by using the stored heat method, also known as the volume (volumetric method), or the heat in place (HIP) method. This method was first developed by the United States Geological Survey (USGS) in the seventies during several national geothermal resource assessments. The method was found suitable as a way to quantify and at the same time facilitate a comparison between the nations geothermal resources (Nathenson, 1975a, 1975b; White & Williams, 1975; Muffler, 1978; Muffler & Cataldi, 1978; Brook et al., 1979). The method has since been used for geothermal resource assessments worldwide and continues to be the most widely recognized geothermal assessment methodology. The method quantifies the amount of stored heat (geothermal energy) in the geothermal resource. The input parameters are limited to the reservoir volume, the volumetric heat capacities of different mediums, the reservoir temperature, the reference temperature, and optionally a porosity parameter. The subsequent workflow then determines how much of this stored geothermal energy can be extracted at the wellhead in the form of actual retrievable energy which in turn can be used for direct-use applications and/or generating electricity (Muffler & Cataldi, 1978).

Several studies have computed various types of maps that visualise the amount of stored heat in the ground for specific stratigraphic intervals (Calcagno et al., 2014; Marrero-Diaz et al., 2015; Trumpy et al., 2016; Frick et al., 2022). In most cases, these studies

have used the baseline methodology described by the USGS. The results are often presented with the unit Joule per square meter (J/m^2) for each calculated cell within a raster (grid) as a way of visualising the spatial differences between areas. The resulting map showing the amount of stored heat is often accompanied by additional computed maps that illustrate variations in the depth to the formation top boundary, reservoir thickness, and the reservoir temperature.

A geothermal assessment study by Balling et al. (2019) serves as an example of how the stored heat method can be used in a Nordic setting for various geothermal aquifers. The study brings forward new data about the temperature distributions and the amount of stored heat in four major geothermal reservoirs in the Danish Basin. The study found that reservoirs with a temperature range of 45 – 80 °C cover large regional on-shore areas in Denmark. The study also provides valuable insights into how the geothermal system responds when exploited over longer periods and how that affects the reservoir performance. A different approach to geothermal assessment was performed in Finland by Arola et al. (2019). This study considers the geothermal potential in the uppermost 300 meters of the ground (bedrock and Quaternary sediments). The study is set apart from other geothermal assessments as it produced a map for shallow geothermal energy potential, whereas other studies more commonly consider deeper geothermal potential. Their study highlights the significance of recognizing shallow geothermal energy as a part of the usable geothermal resource and not only deeper-situated reservoirs.

Geothermal investigations in Sweden have historically focused on two options for geothermal energy extraction: to utilize the warm aquifers waters in the deep-situated sedimentary reservoirs in southern Sweden or to exploit areas of relatively higher heat flow in the Precambrian crystalline basement (Malmqvist et al., 1978; Alm & Bjelm, 1995). These two options continue to be the primary focus of geothermal investigations in Sweden (Juhlin et al., 2022). The first mention of the stored heat method in a Swedish context was in the late seventies in connection to the national program for geothermal energy (Bjelm, 1977; Bjelm et al., 1979; Bjelm & Persson, 1981). These reports provide a first-generation estimate for the stored heat in several sandstone aquifers in SW Scania. Their assessments of the stored heat can be viewed as rough estimates because the stored heat is calculated based on fixed borehole parameters without considering the spatial variability of the parameters. The results were later reported in the Atlas of geothermal resources in Europe compiled by the European Commission. The Atlas provides a broad overview of geothermal reservoirs identified in Europe (Hurter & Schellschmidt, 2003).

Since then, there has been one more study by Erlström and Rosberg (2022) using the stored heat method in Sweden. The study applies parts of the method on the Campanian Lund Sandstone aquifer in SW Scania. The Lund Sandstone is to this day the only deep geothermal aquifer exploited in Sweden with almost 40 years of production. The geothermal plant in Lund utilizes approximately 20 °C warm water from a confined sandstone aquifer at a depth of 640 – 800 meters. The system is designed with a set of heat pumps and heat exchangers in a closed loop system together with several production and reinjection wells coupled to the district heating system (Bjelm & Lindeberg, 1995).

Another notable geothermal project is the Lund deep geothermal exploration project. Between the years 2002 and 2003, a 3700-meter-deep exploration well (DGE-1) was drilled into the Romeleåsen Fault Zone located in Scania. The project targeted a potential reservoir in the fractured crystalline basement associated with the fault zone. The project aimed to find warm fluids and conductive fractured bedrock conditions that could be exploited for direct-use in the Lund district heating system. The investigations showed that the temperatures and conductivity of the rock mass were not sufficient for further development (Rosberg & Erlström, 2019). At the same time as the Lund deep geothermal exploration project, an additional geothermal project was conducted in the nearby city of Malmö. Two exploration wells (FFC-1 and FFC-2) were drilled targeting Mesozoic sandstone aquifers at a depth of 1600 – 2100 meters. Although, the wells encountered water of approximately 55 °C with the required productivity, execution of a full project was halted due to competition from alternative energy resources in Malmö at that time. However, an extension of the FFC-1 borehole was done some years later in order to investigate the feasibility of EGS technology (Engineered Geothermal Systems) (Rosberg & Erlström, 2021; Juhlin et al., 2022). While neither of these deep geothermal projects in the end focused on sedimentary aquifers as a potential geothermal reservoir, they both shed light on the potential geothermal resources in Sweden and the advancements made in the field.

However, despite the recent geothermal developments focusing on the Precambrian crystalline basement, there is potential to improve the assessment of other geothermal resources in Sweden. This especially applies to the deeper aquifers in the sedimentary bedrock of SW Scania. One of those aquifers is the Cretaceous Arnager Greensand which was first recognized as a potential geothermal reservoir during the seventies (Malmqvist et al., 1978). The top of the formation in SW Scania is found at depths between 1100 – 1850 determined from borehole drillings. The formation has been identified as one of the more promising formations for CO_2 storage (Hurter & Schellschmidt, 2003; Anthonsen et al., 2014; Mortensen et al., 2016; Mortensen & Sopher, 2021). The Arnager Greensand is described in Erlström et al. (2018) as one of several Mesozoic sandstone intervals in the Öresund area that have geothermal utilization potential. The aquifer shows high permeability and porosity values in certain areas (Juhlin et al., 2013) which are key parameters when assessing the feasibility of geothermal utilization.

1.1 Objective and aim

The objective of this project is to evaluate the stored heat (HIP) method, as a way of quantifying the amount of stored energy in the ground. The initial parts of the study focus on describing the underlying concepts of geothermal energy systems. This will transition into a summary of the stored heat method. The background

chapter will provide a geological description of the Arnager Greensand, including distribution, age, lithology, and reservoir properties. Based on this, a suitable stored heat method will be tested on the Arnager Greensand. The project aim is to create a geothermal potential map which shows the stored heat in the Arnager Greensand over SW Scania. The results will be given in J/m^2 for the estimate of the total amount of stored heat. The ambition is that the resulting maps and calculated stored heat values can be used as a basis for future geothermal developments in SW Scania.

2 Background

2.1 Geothermal energy

Geothermal energy can simply be described as energy in the form of heat generated in the interior of the earth. Deep geothermal energy is commonly set apart from more shallow geothermal energy with an arbitrary depth of 400 meters (Pahud, 2002; Erlström et al., 2016; Stober & Bucher, 2021a). The distinction between these two classifications of geothermal energy is related to the fact that the temperature of the upper few tens of meters of the subsurface is influenced by the seasonal variations of the sun (Fetter, 2014). The two domains are also distinguished from each other due to the different techniques utilized to extract the geothermal energy. Shallow geothermal energy can be used for cooling and heat storage applications whereas deeper geothermal energy is typically viewed as a heat source characterised by higher temperatures (Pahud, 2002).

Deep geothermal heat originates from the radiogenic decay of unstable nuclides (uranium, thorium, and potassium) and the residual heat originating from the formation of the planet (Van Schmus, 1995; Gando et al., 2011; Stober & Bucher, 2021a). The generated heat continuously flows to the surface of the earth and is transferred by three major heat-transfer mechanisms - conduction which involves the diffusion of heat through a medium, convection which describes the transport of heat caused by fluid motion, and radiation in which all hot bodies radiate electromagnetic energy through a wide spectrum of wavelengths (Banks, 2012; Zarrouk & McLean, 2019b). Conduction is the dominant heat-transfer mechanism in the crust because crustal rocks are relatively solid and have low permeability. Convection occurs under certain circumstances when water at depth is heated and thermally expands carrying far more energy in comparison to thermal conduction (Zarrouk & McLean, 2019a). Advection is a form of convection that occurs when gravity forces geothermal fluids through permeable rocks which can lead to downslope or counterflow movements in geothermal systems (Banks, 2012; Zarrouk & McLean, 2019b).

The geothermal gradient describes the temperature change with depth. The gradient varies greatly depending on the geological terrain and does not increase linearly with depth (Banks, 2012). An average value for the conductive geothermal gradient between the mantle and the earth surface varies between 20 – 30 ˚C/km with a heat flux of 40 – 60 mW/m^2 (Armstead, 1978). Elevated geothermal gradients are found in connection to plate boundaries (convergent or divergent plate boundaries) associated with extensive geological processes such as volcanism (Banks, 2012). The natural geothermal gradient in these plate boundary environments can reach as high as 100 ˚C/km (Zarrouk & McLean, 2019a). Outside of plate boundary environments, such as the Baltic Shield which almost encompasses the entire area of Sweden, the geothermal gradient in the crystalline basement is more stable with typical values ranging from 15 to 20 ˚C/km (Juhlin et al., 2022). In the southern regions of Sweden, the geothermal gradient in the sedimentary bedrock is lightly higher than that in the northern crystalline Precambrian bedrock (Erlström et al., 2016). Local occurrences of notable elevated geothermal gradient in these areas are primarily attributed to the lower thermal conductivity of the sedimentary bedrock. The highest recorded geothermal gradient in Sweden, ranging between 35 and 40 ˚C/km, was observed in the sedimentary bedrock on the island of Gotland situated in the Baltic Sea (Karlqvist, 1982; Erlström et al., 2022).

The thermal conductivity of a rock is mainly controlled by the quartz content. While many rocks contain minerals with relatively high thermal conductivity, it is the quantity of quartz that predominantly influences the thermal conductivity of the rock. The density also plays a significant role in determining the thermal conductivity of the rock. A high quartz content together with a high density will give the rock a higher thermal conductivity (Banks, 2012). Granites with a dense interlocking crystal structure and low porosity have a relatively high thermal conductivity often between 3 and 4 W/mK. Saturated rocks such as fluid-bearing sandstones commonly have a lower thermal conductivity of less than 2 W/mK (Erlström et al., 2016).

A general rule describing the relationship between thermal conductivity and the geothermal gradient is that the geothermal gradient increases in less conductive rocks and decreases in more conductive rocks. An effect of this is that thick layers of rocks with low thermal conductivity such as low-conductivity mudstones and limestones can trap heat underneath by thermal blanketing or insulation processes (Lienau et al., 1989; Banks, 2012). In crystalline bedrock settings, certain granitic bodies can have a high internal heat production from the decay of radioactive elements, such as uranium and potassium, which results in an increased geothermal gradient (Lienau et al., 1989; Banks, 2012). This principle applies not only to crystalline rocks but is also observed in SW Scania in boreholes that encounter the Alum Shale which is a uranium-rich mudstone with a high content of organic material (Erlström et al., 2011). The decay of uranium in the Alum Shale leads to an increased geothermal gradient within those intervals where it is present in the subsurface. Geothermal anomalies can also occur via advection when heat is transported more rapidly between two locations. Fault networks allow for the infiltration of groundwater to great depths where the fluids get heated by either elevated or normal geothermal gradients which then can potentially ascend to the surface (Lienau et al., 1989; Banks, 2012).

2.2 Geothermal energy terminology

The geothermal literature uses four recurring terms: geothermal reservoirs, geothermal aquifers, geothermal systems, and geothermal resources. A natural geothermal reservoir is a porous and permeable formation that contains hot water or steam and holds a large heat supply which gets replenished by a heat transfer mechanism (Toth & Bobok, 2017). The geothermal reservoir stores heat both in the rock matrix and in the fluids that occupy the pore spaces and fractures within the rock (Gupta & Roy, 2007). The geothermal reservoir term is often used interchangeably with a geothermal aquifer which refers to deep permeable water-bearing layers (Limberger et al., 2018). A geothermal system is a confined volume in the crust where a natural heat transfer mechanism moves heat from a heat source to a heat sink (Zobin, 2017). The system is divided into three parts – a heat source, a reservoir where the heat accumulates, and a barrier that holds the accumulated heat in place (Gupta & Roy, 2007).

Muffler and Cataldi (1978) introduced an alternative terminology that explains the technological and economic constraints of the geothermal system. This nomenclature defines a geothermal resource as the total amount of energy in the crust beneath a specific area relative to a local mean annual temperature. The resource represents a portion of this geothermal resource base that can be extracted economically in the near future (Muffler & Cataldi, 1978).

2.3 Geothermal system classifications

There are numerous classification schemes proposed for geothermal systems. Temperature classification is the more common approach where a geothermal system is classified into three main temperature categories - low-temperature resources (under 90 °C), intermediate-temperature resources (90 – 150 °C), and high-temperature resources (above 150 °C) (Muffler & Cataldi, 1978). The major drawback of the temperature classifications is that it does not account for the enthalpy of the geothermal system. This can be exemplified by that two geothermal systems can have the same temperature but produce either vapour and/or water depending on pressure. The vapour phase will contain a greater amount of energy (higher enthalpy) compared to the liquid phase. Kaya et al. (2011) proposed an enthalpy classification that considers the relationship between the energy contained in the liquid versus the vapour phase. The basis of the enthalpy classification is that in a geothermal system, there will be multiple concurrent heat transfer mechanisms. The classification scheme is built on different temperature and enthalpy ranges corresponding to a one-phase or two-phase geothermal system, in which a two-phase system might be liquid, or vapour-dominated (Kaya et al., 2011).

Another classification scheme proposed by Lee (2001) considers the exergy at the geothermal wellhead. The exergy classification is motivated by that geothermal resources should primarily be classified by the ability of the fluid to perform thermodynamic work (Lee, 2001). The thermodynamic property exergy is a reoccurring term in the geothermal energy literature and is described by DiPippo (2015) as “the maximum work (or power) output that could theoretically be obtained from a substance at specified thermodynamic conditions relative to its surroundings”. The exergy term can be explained simply, in the context of geothermal fluids, as the quality of the energy content of the fluid (Zarrouk & McLean, 2019b). The major advantage of the classification is that it describes the maximum work available at the wellhead (surface conditions) compared to the more unknown conditions in the subsurface (Zarrouk & McLean, 2019b).

A more geological approach is to classify geothermal resources by play types which can be described as a regional area with the same geological conditions (Moeck, 2014). This can for example be if the geological system is primarily convection or conduction-driven and/or if the geological setting is in an intracratonic basin or orogenic belt (Moeck, 2014). A classical classification system by White and Williams (1975) divides the geothermal resource into different categories: hydrothermal convection, hot igneous, and conduction-dominated system. This scheme uses a more objective approach because the geothermal systems get assigned a category based on temperature characteristics and the main source of the geothermal energy.

2.4 Geothermal plant technologies

Several technologies are applied to generate electricity or extract heat from geothermal energy resources. Using dry or flash geothermal power plant technologies, steam is used to drive turbines in the production of electricity. Dry steam power plants use the vapour directly to drive the turbine, while a flash steam power plant flashes the hot water to steam by reducing the pressure (Stober & Bucher, 2021d). The geothermal fluid can also be used to heat a secondary fluid with a lower boiling point in a binary-cycle power plant, which then drives the turbine. This allows for the utilization of lower temperature fluids around 100 °C in the generation of electricity (Banks, 2012; Stober & Bucher, 2021d). The Enhanced-Geothermal-System (EGS), also known as a hot dry rock system, is a technique based on creating artificial fractures in non-permeable rock formations where the temperatures are high enough for power production. Water is then injected into the artificial formation and circulated back to the surface to extract the heat carried by the fluids (Stober & Bucher, 2021d).

Direct utilization of a geothermal resource uses the geothermal fluid directly. The system could involve the use of heat exchangers to convert energy from the geothermal fluid to a secondary fluid (Norden, 2011). The use of heat pumps is also considered in the direct-use category. In the context of district heating systems, if the temperature of the geothermal fluid is not sufficient, then heat pumps are necessary to raise the temperature of the fluid to the level required by the district network (Alm & Bjelm, 1995; Norden, 2011).

The direct-use system consists of a configuration of several wells in which the purpose is to circulate the fluids up from the aquifer and then back into the subsurface. The production wells discharge relatively hot water from the formation to the surface and the reinjection wells recharge the cooled fluids back into the subsurface after the heat exchange. A well configuration of a production and a reinjection well is called a well-doublet (Limberger et al., 2018). The recharge of

the fluids to the same level of discharge helps to maintain flow and pressure in the aquifer which will improve the resource recovery (Kaya et al., 2011; Rivera Diaz et al., 2016). The recharge of cooled water forms a moving temperature front that migrate towards the production well. Once the discharge and recharge areas become influenced by each other a state of thermal breakthrough occurs and the reservoir temperature drops which reduces the production efficiency (Limberger et al., 2018). This signifies the importance of considering the spacing between the doublets when planning for a geothermal project (Willems et al., 2017).

2.5 Geothermal resource assessment methods

The Geothermal resource assessment methods are divided into static assessment methods that do not require production data from exploited geothermal systems and dynamic assessment methods that require production data to quantify the geothermal energy (Ciriaco et al., 2020). Several static assessment methods are outlined in the classical paper by Muffler and Cataldi (1978) including the surface heat flux, stored heat (volume), planar fracture, and magmatic heat budget methods. The most recognized static assessment method is the stored heat method. The most viable dynamic assessment method applies numerical reservoir simulations to simulate the heat flow in complex reservoir geometry bodies (AGRCC, 2010b; Ciriaco et al., 2020). The following section will further present the stored heat methods in line with the objective of this paper. The method is particularly valuable during early-stage exploration when there is limited data available (Ciriaco et al., 2020) as is the case for most geothermal aquifers in SW Scania.

2.5.1 The Stored Heat "Heat-In-Place" method

The stored heat method, also known as the volume (volumetric) method, also mentioned as the Heat-In-Place (HIP) method is described by Williams et al. (2008) as a way of estimating the amount of recoverable heat from a porous and permeable rock reservoir by using a thermal recovery factor to account for the producible fraction of the stored heat. The method has developed over time which has resulted in several modified versions (Muffler & Cataldi, 1978; Williams et al., 2008; Garg, 2010, 2011; Garg & Combs, 2015). One such method modification was the implementation of Monte-Carlo simulations to consider the uncertainties associated with the parameters. The method developments have often led to inconsistent applications by different working groups regarding the interpretation and implementation of the input parameters.

The original concept of the stored heat method is focused on the conversion from thermal energy to electric power. The electric power potential is determined by the amount of thermal energy that can be extracted at the wellhead and the efficiency with which this available thermal energy can be converted to electric power. The thermodynamic and economic limitations become known when the reservoir fluid is available at the wellhead (Muffler & Cataldi, 1978; Williams, 2004). Although the literature places significant emphasis on electric power generation; it is possible to apply the method for both electric power generation and direct-use depending upon the amount of energy that can be extracted at the wellhead (Williams, 2014).

The input parameters to the stored heat equations are – the reservoir volume, the volumetric heat capacities of different mediums, the reservoir temperature, the reference temperature, and the formation porosity. The following section will expand on these parameters as there are three recognized approaches to calculating the stored heat that use these parameters differently (Ciriaco et al., 2020). The USGS considers two ways of calculating the stored thermal energy. The first approach considers the heat stored solely in the rock matrix, and the second approach considers the heat stored in the rock matrix and the reservoir fluid separately (Ciriaco et al., 2020). The AGRCC (Australian Geothermal Reporting Code Committee) method is the third approach and considers two additional parameters – a fluid saturation and a water enthalpy parameter (AGRCC, 2010a, 2010b). The most up-to-date review covering the stored heat method is presented in Ciriaco et al. (2020) and the following nomenclature (symbols, derivations, and subscripts) will be derived from there if not specified otherwise. The stored heat equation parameters will be evaluated in greater detail in the following subchapters.

A single reservoir volume can be subdivided into several geohydrological units corresponding to multiple aquifers with their own depth intervals (volume) and temperature conditions (Muffler & Cataldi, 1978; O'Sullivan & O'Sullivan, 2016; Malcolm, 2018). It is important to consider this within the context of a modelling approach since each cell within a raster or grid will have its own volume and temperature conditions. The total thermal energy (stored heat) (Q) for all subdivided units is calculated with Equation (1) (Muffler & Cataldi, 1978; Ciriaco et al., 2020):

$$Q = \sum_{n}^{i=1} \rho_i c_i V_i (T_i - T_f) \qquad \textbf{Equation 1}$$

$\rho_i c_i$ = Volumetric heat capacity of a water-saturated rock (J/°C m^3)

V_i = Volume of i^{th} region of n numbers of lithology (m^3)

T_i = Initial temperature of i^{th} lithology (°C)

T_f = Cut-off or final abandoned reservoir temperature (°C)

The above Equation (1) simply calculates the sum of all stored heat from multiple geohydrological units (aquifers) with their corresponding geological properties (volume, temperature, and volumetric heat capacities). The lithology term refers to a reservoir volume with its own geological characteristics expressed as the areal extent multiplied by the reservoir thickness (Ciriaco et al., 2020).

The two USGS approaches are linked to Equation (1) but differ slightly considering how heat is stored in the subsurface. The first USGS approach considers the thermal energy contained solely in the rock matrix rather than in the reservoir fluid. This follows the assumption that geothermal energy in the reservoir is stored independently of porosity (Ciriaco et al., 2020).

The relationship between the stored heat in the rock matrix versus the reservoir fluids was pointed out early on by Muffler and Cataldi (1978) who state that in most reservoirs 90 % of the thermal energy is contained in the rock matrix and the remaining 10 % in the fluids. Following this reasoning, Equation (1) can be simplified into just considering the heat stored solely in the rock. The stored heat Q in the rock matrix for one whole reservoir volume is calculated with Equation (2) (Muffler & Cataldi, 1978; Ciriaco et al., 2020):

$$Q = \rho_r c_r V(T_i - T_f) \quad \textbf{Equation 2}$$

$\rho_r c_r$ = Volumetric heat capacity of the rock matrix (J/°C m^3)

V = Volume of the productive reservoir (m^3)

T_i = Average initial reservoir temperature (°C)

T_f = Reference or dead-state temperature (°C)

The second USGS approach expands on Equation (2) and introduces a porosity parameter and a value for the volumetric heat capacity of the reservoir fluids which allows for a separate calculation of the thermal energy stored in the reservoir fluids. The total thermal energy calculated using both approaches does not vary more than five percent if the porosity is less than 20 % (Muffler & Cataldi, 1978). The total thermal energy (Q_t) in the rock matrix and the reservoir fluids is calculated with Equation (3) (Muffler, 1978; Muffler & Cataldi, 1978; Arkan & Parlaktuna, 2005; Ciriaco et al., 2020):

$$Q_t = (1 - \varphi)V\rho_r c_r(T_i - T_f) + \varphi V\rho_f c_f(T_i - T_f)$$

Equation 3

$\rho_f c_f$ = Volumetric heat capacity of the fluids (J/°C m^3)

φ = The ratio between the pore space and the bulk volume of the reservoir rock (%)

The third stored heat approach is the AGRCC method which was established as a joint venture by the Australian Geothermal Energy Association (AGEA) and Australian Geothermal Energy Group (AGEG). The goal was to standardise and establish a national framework for geothermal reporting (Lawless et al., 2010). This was motivated by the absence of a universally agreed-upon model for assessing geothermal resources; an issue which remains unsolved to this day (Ciriaco et al., 2020). Equation (4) is comparable to Equation (3) and considers the heat stored in the rock and in the fluid with the addition of heat stored in the steam. The thermal energy Q using the ARGCC method is calculated with Equation (4) (AGRCC, 2010a, 2010b; Ciriaco et al., 2020):

$$Q = V \times [\rho_r c_r(1 - \varphi)(T_i - T_f)] + [\rho_{wi}\varphi S_w(h_{wi} - h_{wf})] + [\rho_{si}\varphi(1 - s_w)(h_{si} - h_{wi})]$$

Equation 4

ρ_{wi} and p_{si} = Density of steam and water at initial reservoir condition (kg/m^3)

h_{wi} and h_{si} = Water and steam enthalpies at reservoir temperature (kJ/kg)

h_{wf} = Water enthalpy at rejection temperature (kJ/kg)

S_w = Relative water saturation of the reservoir (%)

T_f = Reinjection temperature (reference temperature) (°C)

The initial workflow for the stored heat methodology outlined above has undergone substantial modifications. Equation (2) was further refined by Garg and Combs (2015) and O'Sullivan and O'Sullivan (2016) who introduced a saturation term to differentiate between the proportion of water and steam in the rock pores. Further research was conducted by Sadiq and Florida (2013) who considered the internal energy of the system instead of the specific enthalpy in Equation (4). They also proposed with a set of equations that the natural heat flux and the conductive heat flux (thermal recharge) of the geothermal system should be accounted for in the stored heat method (Sadiq & Florida, 2013).

The amount of thermal energy that can be recovered at the wellhead can be estimated with the introduction of a recovery factor parameter (R_f) defined by Equation (5) (Muffler & Cataldi, 1978). The recovery factor describe the ratio between the thermal energy available at the wellhead against the stored thermal energy. The thermal energy available at the wellhead (Q_{wh}) is calculated with Equation (6) based on measurements of fluid thermodynamic properties (Ciriaco et al., 2020). This approach becomes feasible when measurable fluids are available at the wellhead and not in an initial stage of development when there are no productive wells. In the case of the latter, the recovery factors must be estimated based on recovery factors from other active geothermal developments and/or theoretical values. This allows for an estimate of the thermal energy available at the wellhead without direct measurements.

$$R_f = Q_{wh} / Q \quad \textbf{Equation 5}$$

$$Q_{wh} = m_{wh}(h_{wh} - h_{ref}) \quad \textbf{Equation 6}$$

m_{wh} = Extractable mass flow rate (kg/s)

h_{wh} = Enthalpy of the produced fluid (kJ/kg)

h_{ref} = Enthalpy at some reference temperature (kJ/kg)

At this point, the workflow expands on several thermodynamic concepts to convert the thermal energy at the wellhead to available work (exergy) and subsequently provide an estimate for the electric power production. The details of this workflow are specified further by Garg and Combs (2015) who describe the concept of availability as the maximum theoretical work (power) that can be obtained from a substance (water) under specific thermodynamic conditions compared to its surrounding environment. According to Williams et al. (2008), the electric power generation from a potential geothermal system depends on the

thermal energy in the reservoir (Q), the amount of thermal energy that can be extracted at the wellhead (Q_{wh}) and the efficiency of which this is converted from thermal energy to electric power (conversion efficiency). The conversion efficiency (utilization factor) is the relation between the actual electrical energy to the available work (Garg & Combs, 2015).

2.5.2 Monte Carlo simulations

Monte Carlo simulations are numerical statistical methods implemented in the stored heat equations to consider the uncertainties associated with the parameters. The simulations describe the most probable reservoir properties and productivity together with associated uncertainties (Muffler, 1978). The outcome is to generate a probability distribution of the power capacity. The procedure involves determining a minimum and maximum value for the input parameters. A probability distribution function (PDF) is assigned to describe the value range between the minimum and maximum values. The more common distribution types used are normal, triangular, and uniform. The Monte Carlo simulations then make repeated random samplings within the PDF and apply the output values to chosen equations. The number of simulations is selected and produces a large number of likely outcomes (Arkan & Parlaktuna, 2005). This is considered a stochastic approach compared to a deterministic as the input parameters are not fixed (Piris et al., 2021). The result is also presented with probability distribution functions expressed as P90, P50, and P10 representing low, best, and high estimates (Arkan & Parlaktuna, 2005; Piris et al., 2021). The implementation of the Monte Carlo simulations has been extensively discussed in the literature with a focus on how the ranges should be set (Garg, 2010; Sadiq & Florida, 2013; Garg & Combs, 2015). The reliability of the method has been questioned and is associated with overestimations of geothermal resources (Grant, 2015; Ciriaco et al., 2020). Despite this, the stored heat method with the Monte Carlo add-on is continuously being developed with projects improving the reliability and applicability of the method (Pocasangre & Fujimitsu, 2018; Piris et al., 2021).

2.5.3 Stored Heat method parameters

2.5.3.1 Volume

The volume parameter is the most crucial parameter in the stored heat method as it quantifies the size of the reservoir where the fluids can circulate and withdraw heat (Grant & Bixley, 2011). The simplistic way of determining the volume is to treat it as a box defined by the areal and vertical extent (thickness) (Ciriaco et al., 2020). One common approach is to determine the extent and thickness with seismic data supported by well information. The areal extent can also be delineated with several other geophysical techniques such as electrical resistivity measurements and magneto telluric (MT) methods (AGRCC, 2010b; Ciriaco et al., 2020). The problem with the volume identity is that it assumes that the same hydrogeological conditions apply within it. For example, the permeability may vary considerably within the volume and low permeability portions of the volume may not be sufficient enough to support geothermal exploitation over the lifespan of a geothermal project (Grant, 2015).

2.5.3.2 Volumetric heat capacity

The heat capacity of a rock is the amount of thermal energy (heat) in Joules that is absorbed or released upon a temperature change of one Kelvin. The heat capacity can also be expressed as the specific heat capacity per unit mass. This is the amount of thermal energy that is absorbed per mass unit of rock when the temperature increases (Stober & Bucher, 2021c). When the heat capacity is normalised with respect to a constant volume instead of mass, it is referred to as volumetric heat capacity and describes the amount of heat that is absorbed per volume unit of rock per temperature increase (Stober & Bucher, 2021c). The volumetric heat capacity is expressed as ρc in the stored heat equations and is calculated by multiplying the specific heat capacity of a substance by its density.

The term ρc often refers to the volumetric heat capacity of water-saturated rocks in the context of the stored heat methodology (Ciriaco et al., 2020). The volumetric heat capacity differs only slightly over a wide temperature range between different rock types (magmatic, metamorphic, and sedimentary) (Ciriaco et al., 2020). White (1966) recognized that natural substances typically have similar volumetric heat capacities. Compared to the uncertainties associated with the other stored heat parameters, the volumetric heat capacity introduces only minor errors in the stored heat equations (White & Williams, 1975). These minor errors suggest that the volumetric heat capacity can be treated as constant, with a value of 2.5×10^6 J/C m³ for a water-saturated rock in the stored heat equations (Ciriaco et al., 2020).

2.5.3.3 Reservoir temperature

The reservoir temperature is the average reservoir temperature (Muffler & Cataldi, 1978; Garg, 2011; Grant & Bixley, 2011) also described as a characteristic reservoir temperature (Williams, 2004; Williams et al., 2008; Williams, 2014). Regional geothermal gradients can be used to support an assessment of a likely reservoir temperature. Geophysical logging techniques are used to measure the temperature at the bottom of the boreholes, referred to as Bottom Hole Temperature (BHT). These BHT readings are then used to estimate the temperature of the reservoir. The BHT can be influenced by the drilling itself, as drilling fluids are circulated in the hole, and logging is performed afterward. Therefore, it is important to note that the BHT readings do not always represent normalised conditions. But in some cases, this is the only information available unless specific temperature logging has been performed several months later, allowing the conditions in the borehole to stabilise. In the absence of in-situ temperature measurements, chemical geothermometers such as silica geothermometers can be used as proxies to determine the temperature conditions. The geothermometers are more commonly used for high-temperature systems (Williams, 2014).

The BHT readings together with the mean surface temperature can be used to calculate a local geothermal gradient G_t for a specific depth or depth interval as

expressed in Equation (7). The resultant geothermal gradient can be extrapolated in the stratigraphy under the assumption that it remains constant. This enables the estimation of the reservoir temperature at various depths (Tiab & Donaldson, 2012).

$G_t = (T_f - T_s) / D \qquad T_f = T_s + G_t \times D$ **Equation 7**

G_t = Local geothermal gradient (°C/m)

T_s = Mean annual surface temperature (°C)

T_f = Formation temperature (°C)

D = Depth (m)

2.5.3.4 Reference temperature

There are several options for setting the reference temperature and there are multiple terms used to describe this parameter. The selection of the reference temperature depends mainly on the applied power plant technology, but also on the choices made by each country in its implementation (Ciriaco et al., 2020). The use of a lower reference temperature could lead to an overestimation of the available thermal energy (Pocasangre & Fujimitsu, 2018). The geothermal literature predominantly emphasises large-scale power cycles for electricity generation, while limited attention is put on the reference temperature in the context of direct-use.

In Equation (1) the reference temperature T_f is expressed as the cut-off or final abandoned reservoir temperature. The cut-off temperature is explained by Grant and Bixley (2011) as a threshold where there is no economic value in the fluid. It is further explained as the temperature at which wells cease to flow and/or it becomes uneconomic to pump them. The abandonment temperature is equivalent to the cut-off temperature explained by Garg and Combs (2015) as the temperature below which the geothermal reservoir will not produce.

In Equation (2) the reference temperature T_f is expressed as the dead-state temperature or reference temperature. The term dead-state temperature originates from older works by USGS and is similar to the reference temperature (Williams et al., 2008; Williams, 2014). The three commonly used reference temperatures are – separation temperature, ambient temperature, or reinjection temperature (Ciriaco et al., 2020; Piris et al., 2021). The separation temperature is the temperature at which all the heat in the fluids below this point is discarded by the geothermal plant (Malcolm, 2018). The ambient temperature is the annual mean surface temperature value (Malcolm, 2018; Piris et al., 2021). The original USGS national geothermal resource assessments calculated the total thermal energy within the reservoir volume above the dead-state temperature at ambient conditions of 15 °C (Muffler, 1978; Quinao & Zarrouk, 2014).

In Equation (4) the reference temperature T_f is expressed as the reinjection temperature which is the exhaust temperature of the utilized fluids from the geothermal plant (Malcolm, 2018). The reinjection temperature varies depending on the geothermal plant conversion technology. The reference temperature for direct-use purposes is the rejection temperature of the wastewater produced from the geothermal plant (Malcolm, 2018). As an example of setting the reinjection temperature as the reference temperature, a reinjection temperature of 30 °C was used by Calcagno et al. (2014) when investigating the deep geothermal potential within the Tertiary Limage Basin (French Massiff Central). Another example is the Atlas of geothermal resources in Europe which employed a reinjection temperature of 25 °C (Hurter & Schellschmidt, 2003).

2.5.3.5 Recovery factor

The recovery factor has been subject to much discussion mainly due to the addition of in-field production data from active geothermal fields which has been used to derive in-field values for the recovery factor. These values have shown to be different in comparison to theoretical values and because of this there is not a common agreement on how to apply the recovery factor uniformly. Different perspectives on how to implement the recovery can be found in studies by Ciriaco et al. (2020), Malcolm (2018), O'Sullivan and O'Sullivan (2016), and Grant (2015). The below section briefly outlines the recovery factor development.

An early theoretical model by Nathenson (1975a) derived a recovery factor of 0.5 for a uniformly porous, homogeneous, and liquid-phase geothermal reservoir with the use of reinjection fluids. The reinjection concept is described as a cold sweep process whereby the recharge progressively replaces the heated reservoir fluids with cooler water. This process describes an idealised condition where the extraction of the thermal energy can in theory involve the production of a larger volume of fluids than what was originally contained in the reservoir. The reinjection of fluids stimulates the permeability of the rock which increases the reservoir performance (Williams et al., 2008).

The initial USGS national geothermal resource assessments considered the Monte-Carlo approach and used a triangular distribution between 0 – 0.5 with a most likely value of 0.25 (Muffler, 1978). This recovery factor of 0.25 has since been widely used by several geothermal assessments (Grant, 2015). Sanyal et al. (2004) reassessed earlier geothermal assessments and found instances where the actual thermal energy was only one-third of the initial estimate. The outcome of this was that the older geothermal assessments had provided an overly optimistic estimate of the stored heat (Williams, 2004; Grant, 2015).

Previous research had focused on the recovery factor in the context of uniformly porous fluid-bearing reservoirs. However, not enough consideration was taken to the heterogeneity of the geological system especially when considering fracture systems or a combination of both. Williams (2007) investigated this further by considering the relationship between porous versus fracture geothermal reservoirs and the implications it has on the recovery factor. The study applied a fracture flow model by Bödvarsson and Tsang (1982) which showed the sensitivity between the recovery factor and the average fracture spacing. One finding in the study showed that when the average fracture spacing is around 50 meters the fractured reservoir will behave similarly to the cold sweep process of porous reservoirs. Another finding was that when the fracture

spacing increases the recovery factor decreases because the rock itself is increasingly bypassed by the cold sweep process which results in less heat transfer (Williams, 2007).

Williams (2007) furthered his research by implementing self-similar fracture distribution models to investigate the relationship between the recorded flow rate and the variation in the observed recovery factor. A self-similar distribution model can be described briefly as a 2D modelling technique that utilizes fractal geometry, where a fractal is identical to itself on all scales and can be used to describe subsurface fracture structures (Watanabe & Takahashi, 1995). The newfound results were taken into account for updated estimates of the recovery factor considering two geothermal reservoir types: for fracture-dominated reservoirs a range from 0.08 – 0.2 and for sediment hosted reservoirs a range from 0.1 – 0.25 with a maximum value of 0.5 (Williams et al., 2008).

Garg (2010) employed the Monte Carlo approach to investigate the impact of varied ranges of the stored heat parameters. The study points out that the chosen range should consider actual measured field data. A recovery factor of 0 – 0.2 was suggested at an initial exploration stage because without drilling results there is no feasible way to determine if the geothermal system can produce fluids (Garg, 2010; Garg & Combs, 2015). This view of a recovery factor with a zero value was debated by Williams (2014) who argued that as long as there is a permeable volume the recovery factor will be greater than zero. The ARGCC employed a similar view of the recovery factor compared to the ranges suggested by the USGS. The major contribution to the method development was how the method should consider high porosity reservoirs. In the case of when the average porosity exceeds seven percent, the method should implement a recovery factor of 2.5 times the porosity with a maximum of 50 % (AGRCC, 2010a, 2010b).

A major contribution to the implementation of the recovery factor was proposed by Lavigne (1977) who calculated a recovery factor value of 0.33 considering a well-doublet system. The extractable amount of heat R_0 depends on a factor of 0.33 and a temperature fraction between the reinjection temperature and the surface reference temperature often set as the mean annual temperature. This view of the recovery was used in the Atlas of geothermal resources in Europe (Hurter & Schellschmidt, 2003) and has since then been applied in several European geothermal assessment studies (Balling et al., 2019; Piris et al., 2021; Erlström & Rosberg, 2022). The fraction of extractable amount of heat R_0 is calculated with Equation (8):

$$R_0 = 0.33 \times ((T_p - T_{inj}) / (T_p - T_{ref})) \quad \textbf{Equation 8}$$

T_p = Production temperature (°C)

T_{inj} = Reinjection temperature (°C)

T_{ref} = Reference temperature (°C)

2.6 Geological setting and description of the Arnager Greensand

2.6.1 Tectonic framework of the STZ and the Öresund Basin

The Fennoscandian Shield (Baltic Shield) is a stable crustal province of the East European Craton that borders the tectonically active phanerozoic European continent to the southwest. The southernmost part of Sweden, known as the region of Scania, is located in this crustal border transition zone consisting of several structural elements, including Precambrian basement, Early Palaeozoic, Mesozoic, and Paleogene sedimentary formations (Norling & Bergström, 1987; Erlström, 2009). The transition zone includes the Sorgenfrei-Tornquist Zone (STZ) which extends in a northwest-southeast direction from the North Sea through Scania where it connects to the Tessyere-Tornquist Zone (TTZ) in the southeast over the Baltic Sea into Poland (Erlström & Guy-Ohlson, 1994). The STZ and TTZ are two out of five major fault zones that were introduced by Berthelsen (1998) as a part of the Tornquist fan complex crossing the southwest part of the shield. The STZ is characterised by extensive block faulting and has been repeatability active since the Late Palaeozoic with the main events occurring in Mesozoic times which gave the STZ its current appearance (Erlström, 2020).

The tectonic evolution of the STZ is closely linked to the formation of the Danish Basin as the Öresund Basin, centred in the Öresund region, is situated in the transition zone between these geological settings. The Öresund Basin is a marginal part of the Danish Basin (Erlström et al., 2013). The Danish Basin formed in response to rifting during the Late Carboniferous – Early Permian (Vejbaek, 1997) where it later received large amount of sediments in connection to thermal subsidence during a post-rift phase in the Triassic – Jurassic (Liboriussen et al., 1987; Erlström et al., 1997). There are several Triassic – Jurassic extensional events recognized in the stratigraphical record, but these structures are commonly obscured in response to Late Cretaceous – Paleogene inversion movements that overprint the older structures (Norling & Bergström, 1987; Olaf & Nielsen, 1991; Mogensen, 1994; Erlström et al., 1997).

The Öresund Basin features a series of normal extension faults towards the west, and to the northeast lies the Romeleåsen Fault Zone (RFZ) which constitutes the boundary towards the STZ (Figure 1) (Erlström et al., 2013). The normal faults in the Öresund Basin originate from the Carboniferous and were later reactivated in the Triassic period (Erlström et al., 1997; Sivhed et al., 1999). The Triassic period extension resulted in increased accommodation space and thickening of basin strata towards the confining faults (Erlström et al., 2013). The Late Cretaceous inversion movements were caused by a change from a tensional stress regime towards a more compressive one which resulted in reverse faulting along the STZ (Erlström, 2009). The initial inversions are attributed as a response to the Sub-Hercynian Alpine deformation phase. This phase reached its peak intensity during the Campanian epoch and extended until the late Maas-

Table 1. Summary of the SW Scania borehole dataset. The table contains information about the drilling operator and the drilling year. The table also provide the abbreviations which are used to improve the readability of the produced maps. The borehole coordinates are given in the national Swedish SWEREF99 projection.

Borehole	Abbreviation	Drilling operator	Drilling year	Y (SWEREF99)	X (SWEREF99)
Norrevång-1	Nv	OPAB	1971	6183299	376079
Barsebäck-1	Ba	OPAB	1972	6179890	369962
Mossheddinge-1	Mo	OPAB	1973	6164564	393296
FFC-1	FFC-1	Sydkraft - EON	2002	6166931	374902
Magreteholm-1	Mah-1	HGS - DONG	2002	6174037	351271
Svedala-1	Sv	SGU	1948 - 1951	6152816	386937
Eskilstorp-1	Es	OPAB	1971	6149313	375779
Håslöv-1	Hå	OPAB	1972	6145820	376823
Kungstorp-1	Ku	OPAB	1973	6145358	372396
Höllviken-1	Hö-1	SGU	1941 - 1943	6143771	370499
Granvik-1	Gr	Nordstjernan	1947	6143369	371974
Maglarp-1	Ma	OPAB	1971	6139587	377371
Hammarlöv-1	Ha	OPAB	1971	6138859	379112
Trelleborg-1	Tr	SGU	1947 - 1948	6137455	383957
Höllviksnäs-1	Hn	OPAB	1971 - 1972	6142244	369408
Höllviken-2	Hö-2	SGU	1943 - 1947	6141239	369676
Ljunghusen-1	Lj	SGU	1954 - 1955	6141141	367317
Smygehuk-1	Sm	OPAB	1973	6141141	367317
Falsterborev-1	Fa	OPAB	1973	6130415	376188

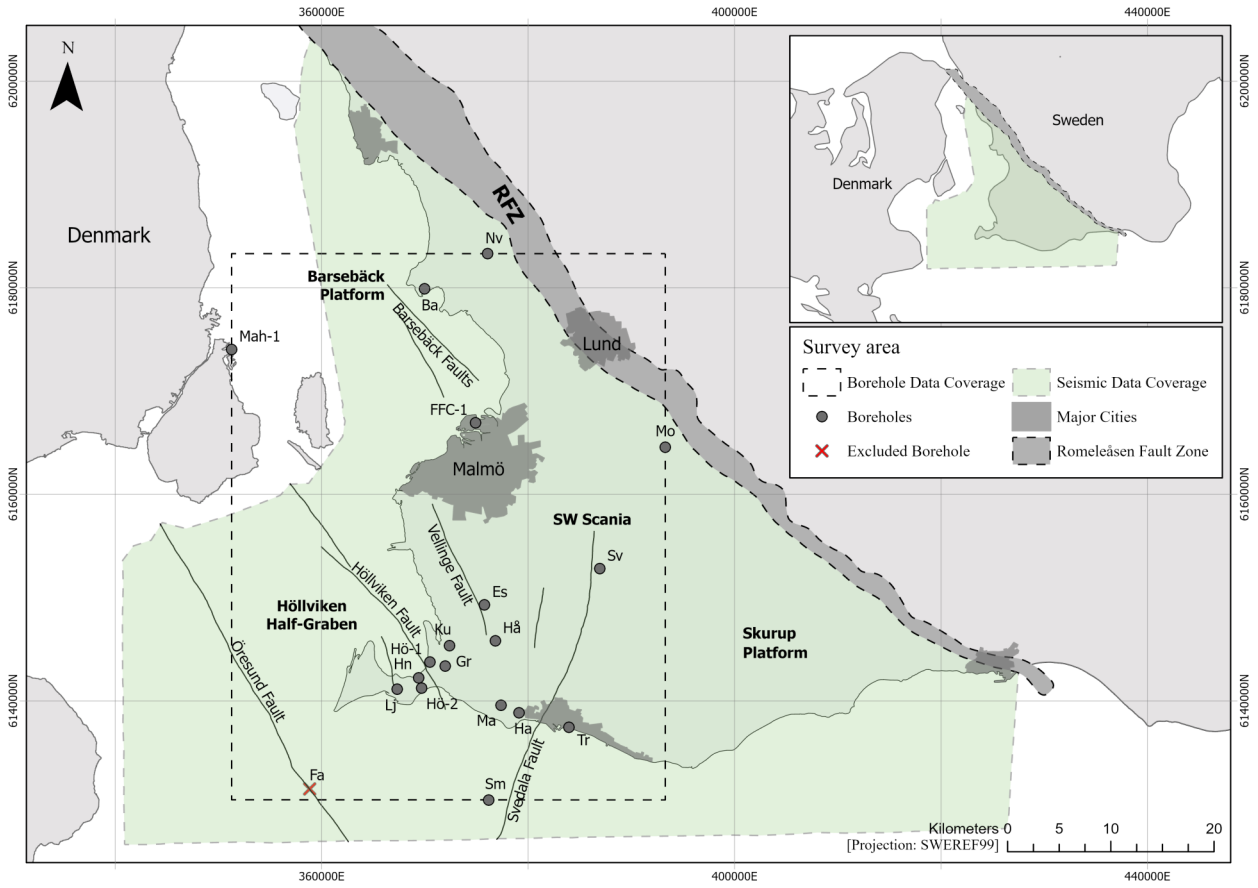

Figure 1. Location map which displays the main structural units of SW Scania alongside borehole positions. The structural units include the Barsebäck platform in the north, the Höllviken Half-graben to the west, and the Skurup platform to the east. The geothermal assessment in this study covers the entire land area southwest of the RFZ. The borehole data coverage is represented by a dashed minimum bounding rectangle. Extrapolation techniques were applied outside of this rectangle and accounts for a portion of the Skurup Platform to the east and a small area in the north adjacent to the RFZ.

trichtian. The inversion movements continued during the Paleogene to Neogene, including the Laramide phase from the Danian to the Thanetian (Deckers & van der Voet, 2018).

The geological evolution of the STZ and the development of the Danish Basin has given rise to a distinctive subsidence and rifting pattern in the Öresund Basin. This has led to the deposition and preservation of a substantial Mesozoic sequence, reaching up to circa 3000 meters in thickness (Erlström et al., 2018). Within this sequence, several intervals are dominated by fluid-bearing sandstones. These intervals hold potential reservoirs to be used as low enthalpy resources. A particularly interesting sandstone interval is the Arnager Greensand which marks the uppermost part of the Lower Cretaceous.

2.6.2 Structural outline of SW Scania

The stratigraphical representation and lithological characteristics of the Mesozoic succession over SW Scania have been investigated by several researchers (Brotzen, 1950; Norling, 1981; Norling & Bergström, 1987). The knowledge about the subsurface is almost exclusively based on well data and seismic surveys, which has been collected at various point over the past 50 years, including the extensive OPAB (Swedish Petroleum Exploration) dataset obtained during the seventies (Table 1) (Figure 1). The main part of the sedimentary succession in SW Scania consists of the 1 – 1.7 km thick carbonate dominated Höllviken Formation overlaying a 450 – 700 m thick interval with Lower Cretaceous, Lower Jurassic, and Triassic strata (Erlström et al., 2018). The area southwest of the RFZ is divided into three structural units - The Barsebäck Platform, the Höllviken Half-graben, and the Skurup Platform. The Arnager Greensand extends across all these structural units (Figure 1 and Figure 2).

The Barsebäck Platform is situated in the northwest part of SW Scania and is a structural unit with a flat crystalline basement surface that dips slightly to the NE towards the RFZ (Figure 2). The basement is covered by over two kilometres of sedimentary strata from the Upper Triassic to the Paleogene (Erlström & Sivhed, 2001; Erlström et al., 2018; Erlström, 2020).

The Höllviken Half-graben constitutes the southern part of the Öresund Basin. The Höllviken Half-graben is characterised by a tilted fault block that dips towards the SW against the bordering Öresund Fault (Figure 2) (Erlström et al., 2018). The basement is significantly displaced along the Öresund Fault, verified by seismics and the Falsterborev-1 borehole which was drilled on the footwall of the Öresund Fault (Sivhed et al., 1999). The Höllviken Half-graben is associated with several other normal faults that strike mainly in a NW – SE direction over the Öresund Basin including the Vellinge Fault and Foteviken faults. The Half-Graben holds the most complete Phanerozoic sedimentary rock succession in Sweden (Erlström, 2020).

The Skurup Platform constitutes the western part of SW Scania and is separated from the other structural units by the Svedala Fault that strikes through the centre of SW Scania in an NNE – SSW direction. The platform is a partly uniform horizontal tectonic block unaffected by regional tectonics covered by a 1500-meter-thick Mesozoic sedimentary sequence primarily Late Cretaceous in age (Erlström, 1994). The Svedala fault has displaced the basement of up to one kilometre (Sivhed et al., 1999). The platform is bounded to the north by the RFZ and to the south by a zone of smaller faults such as the Smygehuk Fault (Thomas et al., 1993; Erlström et al., 1997).

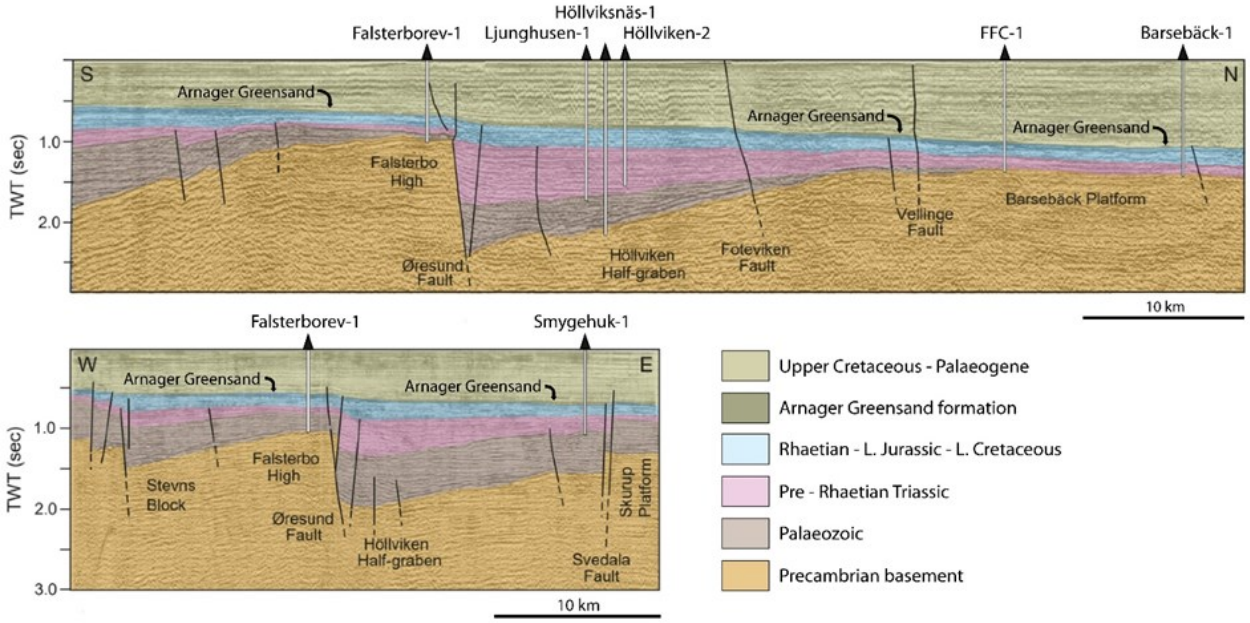

Figure 2. Seismic stratigraphy profiles modified from Erlström et al. (2018). The interpreted profiles show the sedimentary stratigraphy over the Öresund Basin and the SW Scania structural units including the Barsebäck Platform, Höllviken Half-Graben, and Skurup Platform. The Arnager Greensand (dark green) is situated in the transition zone between the Lower Cretaceous and the Upper Cretaceous. The profile also shows the relative position of several boreholes and interpreted fault lines. The seismic profiles cover the off-shore Öresund Basin region in two directions and do not depict the on-shore SW Scania stratigraphy. The profiles are included since they showcase the general stratigraphic arrangement of the Arnager Greensand which can be inferred over on-shore SW Scania.

2.6.3 The Arnager Greensand

2.6.3.1 Depositional setting and distribution

The depositional setting during the Early Cretaceous was predominantly marginal marine and brackish with interludes of coastal lacustrine settings. This resulted in a lithological diverse succession of sandstones, siltstones, and mudstones (Sivhed et al., 1999). The marine influence increased successively during the Early Cretaceous and led to the deposition of the black organic-rich Aptian shale (Sivhed et al., 1999). The Aptian shale is only a few meters thick but is an extensive marker bed in the Early Cretaceous sedimentary succession situated just below the Arnager Greensand (Erlström et al., 2011).

The Arnager Greensand was deposited in a marginal shelf environment at the time of an extensive Cretaceous transgression (Christensen, 1984; Tyson & Funnell, 1987; Sivhed et al., 1999). The Arnager Greensand is interpreted to represent a regional inner-shelf sand deposit. The transgression coincides with the Early Cretaceous – Late Cretaceous boundary (Figure 3). The Arnager Greensand has been dated to Aptian – Cenomanian from biostratigraphical studies on foraminifera and palynomorphs (Vajda-Santivanez & Solakius, 1999; Larsson et al., 2000). The upper part of the formation is widely agreed upon to be Middle Cenomanian in age (Hart, 1979; Solakius, 1989; Packer & Hart, 1994; Hart et al., 2012).

The Arnager Greensand is a saline aquifer with a regional distribution of 8800 km^2 in Swedish territory. The formation was first named the Granvik Sandstone formation in the seventies during exploration surveys on the Falsterbo Peninsula conducted by OPAB. The name was later changed as it was found to correlate with the Arnager Greensand outcropping on the island of Bornholm. The Arnager Greensand covers the region of SW Scania and extends into Denmark and over the southern Baltic Sea into Germany. It is also found in the Vomb Trough and the Kristianstad Basin which are two other Mesozoic basins located further to the north in Scania (Mortensen & Sopher, 2021).

The formation is identified in several boreholes in SW Scania at depths between 1050 and 1800 meters (Erlström et al., 2011; Juhlin et al., 2013). The greatest depths are recorded adjacent to the RFZ, whereas the shallowest depths are in the southern parts of the Öresund Basin. This is related to the fact that the whole Cretaceous succession dips slightly towards the northeast (Anthonsen et al., 2014; Mortensen et al., 2016). The thickness of the formation varies considerably, with a thickness of 20 meters in the northwest to around 60 meters in the south over the Falsterbo Peninsula (Erlström et al., 2011).

The Arnager Greensand is overlain by the Arnager Limestone which is a dense and partly silicified calcilutite (Figure 3) (Sivhed et al., 1999). The limestone has the same approximate distribution over SW Scania as the Arnager Greensand. The thickness of the limestone varies between 10 and 100 meters (Sivhed et al., 1999). The Arnager Limestone has been dated to the early Coniacian (Solakius, 1989; Tröger & Kegel Christensen, 1991; Packer & Hart, 1994; Christensen & Schulz, 1997; Vajda-Santivanez & Solakius, 1999; Madsen et al., 2010). The contact between the two formations is well-defined in the seismic stratigraphy as the significant variation in density and seismic velocity between the two gives a strong difference in acoustic impedance. The result is a strong seismic reflection that is well-mapped in the seismic data cover-

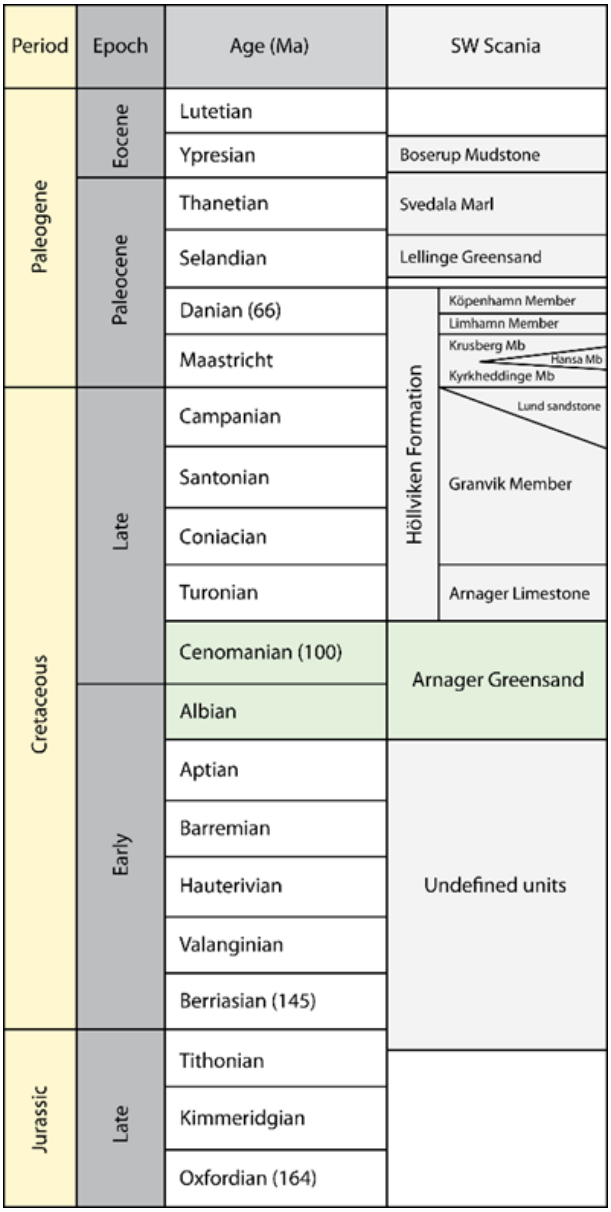

Figure 3. The lithostratigraphic division of SW Scania modified from Erlström (2020). The division covers the Late Jurassic to Paleogene period. The Arnager Greensand is situated in the transition between the Early to Late Cretaceous. The Arnager Greensand is superimposed on an undefined mixed clastic Lower Cretaceous succession which includes alternating beds of sandstone and mudstone such as the Aptian Shale and Lower Cretaceous sandstones. The Lower Cretaceous sandstones have similar reservoir properties as the Arnager Greensand. The Arnager Greensand is overlain by the Arnager Greensand which is a part of the Höllviken Formation which constitutes the upper stratigraphy of SW Scania. The uppermost three members - Lellinge Greensand, Svedala Marl, and Boserup Mudstone only have a local distribution over SW Scania.

ing the Mesozoic sequence of SW Scania (Figure 2) (Erlström et al., 2018).

The Arnager Limestone is the lowermost member of the Höllviken Formation (Figure 3). The lithostratigraphy of the Höllviken Formation was established by Erlström (1990) and consists of clayey carbonate and clastic members that were deposited from the Early Cretaceous to the Paleogene. The thickness and spatial extent of each member varies across SW Scania. The approximate thickness of the Höllviken Formation is around 1000 meters (Anthonsen et al., 2014). A general depositional trend is observed in the formation where sandstone units become more abundant close to the RFZ. One of these sandstone units is the 900-meter -thick Lund Member which is dominated by sandstone commonly referred to as the Lund sandstone (Erlström, 1990; Erlström & Rosberg, 2022).

The Arnager Greensand outcrops only on the island of Bornholm in Denmark. The island of Bornholm is situated in the transition zone between the STZ to the northwest and the TTZ to the southeast over the Baltic Sea. The transition is marked by a bending junction formed by dextral-slip tectonics associated with the Rönne and Arnager Grabens (Erlström et al., 1997). The contact between the Arnager Greensand and the Arnager Limestone can be observed at a cliff section near the village of Arnager. The outcrop has been subject to study by numerous researchers for several decades (Jensen & Hamann, 1989; Solakius, 1989; Packer & Hart, 1994; Christensen & Schulz, 1997; Vajda-Santivanez & Solakius, 1999; Hart et al., 2012). The transition between the Arnager Greensand and the Arnager Limestone on Bornholm is marked by a hardground-phosphorite bed interpreted as a depositional hiatus. The timing and duration of the hiatus are well-defined but the cause of it remains uncertain.

Two hypothesis have been proposed for the cause; the first one suggests that the stratigraphic hiatus is a result of regression and the development of the hardground bed (Christensen, 1984), and the second one suggest that the sedimentation ceased due to relative sea-level rise (Packer & Hart, 1994). Thus, the discussion has been centred around whether it was a shallowing or deepening event. Concurrent research supports the idea the Bornholm area changed from an inner-shelf depositional towards an outer-shelf depositional environment during a transgression (Vajda-Santivanez & Solakius, 1999) and resulted in a sediment-starved shelf during the late Cenomanian to late Turonian period (Hart et al., 2012). The depositional hiatus between the two formations has also been observed in several core drillings in SW Scania (Larsson et al., 2000).

The boundary between the Arnager Greensand and the Arnager Limestone is well-defined. On the contrary, there is uncertainty and variability associated with the lower boundary of the Arnager Greensand. This is partly caused by the fact that the underlying Cretaceous successions in SW Scania are not clearly defined and often have a laterally variable distribution and lithological composition (Erlström, 2020). The base boundary is often difficult to distinguish because of the occurrence of a Lower Cretaceous succession with alternating beds of sandstone and mudstone. There is commonly a diffuse and/or gradual transition between the typical Arnager Greensand lithofacies into these alternating beds. Some of these Lower Cretaceous beds consist of permeable sandstones which also have similar reservoir properties as the Arnager Greensand. The Lower Cretaceous sandstones comprise together with the Arnager Greensand a 100 – 150 meter thick Lower Cretaceous sandstone sequence (Erlström et al., 2011; Juhlin et al., 2013). This whole sequence can be seen to have greater geothermal potential than the Arnager Greensand alone, but in this study, the focus has been on the Arnager Greensand, as it is far better documented in boreholes drillings and seismic data.

The Arnager Greensand is a partly fault confined aquifer with only a few faults with minor vertical displacements over the Arnager Greensand interval (Anthonsen et al., 2014; Mortensen et al., 2016; Mortensen & Sopher, 2021). The aquifer is in contact with the Svedala, Foteviken, and Vellinge Fault in SW Scania and the Öresund Fault in the Öresund Basin (Figure 1 and Figure 2). Over these faults, the Arnager Greensand is deformed as a flexure. Only minor displacements of the Arnager Greensand have been noted over the faults (Sivhed et al., 1999). Any significant disturbances to the continuous distribution of the reservoir are limited to inversion movements along the Öresund and Svedala faults (Juhlin et al., 2013). In the seismic record, this is displayed as a pattern of flexure and bending reflectors crossing these faults. The vertical displacement of the other faults in SW Scania is considerably smaller in magnitude (Sivhed et al., 1999; Juhlin et al., 2013).

2.6.3.2 Arnager Greensand characteristics

The Arnager Greensand is a fine and medium grained unconsolidated quartz arenite (sandstone) (Figure 4) (Sivhed et al., 1999). The Arnager Greensand contains both glauconite as grains and as mineralisation on detrital quartz. It also contains accessory minerals such as feldspars, pyrite, micas, and zircons (Mortensen et al., 2016). The greenish-greyish colour of the sandstone is attributed to the relatively high content of glauconite which is an authigenic mineral that forms through slow marine diagenesis in shallow marine environments such as sediment-starved shelves (Winterer, 2012). The Arnager Greensand matrix contains clay and small quantities of carbonates. The degree of consolidation varies as the detrital grain framework can be embedded by both quartz and carbonate cementation (Sivhed et al., 1999; Erlström et al., 2011).

The petrophysical properties of the Arnager Greensand vary over SW Scania. The formations show porosity values between 7.2 – 31.3 % and gas permeability between 0.15 – 1879 mD. An increase in cementation along with a decrease in average grain size has been noted towards the northeast (Barsebäck Platform) (Sivhed et al., 1999). The Arnager Greensand has been investigated in recent years as a potential storage aquifer for both natural gas and CO_2 as well as for geothermal utilization. Some intervals of the Arnager Greensand display notably high reservoir quality where the permeability exceeds 1 Darcy and the porosity lies within the range of 27 – 30 % (Erlström et al., 2011).

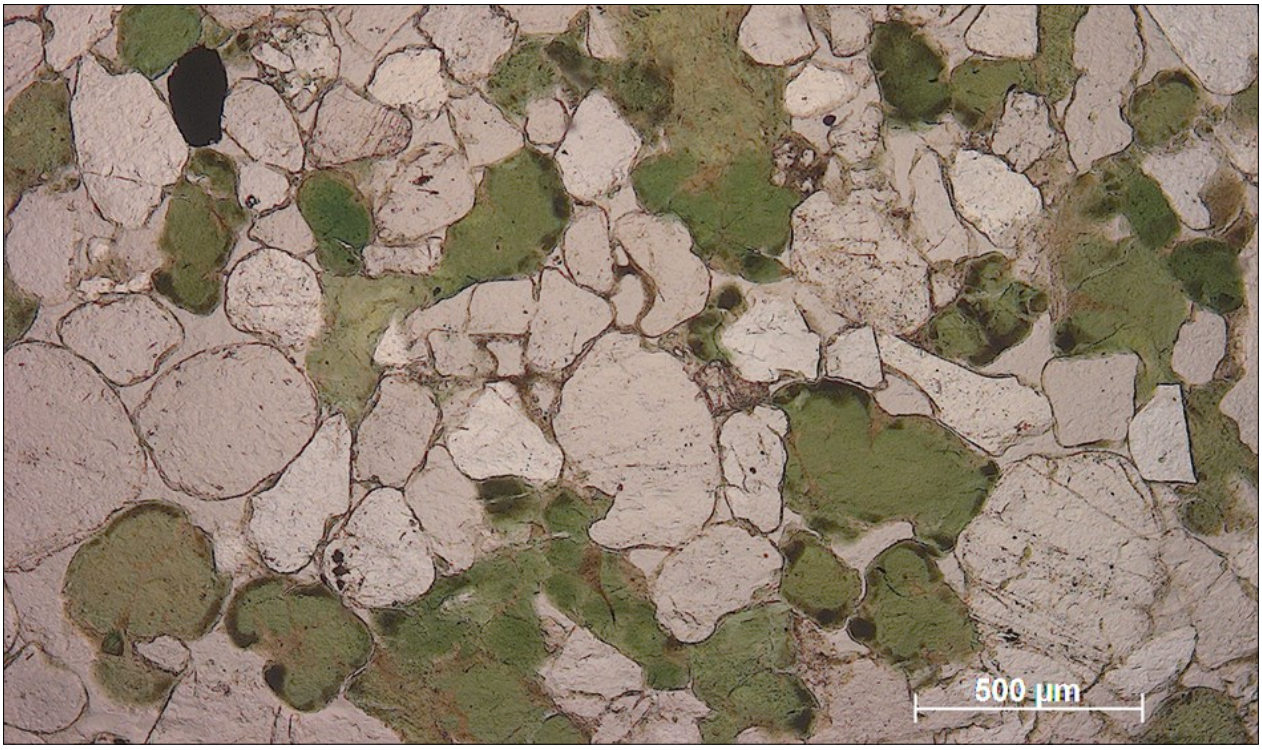

Figure 4. Microphotograph (transmitted light) of the Arnager Greensand from the SGU Geoarchive. The sample is from a depth of 1261 meters (KB) in the Höllviken-2 borehole. The picture showcases quartz grains in white and glauconite in green colour. The Glauconite appears both as grains and mineralization on detrital quartz.

3 Methods

The workflow for the stored heat method (HIP) which was applied in this study is presented in Table (2) and Figure (5). At an initial stage, the study required the digitisation of seismic data from a vintage analogue seismic map (blue marker map) of the top of the Arnager Greensand and a revaluation of the borehole data to get the depth and thickness estimates. The seismic data underwent a time-to-depth conversion process to determine the depth of the Arnager Greensand away from well control. Raster surfaces (grids) for the Arnager Greensand top and the formation thickness were generated using interpolation techniques in a GIS environment. A regional geothermal gradient was combined with the depth data to provide an assessment of the reservoir temperature. Petrophysical data was compiled and further implemented in the stored heat calculations. The stored heat was calculated on a cell-by-cell basis covering the entire land area (SW Scania) southwest of the RFZ. Maps were generated to display the spatial difference in the stored heat and additional maps display the variation in formation depth, reservoir thickness, and reservoir temperature. In the following subsections, the data sources will be outlined together with a more detailed description of the data processing steps.

3.1 Data sources and acquisition

The dataset comes from the Geological Survey of Sweden (SGU) and consists of a combination of older seismic and borehole data (Table 2). The data was acquired and processed during a series of different exploration surveys between 1960 – 2003. The data varies considerably in quality and format.

3.1.1 Seismic Data

Between 1930 and 1980, both land and marine seismic surveys were conducted in SW Scania to investigate the sedimentary bedrock. The initial surveys were performed by SGU (Swedish geological survey) and later by the Swedish Oil and Gas Prospecting Company (OPAB), Swedish Exploration Company (SECAB), and Swedegas AB (Sivhed et al., 1999; Erlström et al., 2018). Exploration boreholes were drilled together with the seismic surveys. The surveys by OPAB focused on depths exceeding one kilometre, while the Swedegas AB surveys focused on shallower formations on land. The combined surveys resulted in the identification of several distinct mappable seismic reflectors. These seismic reflectors were supported by well data and assigned specific stratigraphic horizons and a series of isochrone maps showing these marker horizons (marker beds) exists from these surveys (Sivhed et al., 1999).

One of those distinct reflectors or markers is the so-called blue marker which denotes the strong reflection coefficient that occurs at the interface between the Arnager Limestone and the underlying Arnager Greensand, also referred to as the base Upper Cretaceous marker. The seismic data used in this project is digitised from a blue-marker isochrone map from 1993 (Larsson et al., 1994) (Figure 6). The map itself is originally an interpretation of legacy seismic data. The blue marker isochrone map displays the approximative two-way-traveltime (TWT) in milliseconds (ms) as contour lines down to the transition between the Arnager Greensand and the Arnager Limestone. The map covers SW Scania and the adjacent offshore areas. The map shows the seismic two-way-time between the mean sea level and the reflection at the top of the Arn-

Table 2. The table provides an overview of the data used in the study, including descriptions of the parameters with their respective units, the pre-processing steps performed to integrate the data into the model workflow, and the sources from which the data was obtained.

Input data	Description	Pre-processing	Application	Source
Seismic	TWT values (ms)	Digitisation	Kriging interpolation	Blue Marker map (Larsson et al., 1994)
Borehole	Depth and Thickness (m) (b.m.s.l)	Revision	Co-kriging Interpolation	SGU
Petrophysical	Porosity (%) Permeability (Darcy) Grainsize ρ (g/cm^3) Fluid ρ (g/cm^3)	Tabulation	Stored heat (HIP) equations	SGU
Temperature	Temperature log (°C) (Ljunghusen-1 borehole)	Conversion	Geothermal Gradient Reservoir Temperature	SGU
Terrain map	Coastline polyline feature	Digitisation	Visualisation	Lantmäteriet

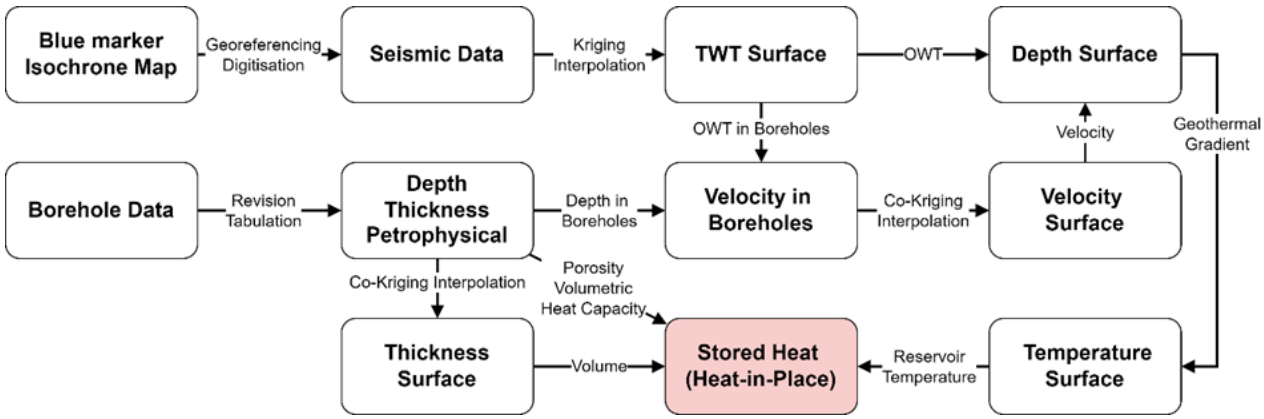

Figure 5. The general workflow applied in the stored heat resource assessment of the Arnager Greensand. The major methodology steps included the digitisation of seismic data, revision of borehole data (depth and thickness), petrophysical calculations, time-to-depth conversion of seismic data, interpolation techniques to generate depth and thickness raster surfaces over SW Scania, and stored heat calculations. The OWT abbreviation stand for One-Way-Time. The red box marks the stored heat output.

ager Greensand. The contour lines are drawn in intervals (resolution) of 20 milliseconds (ms). The map also shows several regional faults cutting through the blue marker, such as the Vellinge Fault, Svedala Fault, Öresund Fault (Carlsberg Fault in the map legend), and the Barsebäck faults. The RFZ is shown in grey and delimits the seismic data coverage to the northeast. The blue marker map remains to this day the primary source material that illustrates the top boundary of the Arnager Greensand.

3.1.2 Borehole Data

The borehole database in this study comprises 17 deep boreholes in SW Scania and one borehole (Margreteholm-1) located on Amager in the south Copenhagen area in Denmark (Table 1) (Figure 1). The boreholes are all drilled into or through the Arnager Greensand. One borehole (Falsterborev-1), which is normally included in the SW Scanian deep borehole dataset, was excluded due to its location on the footwall of the Öresund Fault (Figure 1 and Figure 2). Most boreholes are located on the Falsterbo Peninsula near each other. The Smygehuk-1 borehole is located offshore in the Baltic Sea south of the Swedish coastline. The Barsebäck-1 and Norrevång-1 boreholes are located on the Barsebäck Platform in the north. The Svedala-1 and Mosshedinge-1 boreholes are located further inland and have historically been attributed to the Skurup Platform (Sivhed et al., 1999). The Svedala-1 borehole is located on the footwall of the Svedala Fault and the Mosshedinge-1 borehole is adjacent to the RFZ. Since the two boreholes are located on the margins of the Skurup Platform, it is likely that they are to some extent affected by the nearby faults. This is exemplified in the Mossheddinge-1 borehole by a less characteristic geophysical log response of the Arnager Greensand. The cored Svedala-1 borehole does not include any geophysical logs which hinders a geophysical signature comparison between the two boreholes. The two boreholes are the only ones that penetrate the Arnager Greensand on the Skurup Platform. No deep drillings have been performed on the central regions of the Skurup Platform. This introduces greater uncertainty into the assessment of stored heat in this area, primarily because the distribution of the Arnager Greensand remains uncertain.

The documentation with information about the top and base of the Arnager Greensand comprises a scattered set of borehole reports with geological descriptions, wire-line logs, mud logs, analytical results, borehole protocols, personal comments, structural maps, and map sheet descriptions. A few boreholes were core -drilled which includes the Höllviken-1, Höllviken-2, Svedala-1, Trelleborg-1, and the Granvik-1 boreholes. The geological material from these drillings (cores and cuttings) varies greatly in quality (Larsson et al., 1994). Most boreholes, which make up the bulk of the dataset, only provide depth data through the interpreta-

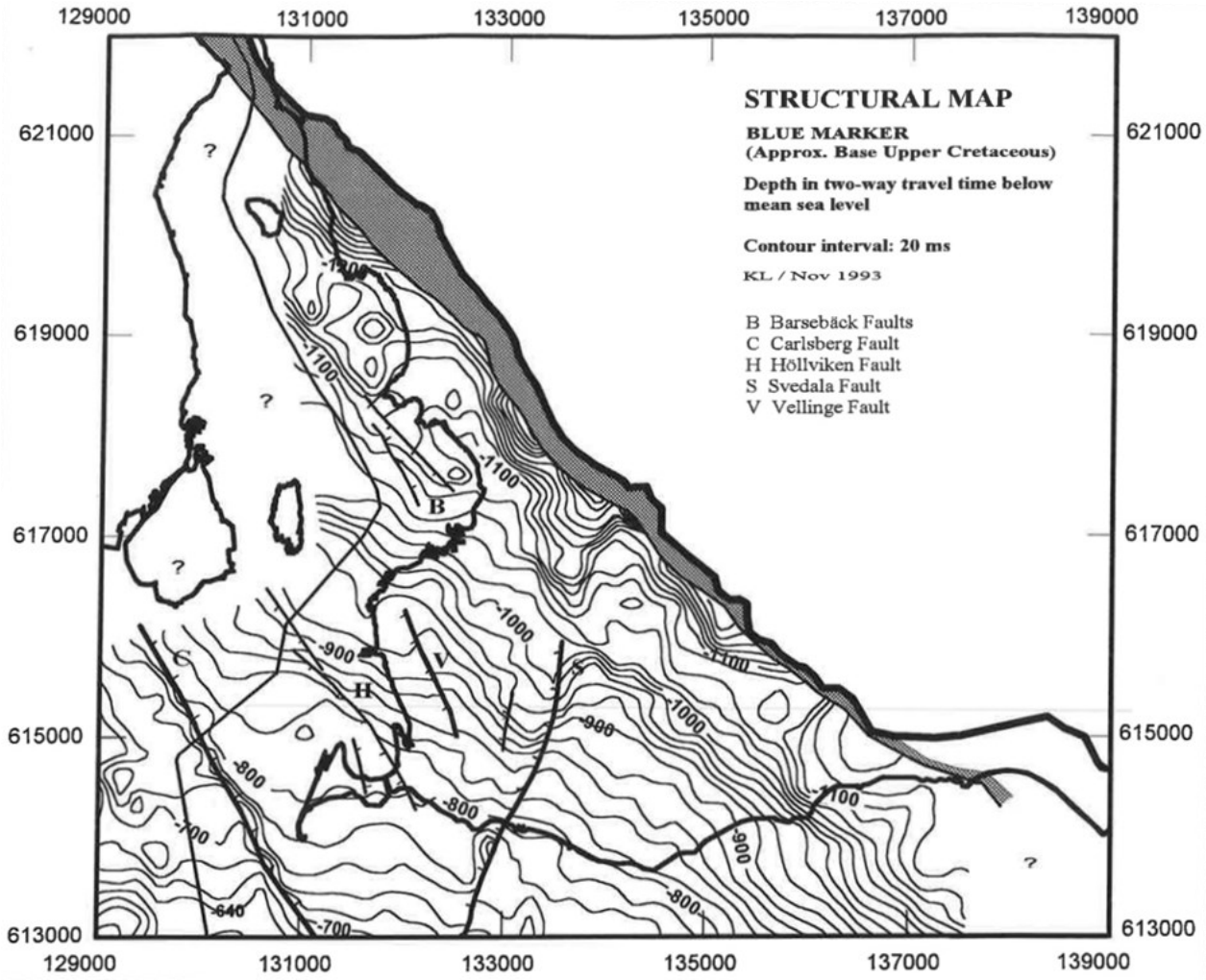

Figure 6. Analogue blue marker isochrone map which shows the reflection from the top Arnager Greensand (Larsson et al., 1994). The contour lines display the approximative Two-Way-Traveltime (TWT) in milliseconds (ms) down to the Base Upper Cretaceous reflection. The map also shows interpreted faults as thick black lines, with the prominent Romeleåsen Fault Zone (RFZ) highlighted in grey colour. The map is derived from the interpretation of legacy seismic reflection data in analogue format. The map is drawn in the old Swedish national coordinate system RT90.

tions of geophysical wireline logs. The quality and format of the source material may vary due to various factors. For instance, some of the boreholes (Höllviken -1, Höllviken-2, Höllviksnäs-1, Svedala-1, Trelleborg-1) were drilled 1940 – 1955 and data gathered from these boreholes is partly missing. The wireline logs also vary greatly in resolution, and it should be noted that there are no geophysical logs from the cored boreholes. Another contributing factor to the scattered dataset is the geological interpretation of the wireline logs which varies in the documentation regarding primarily the base of the Arnager Greensand. This contributes to a spread geo-archive with several reported depth and thickness values.

The borehole depth data in the source material is either given in meters below a drill floor reference level referred to as the Kelly bushing (KB) or the ground level (GL). It should be noted for some boreholes there are no precise depth reference levels given, such is the case for the Trelleborg-1, Granvik-1, Höllviken-1, and Höllviken-2 boreholes. The available depth reference levels are presented in Appendix (1). Two of the boreholes (Granvik-1 and Trelleborg-1) only contain depth measurements to the top boundary of the Arnager Greensand. The drillings were terminated after the top boundary was reached. This means that the Arnager Greensand thickness in the Granvik-1 and Trelleborg-1 boreholes is estimated based on thickness data from adjacent boreholes.

The Bottom-Hole-Temperature (BHT) data were gathered in connection to the wire-line logging operations. Temperature data are available for several boreholes but most of them are not comparable to normal conditions. The measurements were taken too close in time to the drilling operation and the boreholes did not have time to stabilise. The readings may also have been influenced by the circulation of mud during the drilling operations. This means that the reading temperatures are assumed to be a few degrees lower than the actual reservoir temperature (Erlström et al., 2018). The temperature logs from the Ljunghusen-1 and FFC-1 boreholes are the most reliable ones as both were recorded sometime after the drilling operation finished. The temperature readings from these two are in this study assessed to represent normalised temperature conditions.

The database also includes some information on various petrophysical properties of the Arnager Greensand in the Svedala-1, Trelleborg-1, Maglarp-1, Höllviken-1, Höllviken-2, and FFC-1 boreholes. The dataset comprises porosity (%), permeability (mD), grain density (kg/m^3), and fluid density (kg/m^3). Much of this information is found in unpublished reports and borehole protocols. This data is useful since the stored heat equations consider porosity and the volumetric heat capacity for different mediums. The volumetric heat capacities can be calculated based on the density of the rock matrix and the reservoir fluid assuming reference values for the heat capacities. The stored heat equations do not account for the impact of varying permeability in the geothermal reservoir. Hence, the permeability data is an important evaluator of the suitability of the Arnager Greensand as a geothermal reservoir.

3.2 Data processing

3.2.1 Review of the Borehole Data

The top and base of the Arnager Greensand were reevaluated by checking all wireline logs and borehole reports from the borehole dataset and adjustments were made since a few faulty values were found in the borehole reports. These new depth values were considered together with previous interpretations of the top and base boundaries which are presented together with the reevaluated ones. The Granvik-1 borehole was assigned the same formation thickness as the Höllviken-1 borehole and the Trelleborg-1 borehole was assigned the same formation thickness as the Hammarlöv-1 borehole. The vertical reference point was set to below mean sea level for all depth data. The reevaluated depth and thickness database (Table 3) were then used as input values in the data-processing workflow in the calculation of the stored heat for the Arnager Greensand.

The main objective of this project was not to conduct a comprehensive reinterpretation of the Arnager Greensand depth boundaries as this would require a separate sole project. Instead, this project underscores the challenges in interpreting the vintage wireline logs. The results section presents two different geophysical signatures observed over the Arnager Greensand interval. The first one exemplifies when it is relatively straightforward to interpret the top and base boundaries of the Arnager Greensand, along with a second example highlighting the complexities involved in interpreting these vintage wireline logs.

3.2.2 Time-to-depth conversion

The characterisation of the sub-surface geology using reflection seismic data relies on the conversion of seismic TWT data into depth. This process is commonly referred to as time-to-depth conversion and is an important step in accurately interpreting sub-surface structural geology from seismic data. Time-to-depth conversion requires an estimation or model of the seismic velocities in the subsurface. There are many ways to estimate these velocities which can range in complexity from assuming a constant velocity to generating a 3D model of the velocities over the area of interest. An important step in this project was to convert the previous blue marker map using a time-to-depth conversion workflow.

In this project, the blue marker isochrone map (Figure 6) was georeferenced and digitised to derive TWT point values which were later used in the time-to-depth conversion workflow. The georeferencing tool in ArcGis Pro 2.7.3 was utilized in a three-step process to obtain TWT point data. The map was georeferenced from the old Swedish national coordinate system RT90 into the current SWEREF99 coordinate system. A more advanced form of transformation was disregarded as the blue marker map is of good quality with only minor geometric distortion. An affine transformation was used which involved moving and scaling the source map against a coastline line feature from the Lantmäteriet terrain map.

Digitisation was carried out on the TWT-polyline features. This involved manually tracing the TWT contour line features on the analogue map to create a digital representation in shapefile format. The contour lines terminate when intersecting a fault and continue on the opposite side with an offset. Consequently, it was necessary to trace the contour lines accurately along the faults and align them with their corresponding Two-Way Travel Time (TWT) values on the opposite side. Given that there are no visible TWT contour lines to trace along the faults, apart from the thicker fault line itself, digitisation along these faults is difficult and may not be representative of the original interpretation. The contour lines along the Barsebäck faults were also difficult to digitise as it was hard to interpret where the contour lines intersect the fault line. The digitisation in this area should therefore be viewed as a simplification. The digitised polylines were subsequently converted into points with a spacing of 200 meters. This resulted in a point dataset where each point contained a TWT value. Further digitisation was performed on the RFZ and other fault lines on the blue marker map. The combined workflow enabled the transformation of a vintage analogue map into a TWT point dataset which was then used in the subsequent time-to-depth conversion.

The Geostatistical analyst extension in ArcGis was used to perform Ordinary Kriging interpolation on the TWT point dataset. This resulted in a TWT raster surface over SW Scania (Figure 7). Ordinary Kriging is a well-known geostatistical interpolation method that takes into consideration the spatial autocorrelation between sample points. The fundamental concept of Kriging is that it assumes a spatial correlation between the data points which can be used to explain the variation in the spatial surface (ESRI, 2023b). The interpolation gives a statistical measure of accuracy that can be used to improve the fit. The Kriging interpolation workflow within the geostatistical analyst extension is a multi-step process. The extension lets the user investigate suitable interpolation techniques. Subsequent steps include semi-variogram modelling and curve fitting followed by the generation of a prediction surface with cross-validation statistics. The cross-validation step involves a leave-one-out resampling technique that estimates the interpolation errors at the different data points. Initially, all input points are used to estimate the parameters of the interpolation model.

Next, it systematically removes one input point and uses the remaining data points to predict the hidden value. The predicted value is then compared to the actual value. This procedure iterates through all data points and provides statistical measurements of error such as mean values, mean standardised, root-mean-square, root-mean-squared standardised, and average standard (ESRI, 2023d). The interpolation settings and cross-validation statistics for all the raster surfaces are presented in Appendix (2) and Appendix (3).

The TWT raster surface covered SW Scania and nearby offshore areas. A mask was created by merging the digitised RFZ with a coastline feature from the Lantmäteriet terrain map. The resulting mask limits the data processing extent and defines the land area southwest of the STZ where geothermal utilization is feasible. The resulting TWT map is presented in the method chapter as it shows a major step in the time-to-depth conversion (Figure 7).

A TWT value was assigned to each borehole where there was an overlap with a TWT cell using the extract values to point functionally. The raster calculator was then used to calculate the seismic velocity (meters per second) for each borehole. This calculation relied on the depth to the top boundary of the Arnager Greensand and the One-Way-Time (OWT). The OWT represents half of TWT and gives the time taken for an acoustic wave to travel from the surface source to a reflector in the bedrock.

The Geostatistical analyst extension was used to perform a Co-kriging interpolation on the borehole velocity and TWT point datasets. This resulted in a velocity raster which extent is set by the borehole data coverage outlined in Figure (1). Co-kriging is an advanced variant of Kriging interpolation that incorporates multiple variables. It introduces a correlated variable (TWT), also known as a covariate, alongside the primary variable (velocity) to generate an interpolation estimate. This method computes autocorrelation and cross-correlations for each variable, potentially improving the accuracy of the model while introducing the possibility of increased variability (ESRI, 2023c).

The extent of the velocity raster is defined by the borehole data coverage and is smaller in size compared to the TWT raster (Figure 1). Given that the project aimed to produce a stored heat map covering the entire SW Scania; both surfaces needed to match each other in extent and cell size. To achieve this outcome, the velocity raster was extrapolated to the same extent as the TWT raster by configuring the processing extent in the environments pane.

As a final step in the time-to-depth conversion, the depth to the Arnager Greensand top was calculated by multiplying the TWT raster (OWT in seconds) with the velocity raster (meters per second). This resulted in a depth surface to the Arnager Greensand top boundary. The depth values are given with reference to below mean sea level (b.m.s.l).

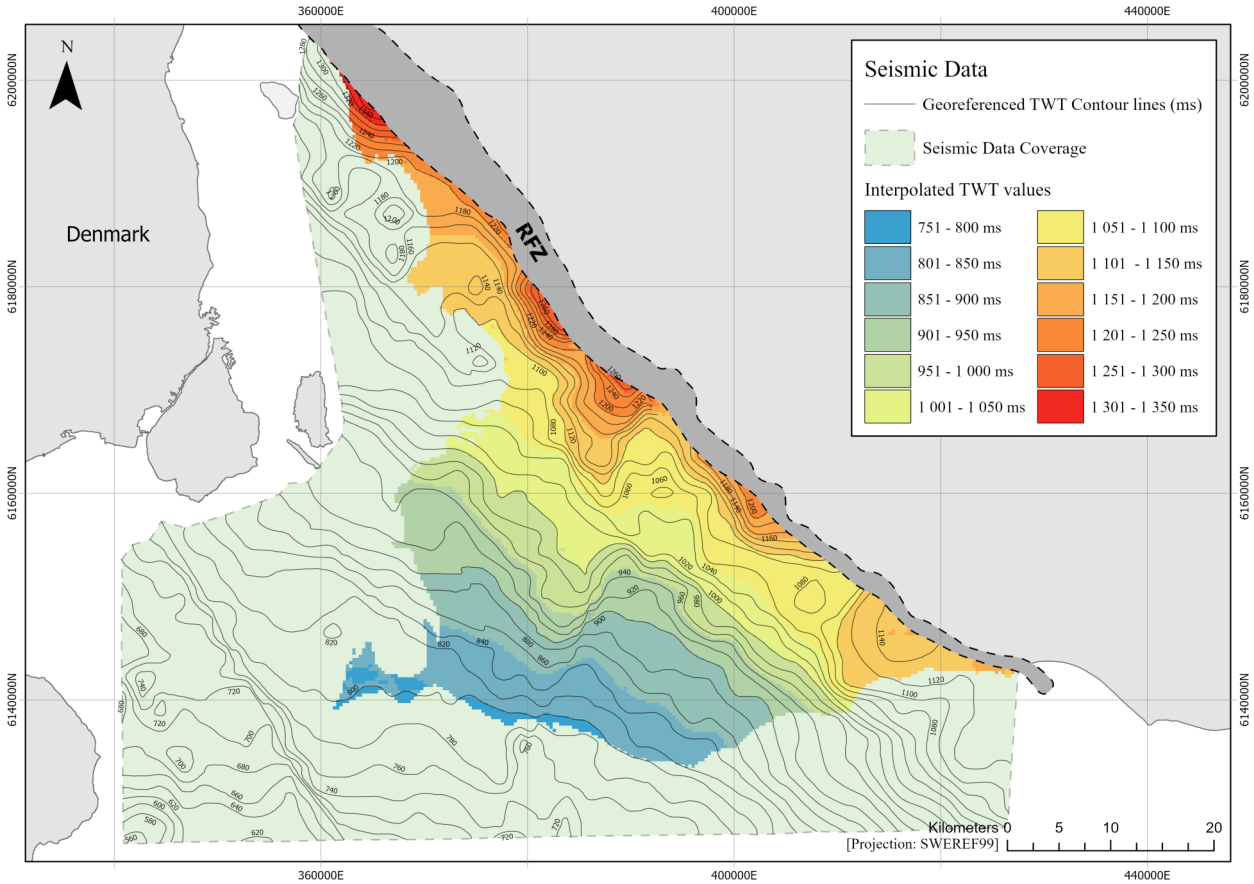

Figure 7. Seismic data map which displays the georeferenced Two-Way-Time (TWT) contour lines derived from the digitization of the blue marker map. The Two-Way-Time raster surface (coloured areas) is interpolated from the point dataset generated from the contour lines. The geothermal resource assessment focuses on the land area southwest of the RFZ corresponding to the highlighted coloured region.

The cell sizes of the TWT and velocity rasters differ because they were generated using different interpolation techniques on separate datasets. The TWT Raster has a resolution of 313 × 313 meters, and the velocity raster has a resolution of 270 × 270 meters. Multiplication of two rasters with different cell sizes in ArcGIS will result in an output that adopts the coarse resolution. A finer resolution was maintained with the snap raster functionality with a convert units cell size projection setting.

3.2.3 Reservoir temperature

A local geothermal gradient was calculated using Equation (7) down to the top boundary of the Arnager Greensand by examining the temperature (BHT) log from the Ljunghusen-1 borehole. The gradient represents a constant temperature increase throughout the entire sedimentary sequence down to the Arnager Greensand top boundary. The geothermal gradient calculation used a mean annual surface temperature of 9 °C (SMHI, 2023). The depth raster was used as input to calculate the reservoir temperature at the top boundary of the Arnager Greensand for each cell over SW Scania. The reservoir temperature was assigned as the T_i parameter in Equation (1) and Equation (3).

3.2.4 Formation thickness estimation

The Geostatistical analyst extension was used to perform a Co-kriging interpolation on the reevaluated borehole thickness data. The thickness was set as the primary variable and the TWT was set as the covariate variable. This resulted in a thickness raster which extent was defined by the borehole data coverage equal to the previous velocity raster (Figure 1). The thickness raster was extrapolated using the same steps as for the velocity raster. A low-pass filter was run in five iterations on the thickness raster. A low-pass filter smooths the data by reducing local variation and removing noise from the interpolation. The filter uses a function that calculates the mean value for the centre cell in a 3 × 3 neighbourhood which reduces the significance of outlier cells (ESRI, 2023a). The thickness surface was assigned as the V_i and V parameter in Equation (1) and Equation (3).

3.2.5 Tabulation of petrophysical properties

The petrophysical data of the Arnager Greensand used in this study include porosity (%), permeability (mD), grain density (kg/m^3), and fluid density (kg/m^3). These petrophysical properties were compiled and basic statistical procedures such as mean and median values were used to assess the variation in each borehole. The parameter overview provided insights into the variability of the petrophysical properties across SW Scania. As outlined in the background chapter, the stored heat equations can be approached in two ways: by accounting for the thermal energy stored in a water-saturated volume of rock or in the rock matrix and fluids separately with a value for the porosity and separate values for the volumetric heat capacities. To account for both approaches, the volumetric heat capacity of the formation fluid and the rock matrix was calculated based on density values and reference values for their respective heat capacities.

3.2.6 Stored Heat calculations

The stored heat calculations considered the two approaches of calculating the stored heat in a water-saturated rock using Equation (1) and in the rock and the fluid separately using Equation (3). The stored heat was calculated on a cell-by-cell basis. A resolution of approximately 270 × 270 meters was maintained for all input rasters. The calculations resulted in a stored heat raster covering SW Scania and two example maps were generated displaying the difference between the two chosen stored heat approaches.

In the ModelBuilder environment in ArcGis, the stored heat equation parameters were evaluated through multiple iteration runs using different input values for the porosity and reference temperature. This was carried out to evaluate the impact the parameters have on the stored heat value. Due to the excessive number of maps that would have resulted, not all iterations are presented in map form. Instead, tables and graphs were produced to display the relationship between the parameters. In addition to this, multiple cases were calculated to evaluate and exemplify the regional difference in stored heat across SW Scania.

There are two ways to present the stored heat. One way is to present the amount of stored heat in a square meter within each cell (J/m^2) and the second way is to present the total amount of stored heat in each cell (Joule). The first way relies on the multiplication with the thickness and the second one with the multiplication with the volume. The volume of a cell is calculated by multiplying the cell size extent with the thickness, for example, a resolution of 270 × 270 meters multiplied by a thickness of 20 meters would result in a volume of 1 458 000 m^3. This volume can be viewed as a voxel cell as it represents a value on a regular grid in 3D space. The volume approach is the only viable approach if a recovery factor is to be applied. The unit derivation of the two ways of representing the stored heat is demonstrated in Equation (9). The parameters are defined the same as in the Equations (1) and (3). The ΔT is the temperature difference between the reservoir temperature and the reference temperature.

$$Q = (J / T \times m^{3)}) \times m \times (\Delta T) = J/m^2$$

$$Q = (J / T \times m^{3)}) \times m^3 \times (\Delta T) = J \qquad \textbf{Equation 9}$$

4 Results

4.1 Borehole Data

The reevaluated depth and thickness data of the Arnager Greensand are presented in Table (3) together with previous depths reported by Sivhed et al. (1999) and Juhlin et al. (2013). The Granvik-1 borehole was assigned a thickness of 55 m as in the nearest Höllviken-1 borehole and the Trelleborg-1 borehole was assigned a thickness of 38 meters as in the nearest Hammarlöv-1 borehole. The thickness interpretations vary between the reevaluated data and the previous estimates. The thickness interpretations differ the most in the Mossheddinge-1, Norrevång-1, Svedala-1, Eskilstorp-1, Maglarp-1, and Smygehuk-1 boreholes. The other boreholes have thickness estimates that are similar to the previous estimates.

Wireline logs from Höllviksnäs-1 and Mosshedinge-1 boreholes are presented in Figure (8). The logs illustrate the contrasting scenarios of straightforward interpretation and difficulty in setting the top and base boundaries for the Arnager Greensand. The Höllviksnäs-1 wireline log shows a clear geophysical signature with a significant change in the spontaneous potential and resistivity over a well-defined interval which is interpreted to be the Arnager Greensand. The interpretation of the Mosshedinge-1 borehole is difficult due to signal distortion and low resolution. A small interval at approximately 1710 meters can be identified as the Arnager Greensand with lower spontaneous potential and varying resistivity. Below this point, there are additional intervals exhibiting fluctuating geophysical signatures.

4.2 Formation depth and Reservoir temperature

The ordinary Kriging interpolation on the TWT point dataset resulted in a TWT raster surface (Figure 7) with a range of 782 – 1342 (rounded to the nearest whole number) milliseconds (ms). The surface is characterised by an overall spatial pattern of increased TWT towards the RFZ. The highest values are observed in the northwest near the city of Landskrona next to the RFZ while high values are also observed along the RFZ. The lowest values are observed in the south on the Falsterbo Peninsula while low values are also observed over the southern parts of the Skurup Platform. The Svedala Fault is a clear geological feature in the centre-most part of the map with a distinct bending flexure pattern. The cell size of the raster is approximately 313 × 313 meters (rounded to the nearest whole number). The raster is visualised with a defined interval classification of 50 ms which yields 12 colour classes.

4.3 Regional thickness estimation

The Co-kriging interpolation on the reevaluated thickness data and the following low-pass filtering resulted in a thickness raster surface between 11 and 56 meters (Figure 12). The surface is characterised by an overall spatial pattern of decreasing thickness towards the RFZ. The greatest thickness is observed over the Falsterbo Peninsula and the lowest is adjacent to the RFZ. The thickness increases locally surrounding the Norrevång-1 borehole and decreases surrounding the Mosshedinge-1 borehole. The raster is visualised with a defined interval classification of 3 meters which yielded 16 colour classes. A comparison between the reevaluated thickness and depth values with the modelled thickness and depth values for each borehole is provided in Appendix (4) wherein a cross plot is presented which shows the relationship between the TWT and thickness values in every borehole.

Table 3. Reevaluated top and base boundaries for the Arnager Greensand, along with the corresponding reevaluated thickness estimates. The previous estimates are obtained from Sivhed et al. (1999) (1) and Juhlin et al. (2013) (2). The table is structured so that the boreholes follow a general north-to-south direction in SW Scania. The total depths of the boreholes are taken from Erlström et al. (2018). The NoData text means that there were no available data for the specific borehole at the time because it had not been drilled or it was not reported in the source data. The Granvik-1 and Trelleborg-1 were assigned a thickness from the nearest boreholes (3).

Borehole	Total depth (b.m.s.l)	Reevaluated Top Boundary (b.m.s.l)	Reevaluated Base Boundary (b.m.s.l)	Reevaluated Thickness (m)	Previous Thickness data (1)	Previous Thickness data (2)
Norrevång-1	2127	1768	1792	24	24	36
Barsebäck-1	2255	1743	1760	17	17	17
Mossheddinge-1	1785	1675	1686	11	No Data	56
FFC-1	2100	1605	1632	27	No Data	27
Magreteholm-1	2677	1601	1629	28	No Data	No Data
Svedala-1	1628	1435	1459	24	24	43
Eskilstorp-1	2463	1353	1381	28	35	35
Håslöv-1	2554	1306	1342	36	37	37
Kungstorp-1	2066	1274	1321	47	47	47
Höllviken-1	1411	1226	1281	55 (3)	51	55
Granvik-1	1254	1245	Unknown	55 (3)	Unknown	Unknown
Maglarp-1	1938	1232	1279	47	48	32
Hammarlöv-1	2369	1204	1242	38 (3)	42	42
Trelleborg-1	1201	1200	Unknown	38 (3)	Unknown	Unknown
Höllviksnäs-1	2605	1190	1242	52	52	52
Höllviken-2	1919	1187	1241	54	55	54
Ljunghusen-1	2276	1182	1230	48	48	48
Smygehuk-1	1660	1071	1117	46	52	57

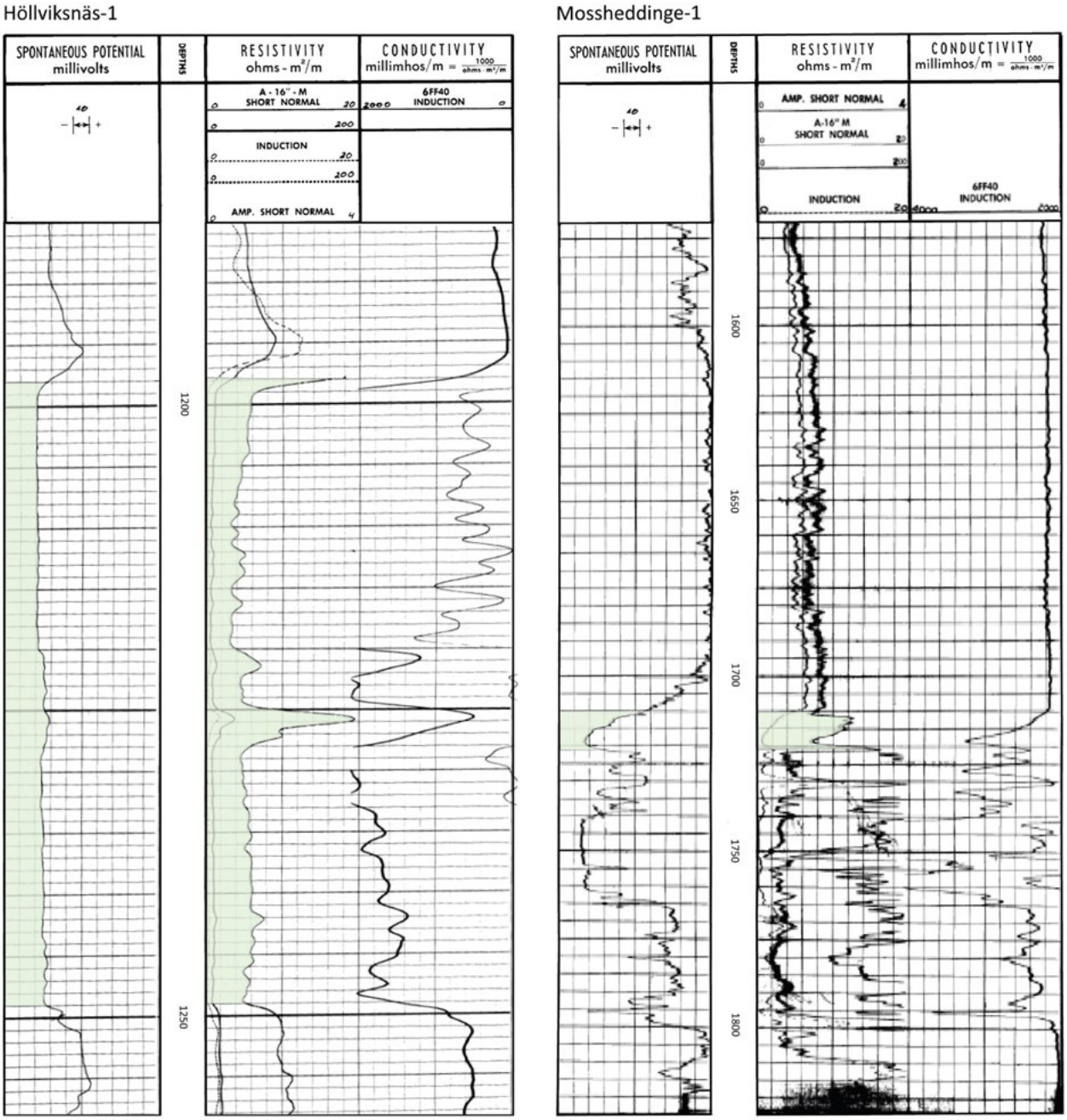

Figure 8. Modified geophysical wireline logs from the Höllviksnäs-1 and Mossheddinge-1 boreholes with the interpreted intervals of the Arnager Greensand marked in green. The logs illustrate the contrasting scenarios of straightforward interpretation in the case of Höllviksnäs-1 and difficulty in the case of Mossheddinge-1 in setting the top and base boundaries for the Arnager Greensand. The logs have been enhanced to improve their visual representation and readability. The depth scale varies between the logs. The logs were retrieved from the SGU geoarchive.

4.4 Petrophysical properties of the Arnager Greensand

The petrophysical properties of the Arnager Greensand are summarized in Table (4). The average and median porosity values are consistent between the boreholes except for a decrease in the Höllviken-1 and FFC-1 boreholes. There are significant differences in permeability between the boreholes, with Maglarp-1 exhibiting extremely high permeability values and FFC-1 displaying lower permeability. The average grain density is consistent between the boreholes except for an increase in the Höllviken-1 borehole. Based on these petrophysical properties the volumetric heat capacities for the rock matrix and the reservoir fluid were calculated using Equation (10). The suggested volumetric heat capacity constant 2.5×10^6 J/C m^3 for a fluid-saturated rock is also presented for comparison.

The specific heat capacity of the reservoir fluid is set to 4180 J/kg K corresponding to the specific heat capacity of fresh water. Given that the formation fluid is saline it is expected that this value should be a lower unknown value as it contains dissolved salts that reduce the amount of heat that can be absorbed by the water. The reservoir fluid was assigned a density value of 1.116 kg/m^3. This is the only reported fluid density

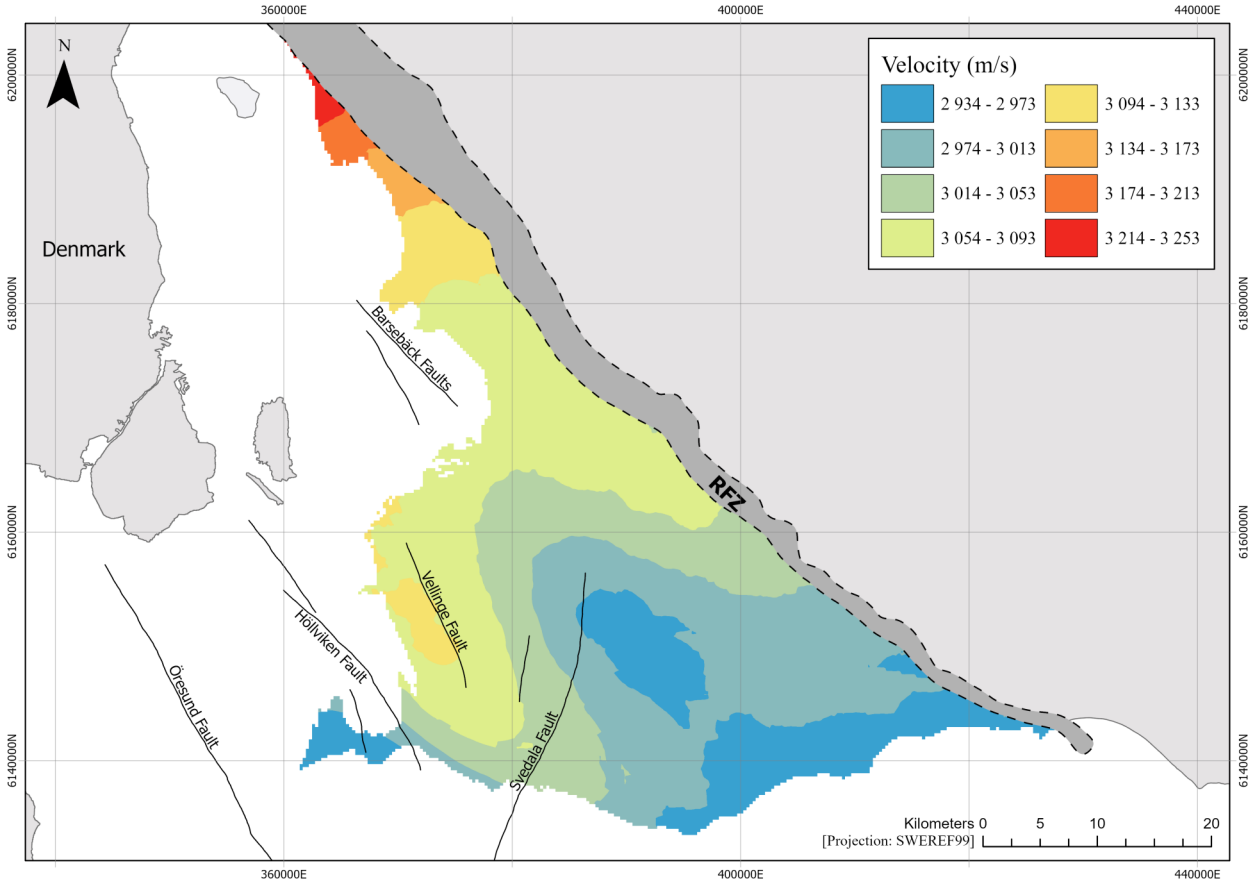

Figure 9. Map of SW Scania which displays the average velocity in meters per second (m/s) down to the Arnager Greensand. The velocity raster was generated by Co-Kriging interpolation techniques using borehole depth data (meters below mean sea level) and two-way-time (ms) values obtained from the respective boreholes. The map highlights the subsurface velocity variations in the region.

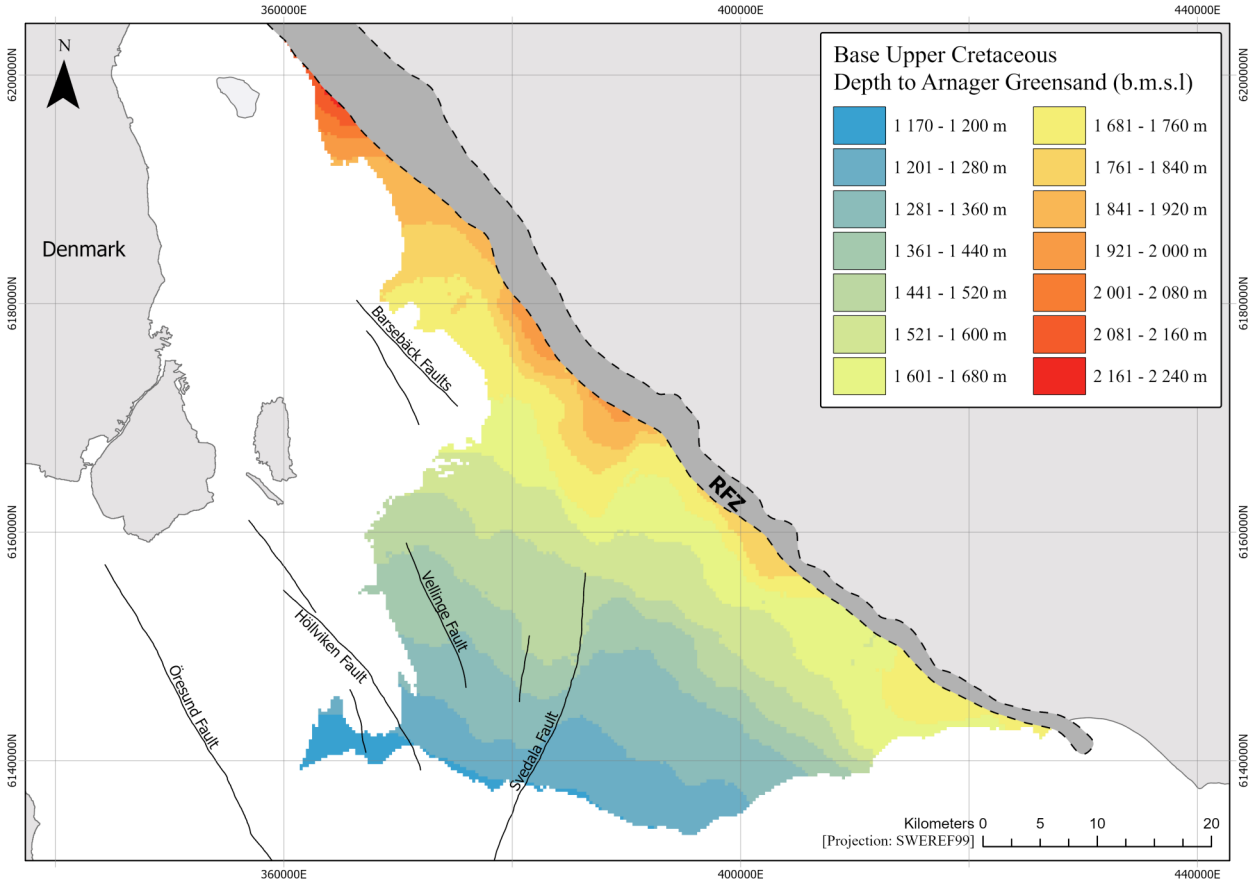

Figure 10. Depth map to the Arnager Greensand top boundary. The map displays the depth (below mean sea level) to the Base Upper Cretaceous boundary which is the boundary between the Arnager Greensand and the Arnager Limestone. The surface was generated by multiplying the velocity and TWT input surfaces acquired from the time-to-depth conversion methodology.

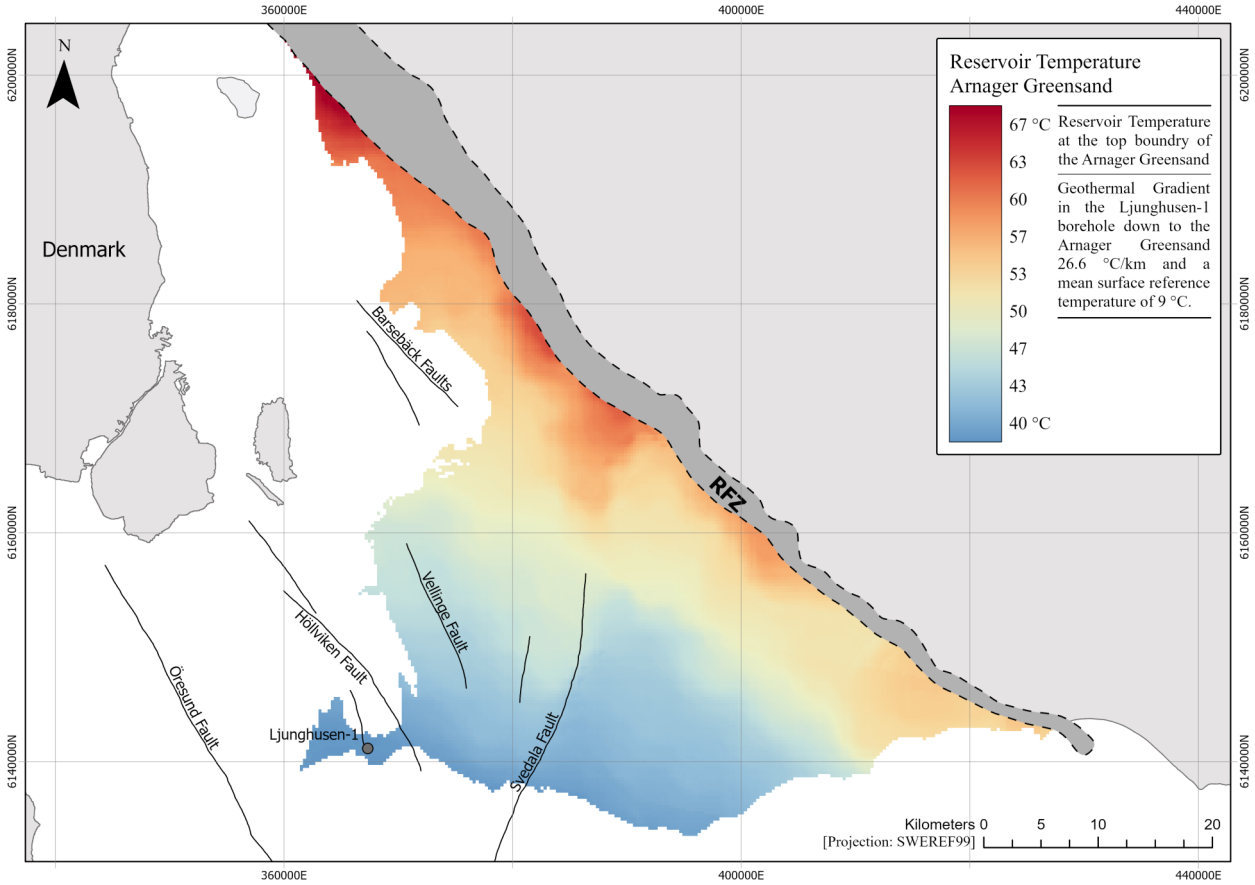

Figure 11. Reservoir temperature map which displays the temperature at the top boundary of the Arnager Greensand. The raster surface was created by applying a regional uniform gradient of 26.6 °C per kilometre with a mean surface reference temperature of 9 °C.

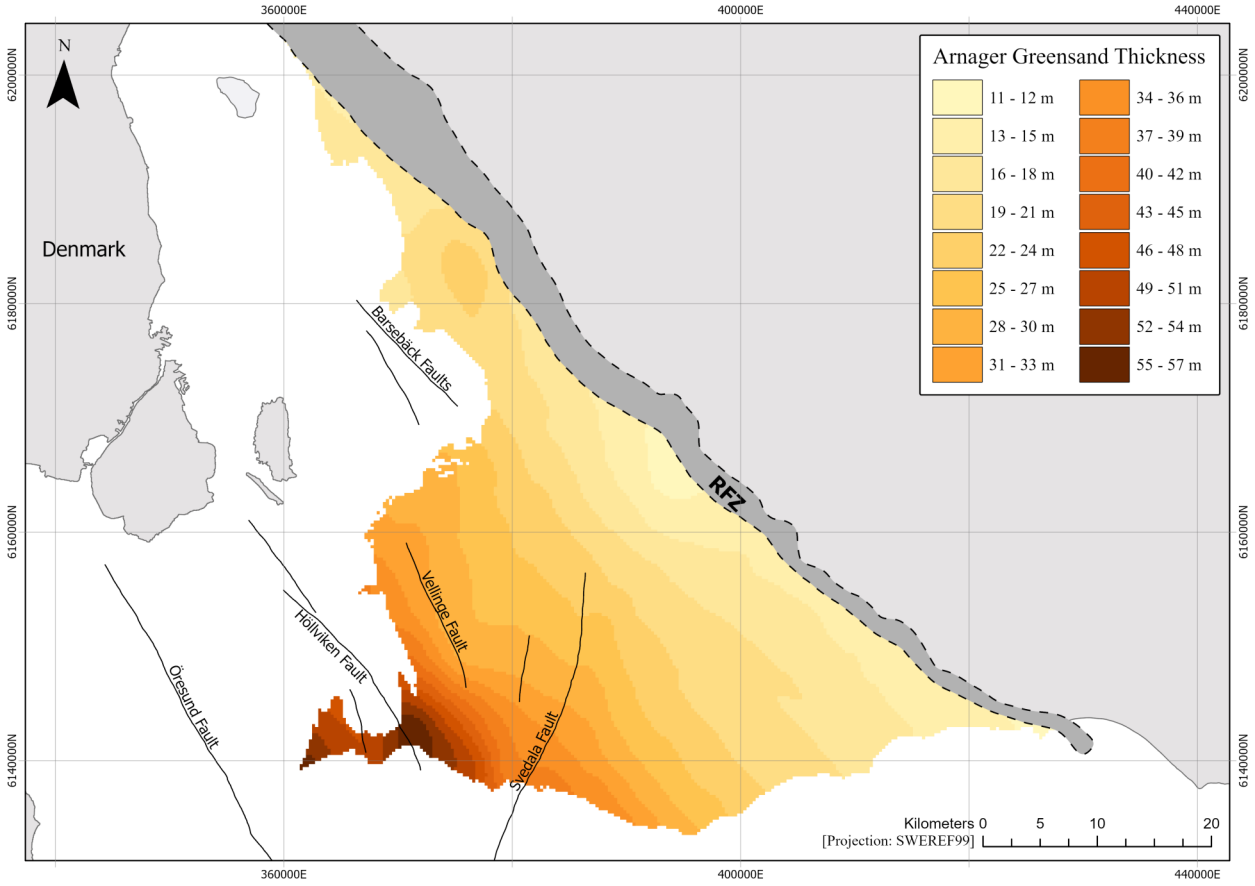

Figure 12. Thickness map of the Arnager Greensand which displays an estimated thickness (m) over SW Scania. The surface was generated with Co-Kriging interpolation techniques using the thickness data from the boreholes (m) and two-way-time values (ms).

data of the Arnager Greensand measured in the Trelleborg-1 borehole (Juhlin et al., 2013). The specific heat capacity of the rock matrix is set to 800 J/kg K (Robertson, 1988). This value was also used in the geothermal assessment study of the Lund Sandstone by Erlström and Rosberg (2022) which allows for a better comparison between the studies on a regional basis. The rock matrix was assigned a density value of 2688 kg/m^3 based on the average grain density in all boreholes (Table 4).

4.5 Stored Heat (Heat-In-Place) maps

The stored heat calculations resulted in several stored heat raster surfaces and model outputs. The calculations yield a large number in the range of 1×10^9 expressed as GJ/m^2. Two maps exemplify the two approaches to the stored heat method. The first one considers the stored heat in the water-saturated rock using the suggested volumetric heat capacity constant of 2.5×10^6 J/C m^3 for a water-saturated rock (Figure 13). The second one considers both the heat stored in the rock matrix and fluid separately using the calculated volumetric heat capacities in Equation (10) (Figure 14).

The stored heat calculation (Equation 1) with a value of 2.5×10^6 J/C m^3 for the volumetric heat capacity of a water-saturated rock and a reference temperature of 9 °C corresponding to the average annual temperature in Scania (SMHI, 2023) resulted in stored heat raster surface with a range of 1.25 – 4.53 GJ/m^2 (Figure 13). The mean stored heat value of the Arnager Greensand over SW Scania for the map case is 2.27 GJ/m^2. When considering the volume approach (Equation 9) this amounts to a total of 3.27×10^{18} J (3270 PJ) stored in the Arnager Greensand in SW Scania. The highest stored heat values are observed over the Falsterbo Peninsula and the lowest values are observed over the Skurup Platform adjacent to the RFZ. A local increase in stored heat is observed surrounding the Norrevång-1 borehole and a local decrease in stored heat is observed surrounding the Mossheddinge -1 borehole. The raster is visualised with a defined interval classification of 3×10^8 which gives 12 colour classes. The maximum and minimum classes are adjusted. The histogram for the stored heat raster surface is presented in Appendix (5).

The stored heat calculation (Equation 3) using the calculated volumetric heat capacities of the rock matrix and reservoir fluid (Equation 10), a set porosity of 24 % corresponding to the average porosity of the Arnager Greensand (Table 4), and a reference temperature of 9 °C resulted in a stored heat raster surface (Figure 14) with a range of 1.37 – 4.99 GJ/m^2. The mean stored heat value in this map case is 2.5 GJ/m^2. This amounts to a total of 3.61×10^{18} (3610 PJ) stored in the Arnager Greensand reservoir in SW Scania. The surface follows the approximate spatial patterns as the previous map but has an overall higher stored heat. The raster is visualised with a defined interval classification of 3.5×10^8 which gives 12 colour classes. The maximum and minimum classes are adjusted. The histogram for the stored heat raster surface considering porosity is presented in Appendix (5).

The total stored heat (Joule) over SW Scania was examined by varying the parameters in the stored heat equations. The presented graphs highlight the variations in stored heat across a range of reference temperatures and porosity values (Figure 15 and Figure 16). The raw data for these graphs is presented in Appendix (6). The graphs only display the stored heat in the rock matrix and the reservoir fluids and do not consider the stored heat associated with the heat capacity of a water -saturated rock which instead is presented in Appendix (6). Figure (15) shows the variation in stored heat by adjusting the formation porosity within a range of 4 – 32 % with a set reference temperature of 9 °C. These porosity values are based on actual measurements of the Arnager Greensand porosity. A porosity value of zero implies that the stored heat in the reservoir fluid is not considered. The graph highlights the relationship between the increased stored heat with a higher porosity. A porosity value of 24 % corresponds to the map in Figure (14). Figure (16) shows the variation in stored heat by adjusting the reference temperature within a range of 4 – 30 °C with a set porosity of 24 %. A reference temperature of 4 °C corresponds to the reinjection temperature applied in the Lund geothermal plant. The graph highlights the relationship between de-

Table 4. Petrophysical properties of the Arnager Greensand in the SW Scanian boreholes. The table provides average and mean values for the petrophysical properties, including porosity, permeability, and grain density. The subscript value shows the number of samples (sample size) from which the average and mean values are calculated. The samples were taken from different stratigraphic intervals where the Arnager Greensand was encountered.

Borehole	Average Porosity (%)	Median Porosity (%)	Average Permeability (mD)	Median Permeability (mD)	Average Grain density (kg/m^3)	Median Grain density (kg/m^3)
Svedala-1	25.7 $^{(15)}$	28.0	111.2 $^{(15)}$	27.0	2680 $^{(10)}$	2673
Trelleborg-1	23.6 $^{(4)}$	26.3	868.3 $^{(4)}$	788.5	2633 $^{(3)}$	2633
Maglarp-1	26.3 $^{(6)}$	26.5	1186.0 $^{(5)}$	1126.0	2632 $^{(6)}$	2633
Höllviken-1	24.7 $^{(32)}$	27.1	228.0 $^{(33)}$	88.0	2710 $^{(28)}$	2689
Höllviken-2	17.2 $^{(5)}$	13.6	429.9 $^{(5)}$	1.8	No data	No data
FFC-1	19.4 $^{(2)}$	19.4	28.4 $^{(2)}$	28.4	2666 $^{(2)}$	2666
All boreholes	24.3 $^{(64)}$	26.6	325.0 $^{(64)}$	65.5	2688 $^{(49)}$	2674

Rock matrix Volumetric heat capacity = 800 (J/kg C) × 2688 (kg/m^3) ≈ 2.15×10^6 (J/C m^3)

Fluid Volumetric heat capacity = 4180 (J/kg C) × 1116 (kg/m^3) ≈ 4.66×10^6 (J/C m^3)

Volumetric heat capacity of a water-saturated rock = 2.50×10^6 (J/C m^3) (Ciriaco et al., 2020) **Equation 10**

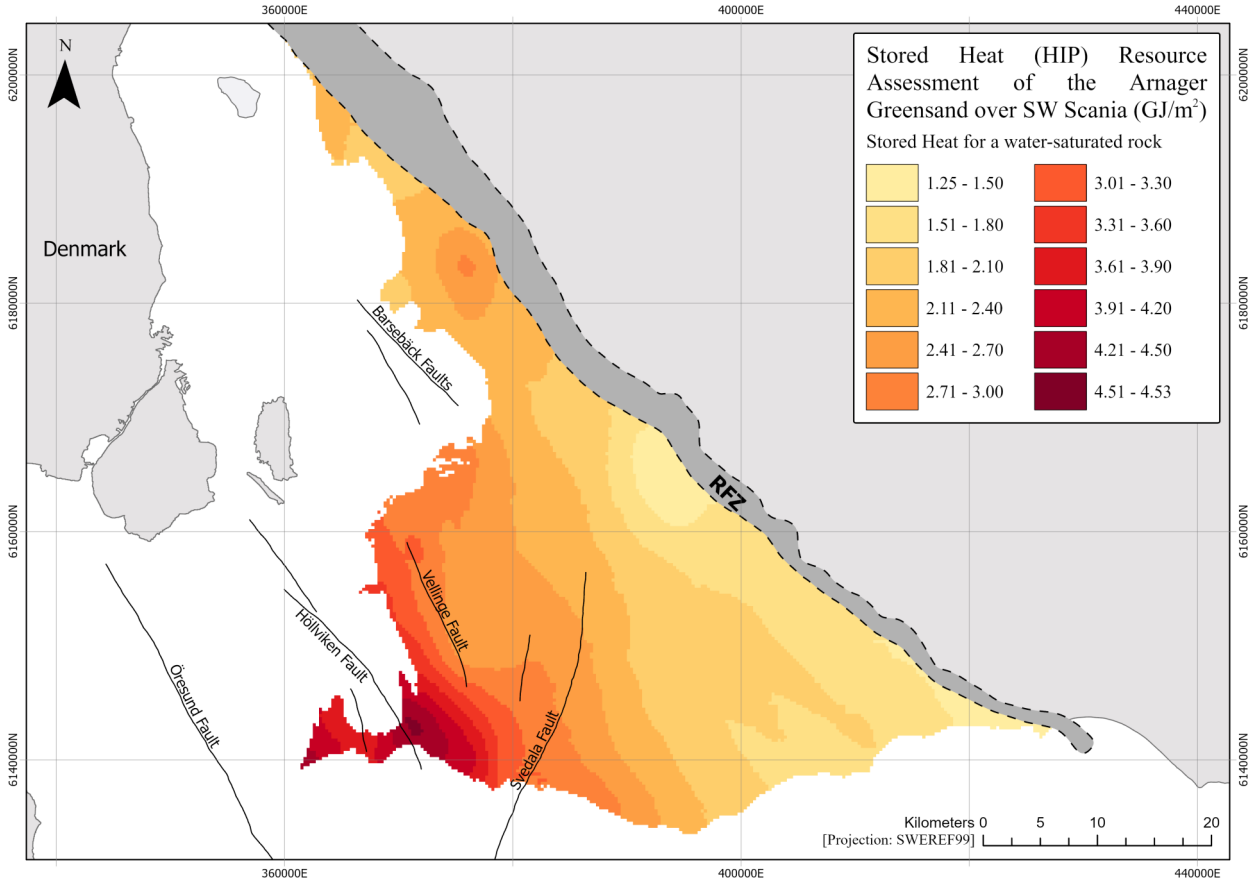

Figure 13. Stored heat (Heat-In-Place) map which displays the estimated amount of heat (GJ/m^2) contained in the Arnager Greensand over SW Scania The stored heat values range from 1.25 – 4.53 GJ/m^2 considering the energy stored in a water-saturated rock using a reference value for the volumetric heat capacity.

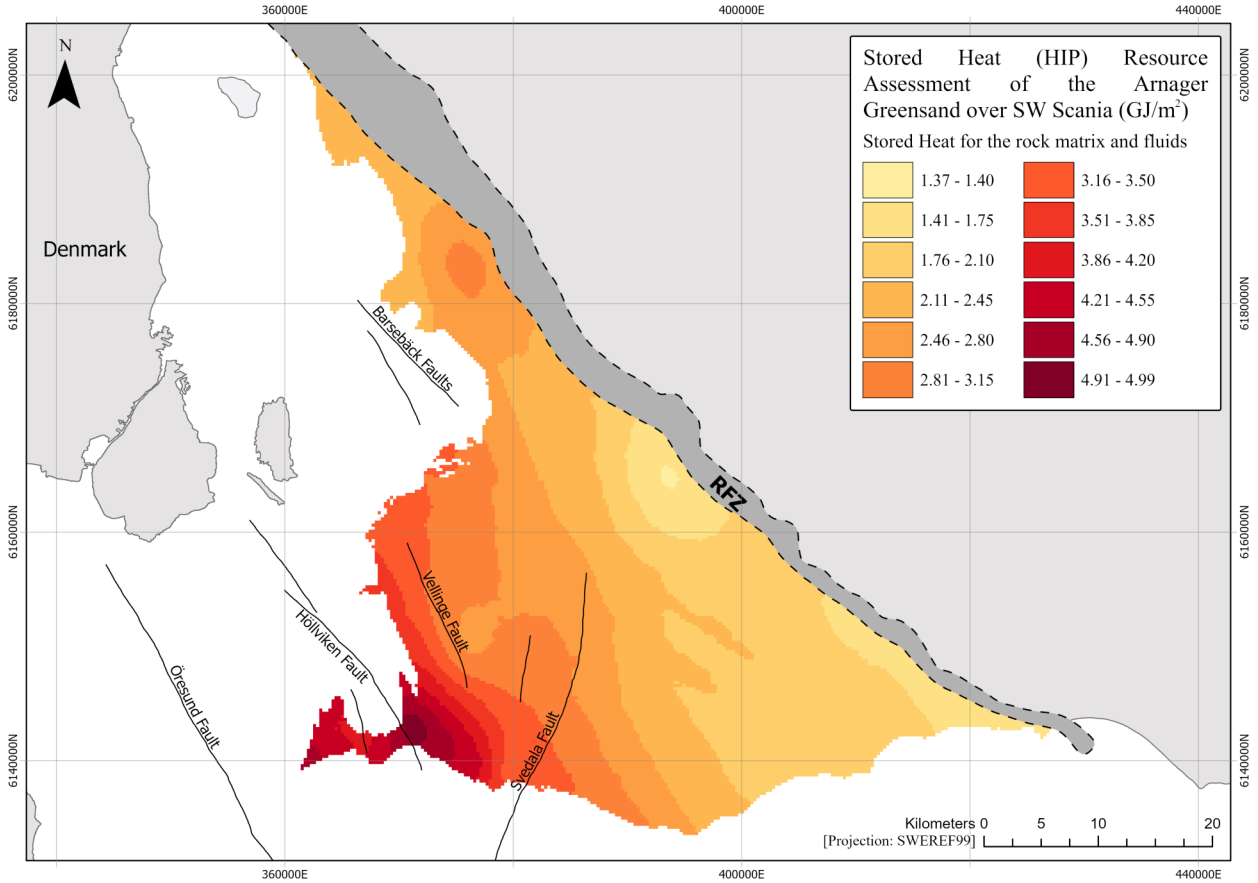

Figure 14. Stored heat (Heat-In-Place) map which displays the estimated amount of heat (GJ/m^2) contained in the Arnager Greensand over SW Scania. The stored heat values range from 1.37 – 4.99 GJ/m^2 considering the energy stored in both the rock matrix and the reservoir fluids.

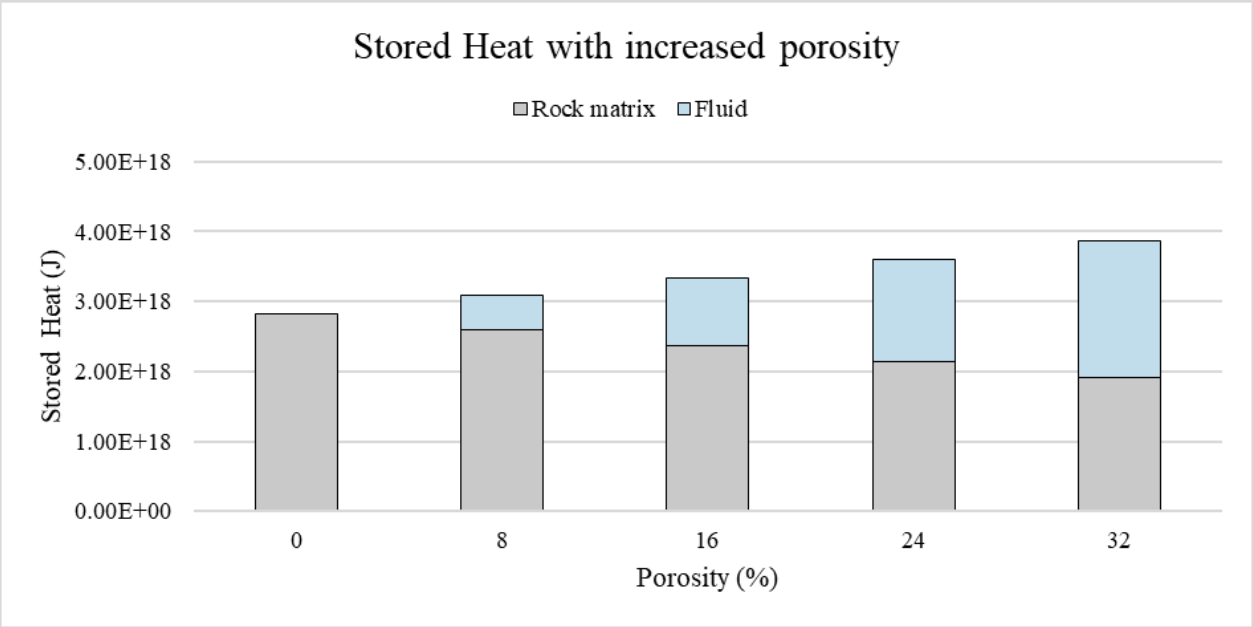

Figure 15. The total stored heat (J) in the Arnager Greensand in SW Scania. The graph displays the stored heat in the rock matrix and the fluids with different values for the porosity. The porosity range is set according to measured porosity values of the Arnager Greensand.

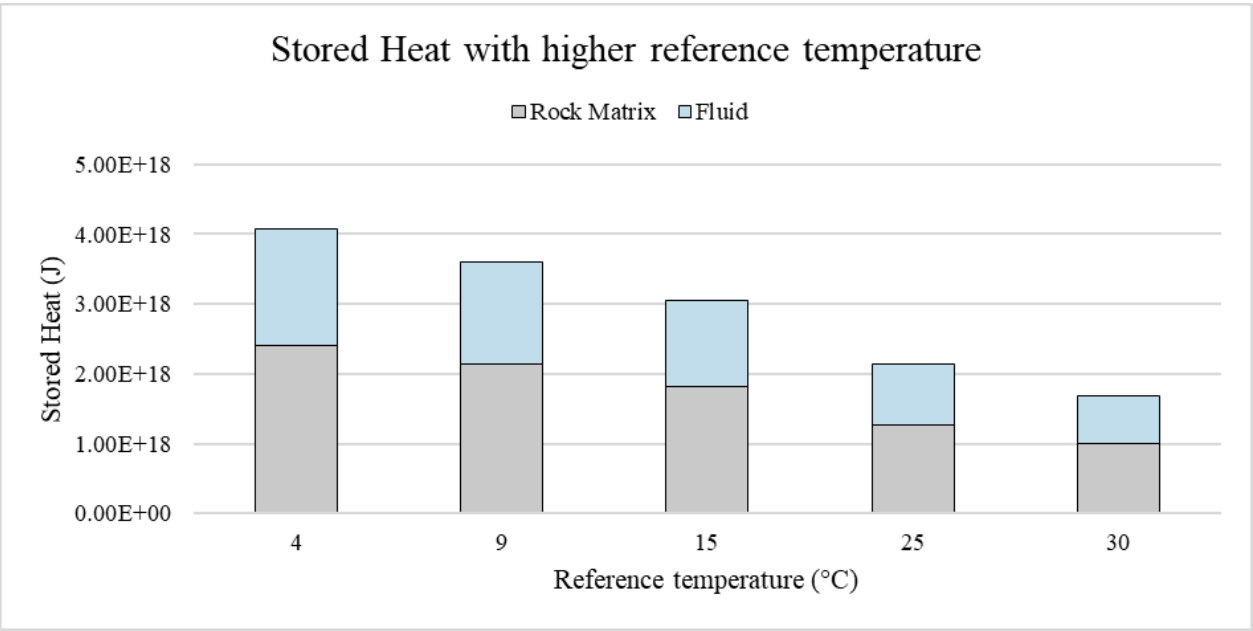

Figure 16. The total stored heat (J) in the Arnager Greensand in SW Scania. The graph displays the stored heat in the rock matrix and the fluid with different values for the reference temperature. The temperature range is set according to commonly used reference temperatures. A reference temperature of 4 °C corresponds to the reinjection temperature of the Lund geothermal plant.

creased stored heat with increasing reference temperature. A reference temperature of 9 °C corresponds to the map in Figure (14).

4.6 Stored Heat case studies

A few different cases with various reservoir properties and resulting stored heat values are presented in Table (5). Each case represents a location in SW Scania corresponding to a specific borehole. The Falsterbo region (Case 1) is based on average porosity data from the Höllviken-1 borehole, the Malmö region (Case 2) from the FFC-1 borehole, the Svedala region (Case 3) from the Svedala-1 borehole, and the Barsebäck region (Case 4) from the Barsebäck-1 borehole. The porosity values reflect a decrease in porosity closer to the RFZ. The reservoir temperature and thickness were taken from the modelled surfaces. The results describe the stored heat and the extractable amount of heat for a hypothetical reservoir volume. The hypothetical reservoir area was set as 1×10^6 m^2 as it considers a possible Influence area of a discharge well related to a common well spacing standard of 1000 – 1500 meters in a well-doublet system (Lopez et al., 2010; Willems et al., 2017; de Bruijn et al., 2021).

Table 5. Input parameters for different case calculations of the stored heat of the Arnager Greensand. The cases exemplify the stored heat at various locations in SW Scania based on borehole data. The Falsterbo region (Case 1) is based on average porosity data from the Höllviken-1 borehole, the Malmö region from the FFC-1 borehole, the Svedala region from the Svedala-1 borehole, and the Barsebäck region from the Barsebäck-1 borehole. The applied recovery factor on the total stored heat is 1/3.

Parameter		Case 1 Falsterbo	Case 2 Malmö	Case 3 Svedala	Case 4 Barsebäck
Thickness	m	55	27	24	17
Cell Surface extent	m^2	72900	72900	72900	72900
Hypothetical Surface extent	m^2	1.00E+06	1.00E+06	1.00E+06	1.00E+06
Cell Reservoir Volume	m^3	4.01E+06	1.97E+06	1.75E+06	1.24E+06
Hypothetical Reservoir Volume	m^3	5.50E+07	2.70E+07	2.40E+07	1.70E+07
Porosity	%	0.25	0.19	0.26	0.12
Top boundary reservoir temperature (model output)	°C	42	52	47	56
Reference temperature	°C	9	9	9	9
Density rock matrix	kg/m^3	2688	2688	2688	2688
Specific heat capacity rock matrix	J/kg °C	800	800	800	800
Volumetric heat capacity rock matrix	J/m³ °C	2.15E+06	2.15E+06	2.15E+06	2.15E+06
Density fluids	kg/m^3	1116	1116	1116	1116
Specific heat capacity fluids	J/kg °C	4180	4180	4180	4180
Volumetric heat capacity fluids	J/m³ °C	4.66E+06	4.66E+06	4.66E+06	4.66E+06
Volumetric heat capacity of water-saturated rock	J/m³ °C	2.50E+06	2.50E+06	2.50E+06	2.50E+06
Stored Heat	J/m^2	4.54E+09	2.90E+09	2.28E+09	2.00E+09
Stored Heat with porosity	J/m^2	5.04E+09	3.05E+09	2.56E+09	1.96E+09
Total Stored Heat	J	4.54E+15	2.90E+15	2.28E+15	2.00E+15
Total Stored Heat with porosity	J	5.04E+15	3.05E+15	2.56E+15	1.96E+15
Extractable amount of heat (R = 0.33)	J	1.50E+15	9.58E+14	7.52E+14	6.59E+14
Extractable amount of heat with porosity (R = 0.33)	J	1.66E+15	1.01 E+15	8.44 E+14	6.47E+14

5 Discussion

5.1 Geothermal resource assessment of the Arnager Greensand

The stored heat values presented in the results describe the geothermal potential of the Arnager Greensand aquifer in SW Scania for a variety of outcomes by setting the stored heat parameters differently. A higher stored heat value corresponds to greater geothermal potential of that area. This study has opted to use two variations of the stored heat method. The first one considers the stored heat in a water-saturated rock, while the second one considers the stored heat in the rock matrix and reservoir fluids separately. This is in line with the objective of this project to evaluate the stored heat method.

The two main geothermal assessments of the Arnager Greensand are presented as maps in Figure (13) and Figure (14). The first assessment considers a reference value for the volumetric heat capacity of a water-saturated rock which gives stored heat values in the range of 1.25 – 4.53 GJ/m^2. This corresponds to a total of 3.27×10^{18} (3270 PJ) stored in the Arnager Greensand over SW Scania. The first assessment is considered a conservative estimate compared to the range of 1.37 – 4.99 GJ/m^2 which results when considering the stored heat in the rock matrix and the reservoir fluids separately. The second assessment corresponds to a total of 3.61×10^{18} (3610 PJ) stored in the Arnager Greensand over SW Scania.

The most promising areas for future geothermal development of the Arnager Greensand as indicated by the stored heat maps are found in the southern parts of SW Scania over the Falsterbo Peninsula. The Falsterbo area exhibits the highest stored heat values which ranges between 3.0 – 4.5 GJ/m^2 for the conservative estimate. There is a gradual decrease of stored heat between the Falsterbo Peninsula and the city of Malmö (Vellinge Fault as location reference). This zone shows relatively increased stored heat values in the range of 2.5 – 3.2 GJ/m^2. The city of Trelleborg similarly displays increased stored heat values. This transitional zone presents opportunities for future geothermal investigations and the potential exploitation of the Arnager Greensand for direct-use applications. The proximity of urban and industrial areas over this zone increases the feasibility of a well-doublet system and integrating it to a district heating system.

Since this is the first-ever geothermal assessment of the Arnager Greensand that considers spatial variability there are no previous estimations to compare the results against. However, its significance can be evaluated by comparing the results with other geothermal assessments conducted in similar geological settings (Figure 17). The Triassic and Jurassic reservoirs in the

Danish Basin, specifically the Frederikshavn, Haldager, Gassum, and Bunter/Skagerrak reservoirs, have stored heat values ranging 10 – 30 GJ/m². However, there are localized areas within these reservoirs where the stored heat can be as high as 30 – 70 GJ/m², and a few exceptional areas with extremely high stored heat values ranging 70 – 110 GJ/m² (Balling et al., 2019). The Lund Sandstone situated at a depth of 640 – 800 meters in SW Scania has a stored heat range of 5 – 8 GJ/m^2 (Erlström & Rosberg, 2022). These above comparisons underscore the stored heat range one can anticipate within the same regional basin system, which includes both the Danish and Öresund Basins, and the Lund Sandstone and Arnager Greensand in SW Scania.

In a European context, the Arnager Greensand stored heat values are similar to those reported for Mesozoic sandstone reservoirs in the North German Basin. These reservoirs have stored heat values ranging from 0 - 3.7 GJ/m^2 and 0 – 4.8 GJ/m^2 considering two temperature models (Frick et al., 2022). The stored heat values are lower compared to the 7.0 GJ/m^2 reported for the Dogger Limestone aquifer. The Dogger Limestone aquifer is situated at a depth of 1500 to 2000 meters in the Paris Basin and features temperatures ranging from 55 – 80 °C (Lopez et al., 2010). The values are also considerably lower compared to a value of 25 GJ/m^2 reported for a Lower Cretaceous aquifer in the Lisbon region at a depth of 1350 meters (Marrero-Diaz et al., 2015). Additionally, the clastic Triassic reservoir in the Upper Rhine Graben at a depth of 2000 meters in France reports a stored heat range of 15 – 30 GJ/m^2 (Dezayes et al., 2008). In summary, when compared to similar geothermal aquifers in Europe, the Arnager Greensand demonstrates comparatively lower stored heat values. This emphasizes the limited potential of the Arnager Greensand to be used as a geothermal resource for direct-use purposes.

Several of these reservoirs above are located at greater depths compared to the Arnager Greensand and many of them have a greater thickness which gives them a much higher stored heat value. Furthermore, the assessment studies may set the stored heat parameters differently, including the reference temperature, as well as the volumetric specific heat and porosity. This is an inherent flaw of the stored heat method. While it may initially appear straightforward to compare the stored heat between different assessment studies, the variation in how the parameters is set makes for a difficult comparison. For example, Calcagno et al. (2014) used a reinjection temperature (reference temperature) of 30 °C and Frick et al. (2022) used a reinjection temperature of 8 °C in their geothermal assessment study.

In geothermal assessments a common approach is to present a stored heat range covering a larger regional area (Kramers et al., 2012; Pluymaekers et al., 2012), while others focus their efforts on a smaller area where the geothermal potential is greater (Marrero-Diaz et al., 2015). Certain studies also opt to present a representative single value for the whole region (Lopez et al., 2010). Additionally, some studies delineate the research area by only accounting for the stored heat that exceeds a certain threshold, for example to only consider areas where the reservoir thickness is greater than 15 meters (Balling et al., 2019). These various approaches to modelling the stored heat can yield either a broad or a narrow range of values, while also accounting for both non-zero and zero values (Figure 17).

5.2 Extractable amount of heat

The conservative estimate of 3270 PJ stored in the Arnager Greensand corresponds to a extractable amount of heat of 654 PJ when considering a recovery factor of 1/5 for sediment-hosted reservoirs proposed by Williams et al. (2008). Another approach is to consider a recovery factor of 1/3 proposed by Lavigne (1977) which results in 1079 PJ for the extractable amount of heat. To put these numbers into perspective, the urban areas of Landskrona, Lund, Staffanstorp, Bjärred, and Lomma in SW Scania consume approximately 4 PJ/year in its district heating system (Ottosson, 2022, as cited in Erlström & Rosberg, 2022). This means that the Arnager Greensand aquifer amounts to about two hundred years of heat consumption. However, a direct comparison between these values is not practical as the total stored heat value is for the entire SW Scania region, whereas Landskrona, Lund, Staffanstorp, Bjärred, and Lomma constitute only a small part of it. Nonetheless, this comparison helps to better understand the size of the resource and how much of the stored heat that can be extracted at the wellhead in the form of actual retrievable energy which in turn can be used for direct-use applications.

Another perspective on the extractable amount of heat is to consider separate geohydrological units beneath existing boreholes. By considering a bigger reservoir volume, which hypothetically could match a potential influence area of a well-doublet system, in comparison to the volume derived from the cell extent in the eled maps, it is possible to calculate the extractable amount of heat relative to the set volume. This approach is considered in Table (5) for the borehole case studies. The greatest extractable amount of heat is observed in case 1 over the Falsterbo Peninsula and the lowest in case 4 over the Barsebäck Platform. The four case studies are limited to the western parts of SW Scania where there is a gradual decrease in the extractable amount of heat towards the RFZ.

This approach can be expanded further to delineate a boundary condition for the geothermal reservoir in different parts of SW Scania. The chosen extent could for example depend on the potential influence area of several production and reinjection wells. However, determining representative values for such extensive areas presents difficulties due to the spatial nature of the stored heat parameters To exemplify this, a representative stored heat range for the Lund, Staffanstorp, Bjärred, and Lomma area is 2.0 – 2.3 GJ/m^2. Considering a 25 km^2 area between these urban areas, and assuming reservoir properties like those observed in the Barsebäck case (Table 5), which aligns closely to the modelled geothermal parameters in this specific area, the amount of stored heat would amount to roughly 50 PJ and an extractable amount of heat of 17 PJ. This shows that the stored heat is considerably lower in the north-west part of SW Scania, in contrast to the higher stored heat values that would result with the same boundary conditions over the Falsterbo Peninsula.

The fraction of extractable amount of heat ex-

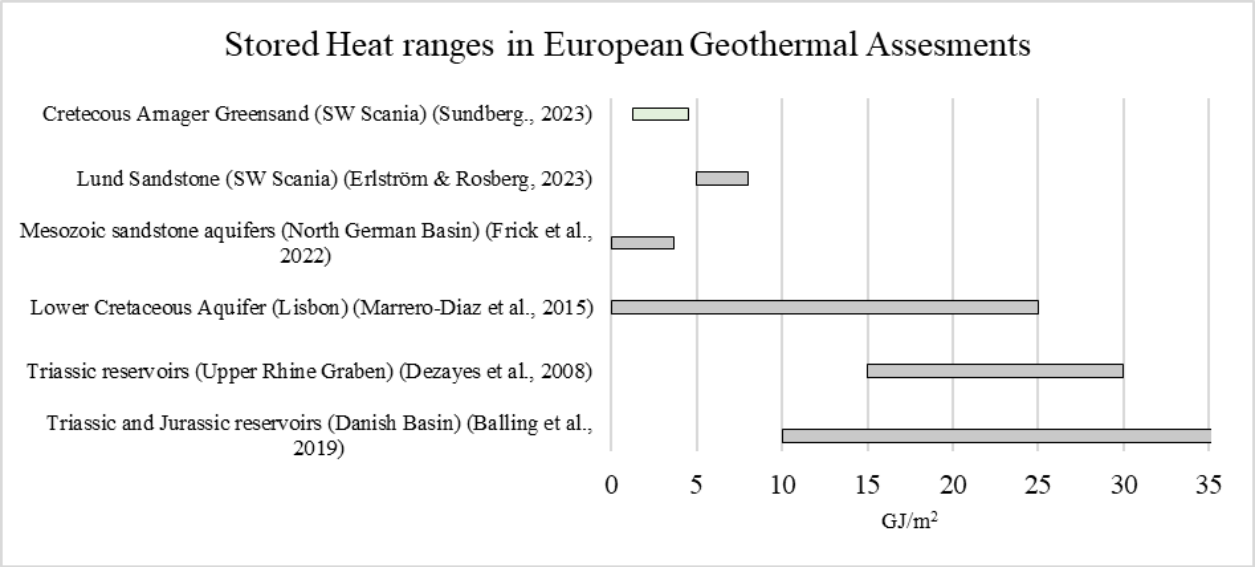

Figure 17. The graph presents a comparison of stored heat ranges from various geothermal assessment studies in Europe and highlights the varying stored heat ranges. These variations primarily stem from the unique geothermal characteristics of each reservoir, encompassing primarily the thickness and temperature conditions. Additionally, the stored heat ranges are influenced by the scale of the assessment, whether it examines a broader regional area with a wider range for the reservoir properties or a more localized area with greater geothermal potential. The ranges can also be influenced by whether the assessment defines the modelled area to exclusively include stored heat values surpassing a specific criterion which often results in that these assessment typically do not include zero-values in their reporting.

pressed in Equation (8) is based on a well-doublet system. The extractable amount of heat is site-specific as the recovery factor depends on a temperature fraction between the reinjection temperature and the reference temperature. One approach to this has been to consider the temperature fraction as constant where the reinjection temperature and reference temperature are equal which results in a recovery factor of 1/3 (Calcagno et al., 2014; Erlström & Rosberg, 2022). In the case of the Arnager Greensand, it is difficult to determine a feasible reinjection temperature of a potential geothermal plant as it would be limited by technological constrains. One way to investigate this further is to examine the temperature fractions of the Lund geothermal plant and the Margareteholm geothermal plant in Denmark, although the Lund geothermal plants consists of a complex configuration of several production and reinjection wells and the Margareteholm plant is more of a basic well-doublet system. This makes is so that Equation (8) is not directly applicable in the case of the Lund geothermal plant.

The Lund Geothermal plant has a production temperature of 20 °C and a reinjection temperature range of 4 – 7 °C (Erlström & Rosberg, 2022). This gives a range of 0.36 – 0.44 for the extractable amount of heat using Equation (8) with a reference temperature of 8 ° C. The Margareteholm plant discharges fluids from the Lower Triassic Bunter sandstone formation at 2650 meters depth. The plant has a production temperature of 74 °C and a reinjection temperature of 18 °C (Balling et al., 2019). This gives a value of 0.28 for the extractable amount of heat with the same reference temperature as above. These examples show the variation in the extractable amount of heat from two markedly different aquifers, each characterised by its own temperature conditions and the reinjection temperature specific to their respective geothermal plants.

5.3 Spatial Distribution and its impact on the Stored heat

One objective of this study was to investigate the regional spatial distribution of the Arnager Greensand and its effects on stored heat results. It is important to consider the anisotropy (combined vertical and lateral differences) of the Arnager Greensand when viewing the stored heat results. The presented maps show the spatial variability of the stored heat (Figure 13 and Figure 14). An overall trend can be observed in both maps where the stored heat is greater over the Falsterbo Peninsula and decreases toward the RFZ. The stored heat is also relatively lower over the Skurup Platform compared to the rest of SW Scania. The increased stored heat over the Falsterbo Peninsula is attributed to the fact that the Arnager Greensand is thicker in these regions. There are two deviations to the regional spatial pattern observed as a halo or bullseye effect surrounding the Norrevång-1 and Mossheddinge-1 boreholes. The halos are caused by the interpreted thickness in the boreholes which deviates from the regional thickness trend (Appendix 4). This in turn affects the interpolated thickness surface which leads to increased stored heat around the Norrevång-1 borehole and lower stored heat around the Mossheddinge-1 borehole.

This observation in the stored heat spatial distribution underscores that the stored heat equation is predominantly controlled by the volume parameter (thickness and areal extent). The case examples in Table 5 further demonstrate that the stored heat increases notably where the Arnager Greensand thickness is greater. A previous study by Arkan and Parlaktuna (2005) supports the above notion that the volume of the aquifer is the primary factor affecting the stored heat results. This was established through sensitivity analysis of the stored heat parameters.

The Arnager Greensand exhibits two distinct spatial distribution patterns. That is a decrease in thickness and an increase in depth towards the RFZ (Erlström et al., 2011; Anthonsen et al., 2014; Mortensen et al., 2016). This inverse relationship is interesting to investigate, especially in the context of the stored heat methodology, as a substantial increase in reservoir temperature might potentially offset the impact of a relatively small thickness. This inverse trend is not clearly identified in the maps as it would display as an increase in stored heat adjacent to the RFZ where the reservoir temperature is the highest. The reason behind this is that the reservoir temperature is the second most controlling factor of the stored heat equations followed by the porosity and density which have a lesser impact (Arkan & Parlaktuna, 2005).

5.4 Stratigraphical boundary interpretations of the Arnager Greensand

There are several interpreted top and base boundaries of the Arnager Greensand which results in different reported thickness values (Table 3). This study introduces additional boundary interpretations and discusses the challenges in deducing these. The challenges are primarily due to the constraints of the limited dataset and the uncertainties regarding the diffuse base boundary transition towards the Lower Cretaceous strata, which includes the Lower Cretaceous sandstones with similar properties to the Arnager Greensand and the Aptian Shale marker-bed. The uncertain definition of the base boundary complicates an estimate of the Arnager Greensand thickness. Adding to this, the geophysical signal of the Arnager Greensand can not be correlated against the core material since both techniques were never applied in the same borehole. This is a contributing factor to the absence of a well-defined lithostratigraphic division for the Lower Cretaceous in SW Scania. On the contrary, the top boundary is more easily distinguishable in the seismic and borehole data which makes it more easily mapped.

This study aimed for a regional modelling approach to show the broad geological trends of the Arnager Greensand. While minor adjustments in the top and base boundaries will not significantly affect the stored heat spatial pattern, the varying boundary interpretations underscore the difficulties in accurately placing the Arnager Greensand within the Lower Cretaceous framework of SW Scania (Table 3). However, a substantial adjustment of the boundaries may result in a ten-meter variation in thickness which would impact the stored heat results.

This is exemplified in the Mossheddinge-1 borehole, where prior studies interpret the Arnager Greensand to be thicker and situated further up in the stratigraphy (Juhlin et al., 2013). This borehole has long been considered hard-interpreted as sandy and glauconitic sediments occur over an interval spanning 150 meters (Sivhed et al., 1999). This is shown in Figure (8) where the geophysical signature fluctuates between what is interpreted as alternating beds of sandstones and mudstones. These alternating beds are primarily located beneath the Arnager Greensand. The transition also lack good resolution which makes it hard to determine the base boundary.

From a broader standpoint, if the Arnager Greensand were to be situated higher up in the stratigraphy in the Mossheddinge-1 borehole, as suggested by Juhlin et al. (2013), this would result in a decrease in reservoir temperature. Conversely, a greater thickness of the Arnager Greensand in Mossheddinge-1 borehole would increase the stored heat in the region. This reasoning is relevant to all borehole interpretations, underscoring the significance of accurate boundary interpretations as it influences the subsequent interpolations and the stored heat estimates.

The Lower Cretaceous sandstone sequence which includes the Arnager Greensand and the Lower Cretaceous sandstones could be assessed using the concept of net-sand. This approach would involve interpreting the permeable sandstone units within the whole sequence by summing up their cumulative thicknesses. The interlayering of non-permeable lithologies would not be taken into consideration. This approach was taken by Erlström and Rosberg (2022) in the geothermal assessment of the Lund Sandstone.

The thickness of the Lower Cretaceous sandstones is estimated to vary between 4 to 27 meters in SW Scania (Juhlin et al., 2013). Considering these Lower Cretaceous sandstones, the stored heat would substantially increase over the Lower Cretaceous interval using the net-sand approach. To exemplify, the thickness would increase from 27 to 37 meters in the FFC-1 borehole and the stored heat would increase from 2.90 GJ/m^2 to 3.98 GJ/m^2. Similarly, the thickness in the Barsebäck-1 borehole would increase from 17 to 32 meters and the stored heat would increase from 2.00 GJ/m^2 to 3.76 GJ/m^2. In practice, accurately determining these thicknesses is difficult as the spatial distribution of the Lower Cretaceous sandstones remains highly uncertain across SW Scania (Erlström et al., 2011).

5.5 Parameter evaluation

There are both spatial and static parameters used in this study. Spatial parameters in this context refers to parameters that exhibit spatial variability and static parameters refer to constant values that are uniformly applied to all cells. The spatial parameters include the thickness and reservoir temperature, and the static parameters include the volumetric heat capacity, reference temperature, and porosity. It would be possible to generate a spatial surface for the porosity, but this would demand more data on the petrophysical properties. The current petrophysical dataset is limited to a select few boreholes and generating additional spatial surfaces such as a porosity surface would potentially introduce further uncertainties.

There is a clear relationship between the reservoir volume, reservoir temperature and the volumetric heat capacity. This relationship shows that a thicker and hotter reservoir with a higher volumetric heat capacity holds the greatest geothermal potential (Table 5). In practical terms, this can be understood as the multiplication stacking of raster surfaces corresponding to a parameter, where a higher cell value results in a higher stored heat estimate. Future studies should focus on modelling the reservoir thickness and reservoir temperature in greater detail as these two parameters would have the most bearing on the stored heat.

5.5.1 Volumetric heat capacity

The Arnager Greensand rock matrix has a volumetric heat capacity of 2.15×10^6 J/m³ °C which falls within a reference range of 1.6 – 2.8 reported for sandstones (Stober & Bucher, 2021b) and a broader range of 2.0 – 6.5 (Banks, 2012). The reference value of 2.5×10^6 J/C m^3 for the volumetric heat capacity of a water-saturated rock also falls within these ranges. This indicates that the volumetric heat capacity values used in this study are within reasonable assumptions. However, the value of 4.66×10^6 J/m³ °C for the volumetric heat capacity of the reservoir fluid is uncertain because it is calculated based on a single measurement of the density fluid.

5.5.2 Porosity

The Arnager Greensand shows high porosity values with a average porosity of 24.3 % and a median porosity of 26.6 % (Table 4). The porosity has a large influence on the second approach to the stored heat equation as the fluids have considerably higher volumetric heat capacity compared to the rock matrix (Equation 10). A high porosity value results in larger value for the stored heat. This relationship between the stored heat in the rock matrix versus the reservoir fluid is presented in Figure (15). The graph shows that a porosity value of 32 % amounts to approximately 50 % of the total stored heat. A porosity value this high is considered extreme and does not represent the whole Arnager Greensand aquifer. However, for certain stratigraphic intervals in the boreholes over the Falsterbo Peninsula the porosity exceeds 30 %. This indicates that a substantial part of the stored heat in the Arnager Greensand is contained in the reservoir fluids over the Falsterbo Peninsula.

5.5.3 Reference temperature

A lower reference temperature increases the stored heat for each cell as the ΔT becomes greater. This relationship is presented in Figure (16) where a reference temperature of 4 degrees corresponding to the reinjection temperature of the Lund geothermal plant results in a total of 3690 PJ for the first stored heat approach and 4070 PJ for the second approach. This shows that setting the reference temperature higher leads to a more conservative estimate, while a lower reference temperature may lead to an overestimate of the stored heat.

5.6 Aspects of the Stored Heat method

5.6.1 Permeability

A geohydrological parameter to consider when evaluating the Arnager Greensand as a potential geothermal resource is permeability, as the stored heat equations do not consider the effects of permeability differences (Williams, 2014). The permeability may vary considerably within a reservoir which will prevent fluids to sustain a geothermal plant over the lifespan of a geothermal development (Grant, 2015). The Arnager Greensand shows high permeability values over the Falsterbo Peninsula, yet there are notable differences in the permeability between the boreholes and at different stratigraphic intervals (Table 4). Previous research suggests that in the northernmost part of the region, the Arnager Greensand grades into a finer grain size, which results in a lower permeability in the range of 100 – 200 mD (Erlström et al., 2011). Over the central Skurup Platform, there are no deep-drillings conducted and the petrophysical properties of the Arnager Greensand remains unknown over this region.

5.6.2 Thermal recharge

The stored heat equations only consider the heat in place and disregard the effects of heat replenishment by conduction from confining layers during geothermal exploitation. This process is commonly referred to as thermal or heat recharge (Poulsen et al., 2015; de Bruijn et al., 2021). This occurs when the reservoir cools down due to the reinjection of cold water. This causes a temperature difference between the confining layers and the reservoir which leads to heat flow from the confining layers into the reservoir. If the reservoir has low-permeability confining layers vertically, the fluid flow will be minimal, and the heat transfer mechanism will be conduction. This is known as vertical thermal recharge. In contrast, lateral thermal recharge occurs when heat moves laterally within the reservoir to the area that has cooled down around the reinjection well. The heat transfer mechanisms in this case will be both conduction and convection which will occur when the permeability is high (de Bruijn et al., 2021).

Studies have shown that recharge from confining layer can influence the total energy output of reservoirs (Poulsen et al., 2015; de Bruijn et al., 2021; Wang et al., 2021). This effect is expected to be more pronounced in thinner reservoirs due to their larger contact area with the confining layer which results in a higher relative contribution of recharge. Another important factor in relation to the thermal recharge is the production rate of the geothermal plant. A low production rate stimulates the heat flow from the confining layers to the reservoir under a longer period which may yield the largest relative contribution of vertical recharge. The spacing between wells increases the distance over which the cooled-down reservoir fluids interacts with the confining layers. As a consequence, this could lead to a reduction in the rate at which the production temperature drops (de Bruijn et al., 2021).

In the case of the Arnager Greensand, these three key factors are important to consider as the reservoir is thin and a part of a mixed clastic Lower Cretaceous succession which includes alternating beds of mudstones and sandstones, such as the Aptian shale and the Lower Cretaceous sandstones. The mud facies in this sequence may contribute to the total energy output of the sequence through thermal recharge. Understanding this system behaviour is crucial and should be further evaluated for the Arnager Greensand as it will enhance the overall reservoir performance.

5.7 Model evaluation – strengths and limitations

The strength of the presented model is that it provides for the first time a comprehensive regional overview of the spatial configuration of the Arnager Greensand

and its potential as a geothermal resource. This includes information about the formation depth, thickness, and reservoir temperature, as well as the resulting stored heat maps. The study highlights the regional trends of the Arnager Greensand and pin-points regions in SW Scania which are of interest for geothermal technical utilization. This study also provides sufficient metadata in connection the maps. Specifically, how the maps were generated and how they should be viewed, and also what parameters were taken into consideration. The maps serve as a foundation for future geothermal investigations, supporting the identification of specific areas to zoom into and explore where local geothermal conditions need to be investigated in greater detail.

The major limitation of the model is that it is based on a small dataset comprised of 18 boreholes. There is a lack of data mainly over the Skurup Platform as the borehole dataset is situated exclusively in the eastern part of SW Scania. The model is limited by both the data quality and the lack of petrophysical data. The major weakness of the model is that it relies on extrapolation over the Skurup Platform and a smaller area surrounding the city of Landskrona. These two areas are outside of the borehole data coverage. Extrapolation was performed because one of the objectives of this study was to create a stored heat map that covers the entire SW Scania. A full coverage map adds value in the comprehensive understanding on the Arnager Greensand. The extrapolation results in large uncertainties regarding the geothermal parameters over the Skurup Platform. This should be taken into consideration when viewing the results.

5.7.1 Velocity and thickness map evaluation

The time-to-depth conversion involves steps of extrapolation. The velocity values assigned to the cells over the Skurup Platform are extrapolated from the low velocity in the Svedala-1 borehole (Appendix 4). The extrapolation is apparent when examining the velocity map, where a substantial area is marked by the low velocity blue colour class (Figure 9). Similarly, the low thickness in the Mossheddinge-1 and Svedala-1 borehole extrapolates over the Skurup platform, contributing to a large number of cells with a relatively low thickness (Figure 12).

The velocity range down to the Arnager Greensand is 2933 – 3253 m/s. The velocity values represent the mean velocity for the whole sedimentary column down to the Arnager Greensand. This simple approach of using a mean velocity adapted in this study cannot account for the lateral variations in seismic velocity, related to variations in lithology and thickness of the Höllviken Formation members situated above the Arnager Greensand (Figure 3). For example, the Granvik Member which is situated above the Arnager Limestone and is made up of a fine-grained marl limestone with interlayers of silt-mudstones with a thickness between 200 – 400 meters (Sivhed et al., 1999). Similar reasoning can be used by looking at the shallow-marine sandstone units (Lund Sandstone and Hansa Member) that cut into the stratigraphy from the RFZ. A mean velocity value is less applicable in this region of Scania as the stratigraphy becomes more complex adjacent to the RFZ.

A more detailed modelling of the seismic velocities could result in a more accurate depth conversion. However, due to the significant effort involved in performing such modelling, it was not feasible in this study. It is also likely to be the case that the errors in the depth conversion of the reservoir only lead to a relatively small error in the stored heat estimates when compared to other factors such as the uncertainty of the reservoir thickness. In summary, for the purpose of this project in outlining general geological trends, the basic velocity model was considered satisfactory and fulfilled its purpose of generating a depth surface.

5.7.2 Depth map evaluation

Similar depth maps as the one created in this project have been generated for the Arnager Greensand in the past using various techniques. Some of these maps are schematic graphical representations, while others are more advanced, employing similar time-to-depth conversion techniques as used in this project. In a study by Davies Jones (2019), old analogue OPAB data were digitised and converted using a time-to-depth workflow, which involved the interpretation of different stratigraphic horizons and interpolation between boreholes. The resulting depth map of this study only covers a small part of SW Scania as it does not employ any extrapolation over the Skurup Platform. This study is a proof-of-concept that alternative approaches to the time-to-depth conversion are possible instead of using the pre-existing interpretations from the blue marker map. However, the final depth map in the study by Davies Jones (2019) displays large similarities to the blue marker map used in this study. Hence, a re-interpretation of the vintage data was out of the scope of this project, the use of the pre-existing blue marker map was found suitable given the focus and time available in this project.

5.7.3 Reservoir temperature map evaluation

The geothermal gradient is calculated from one single BHT log measured in the Ljunghusen-1 borehole. Subsequently, the reservoir temperature is estimated by applying this constant geothermal gradient over the whole reservoir which introduces uncertainties to the stored heat results. The uncertainties are mainly related to that the reservoir temperature is coupled to the reservoir depth, and will not consider variations in thermogeological conditions, such as thermal conductivity.

The formation temperature in the Öresund Basin is estimated to range between 45 - 50 °C at a depth of 1500 meters, between 60 - 70 °C at 2000 meters, and between 70 - 90 °C at 2500 meters (Erlström et al., 2018). These temperature estimations are consistent with the reservoir temperatures presented in this study. For instance, the reservoir temperature is about 40 °C at a depth of 1200 meters beneath the Falsterbo Peninsula, and it reaches 50 °C at a depth of 1500 - 1600 meters below the Malmö region. The results from this study also indicate localised temperature peaks within the 1900 – 2100 depth range in the northwestern part of SW Scania adjacent to the RFZ with temperatures ranging from 60 - 65 °C.

5.8 The Arnager Greensand as a geothermal resource

In terms of geothermal resource classifications, the Arnager Greensand would be classified as a low-temperature resource because the reservoir fluids do not exceed 90 °C, or as a low-enthalpy how-water resource due to the fluids having a low energy content. According to the classification by White and Williams (1975), the Arnager Greensand would be considered a conduction-dominated system. Building on this, Lund (2009) explains that geothermal resources like this often occur in sedimentary basins, where an elevated geothermal gradient can be attributed to either a low thermal conductivity of the host rock or high heat flow. For the Arnager Greensand, we assume that lower thermal conductivity results in a slightly higher geothermal gradient, leading to increased temperatures in both the rock matrix and reservoir fluids. Additionally, there is a possibility of minor sub-horizontal fluid flows caused by advection in the aquifer given it is gently dipping towards the RFZ.

The reservoir properties of the Arnager Greensand are expected to vary locally, as it was deposited as an extensive fine-to-medium-grained unit over a large area in a marginal marine environment, with interludes of coastal lacustrine settings. The clastic sediments are believed to originate from the erosion of the Fennoscandian shield and/or the islands situated in the Danish-Polish Trough (Larsson et al., 2000). The glauconite characterising the Arnager Greensand formed through subsequent autogenic processes. Glauconitisation in sandstones is considered a secondary-porosity-forming process, occurring after the initial deposition of the host rock which may reduce porosity and permeability (Díaz et al., 2003)

The unconsolidated nature of the Arnager Greensands is another distinguishing feature. It has been observed that production and reinjection wells located in these unconsolidated sand formations may require the removal of particles from the fluids for successful geothermal utilization. An example of this is the geothermal exploitation of the Upper Pannonian sandstones in Hungary, which contain a poorly cemented, heterogeneous, and argillaceous formation. The presence of loose sand particles in the geothermal plant shortens its lifespan, necessitating several stages of sand removal to protect the geothermal pump and maintain the reservoir permeability around the reinjection wells (Zarrouk & McLean, 2019b)

The Late Cretaceous – Paleogene tectonic inversion events which occurred after the Arnager Greensand was deposited (Erlström, 2020) resulted in minor effects on the stratification over the SW Scania faults (Figure 1 and Figure 2). Studying these faults in the context of a geothermal assessment is essential as secondary fracture-related porosity can have a more significant impact on the permeability of the system compared to primary porosity (Limberger et al., 2018). Geothermal systems dominated by fracture related porosity often exhibit high permeability but relativity low fluid volumes (Williams et al., 2008). Therefore, it is crucial to recognize that the Arnager Greensand might potentially be both a porous fluid-bearing reservoir and a fractured reservoir along the SW Scania faults. The seismic resolution across the faults is low and the detailed geometry of them remains largely unknown.

A comprehensive understanding of the heat transport mechanism, petrophysical properties, and spatial arrangement of the Arnager Greensand is important, as it directly impact the overall reservoir performance. Further research in this area should prioritise in-depth lithological and petrophysical studies as past research has predominantly focused on biostratigraphy. The addition of new seismic data, especially over the SW Scania faults, would also contribute to a better understanding of how the Arnager Greensand interval was affected by the Late Cretaceous - Paleogene tectonic inversion events.

6 Conclusions

- This work presents the first geothermal assessment of the Arnager Greensand over SW Scania using two variants of the stored heat method. The first method estimates that the Arnager Greensand stores approximately 3270×10^{15} (petajoules) of geothermal energy. The stored heat in the reservoir varies between 1.25 – 4.53 GJ/m² (gigajoules per square meter). The second method assesses the stored heat in the rock matrix and reservoir fluids separately by considering a porosity parameter which results in a total stored heat of 3610×10^{15} with values ranging between 1.37 and 4.99 GJ/m².

- The greatest amount of stored heat is found over the Falsterbo Peninsula and the lowest over the Skurup Platform and areas along the Romeleåsen Fault Zone. The increased stored heat over the Falsterbo Peninsula is attributed to a greater thickness of the Arnager Greensand in this region. A region with relativity increased stored heat extends from the Falsterbo Peninsula northward to the city of Malmö and eastwards to the city of Trelleborg. The Arnager Greensand in this region features noteworthy thickness and potentially high porosity and permeability reservoir characteristics. This offers promising prospects for future local geothermal investigations. The proximity to urban and industrial areas significantly boosts the feasibility of integrating a well-doublet system into a district heating system.

- The Arnager Greensand over SW Scania exhibits lower stored heat values compared to aquifers in similar geological settings. These stored heat findings underscore the limited potential of the Arnager Greensand for utilization as a geothermal resource on a regional basis.

- The Lower Cretaceous sandstones constitute together with the Arnager Greensand a Lower Cretaceous sandstone sequence that can be assessed using the concept of netsand. Considering the Lower Cretaceous sandstones and the Arnager Greensand as a combined aquifer with a greater cumulative thickness, the geothermal potential would increase over the Lower Cretaceous interval in SW Scania.

- This study applies a rather simplified view on the recovery factor where the extractable amount of heat amounts to 1/3 proposed by Lavigne (1977) considering a well-doublet system. The extractable amount of heat is calculated for four case examples considering a possible influence area of such a doublet system. The extractable amount of heat is the greatest over the Falsterbo Peninsula and decreases towards the RFZ based on the borehole case studies presented in this work.

- The volume parameter has a great bearing on the stored heat results. This parameter is inferred by the interpretation of the top and base boundaries of the Arnager Greensand, which is uncertain in some boreholes, where the boundaries can only be interpreted from vintage wire-line logs of poor quality. This leads to uncertainties in the thickness estimates for some boreholes.

- The stored heat method emphasises that large reservoirs characterised by high temperatures hold the greatest geothermal potential. The stored heat is also influenced by the chosen reference temperature and volumetric specific heat. A higher reference temperature results in a more conservative estimation, while a lower reference temperature may lead to an overestimation of the geothermal resource.

- The main drawback of the stored heat method is the volume parameter as it assumes that the same geological conditions apply within the whole volume. The issue of scale also presents challenges since this method has been used for both regional and more local assessments. This becomes problematic as the volume must be placed in relation to the area of influence from a potential geothermal plant in order to estimate the extractable amount of heat. The influence area is hard to determine as it might revolve around a well-doublet system or a more complex configuration of multiple production and reinjection wells.

- The Arnager Greensand is a rather thin reservoir and is also part of a Lower Cretaceous succession which includes alternating beds of mudstones and sandstones, such as the Aptian shale and the Lower Cretaceous sandstones. The mud facies in the Lower Cretaceous succession could contribute to the total energy output of the sequence through thermal recharge. The effects of thermal recharge should be further explored in future studies to better determine the suitability of the Arnager Greensand as a geothermal resource.

- The stored heat equations do not consider the effects of permeability differences in the reservoir. In practical terms, this means that a low permeability reservoir could hold an enormous amount of stored heat, but geothermal utilization would not be feasible as the reservoir fluids would not be readily available at the surface. Considering the timeframe of 30 – 40 years for successful geothermal developments, this parameter becomes even more important as fluids need to be supplied continuously over this timeframe.

- There is a need for further deep drillings to better determine the spatial configuration of the Arnager Greensand. The additional depth and thickness data would better guide the interpolations over the Skurup Platform and contribute to a better subsurface model. The current borehole dataset is limited to boreholes situated in western parts of SW Scania in which some only contain data on the petrophysical properties. The properties of the Arnager Greensand over the Skurup Platform are highly uncertain, leading to considerable unknowns in the geothermal parameters for this area in the assessment. Future studies should focus on modelling the reservoir thickness and temperature in greater detail as this would have the most bearing on the stored heat. Future studies should also investigate the Monte-Carlo approach to consider the uncertainties associated with the input parameters.

- This study shows that the stored heat method is a valuable tool in the early exploration of a potential geothermal resource. This method is a great starting point when looking into the geothermal potential of geothermal aquifers such as the Arnager Greensand. It proves useful as it with limited means can calculate a rough estimate of the geothermal potential. The maps which are created in this study capture the regional trends of the Arnager Greensand and highlight areas in SW Scania with potential for future geothermal investigations. The resulting maps and stored heat values in this study can be used as a basis for future geothermal developments.

- To better our understanding of the potential use of the Arnager Greensand as a geothermal energy resource it is necessary to perform additional deep-drillings, seismic surveys, and gather additional thickness data. New BHT data are also essential for more accurate reservoir temperature estimates. There is also a need for further lithological studies as previous research has predominantly focused on biostratigraphical studies. Additional deep-drillings would not only offer insights into Arnager Greensand but also provide valuable data on other promising sandstone intervals in the Öresund area with geothermal potential. A comprehensive understanding of these intervals is crucial, as the Arnager Greensand, along with several other geothermal aquifers in SW Scania, should be acknowledged as national renewable energy assets.

7 Acknowledgements

This thesis has been a valuable experience for me as it has given me the opportunity to apply my geological knowledge on an interdisciplinary subject. I have learnt a great lot about several topics which are associated with geothermal energy. All of this would not have been possible without the guidance from main supervisor Mikael Erlström (LU and SGU) who introduced me to the project and the stored heat method. I would like to thank Mikael for his dedication to the project and his approach to pedagogical teaching. I would also like to thank my second supervisor Daniel Sopher (SGU) who helped me with the more computational parts of this project. Daniel comes from a geophysical background, and I have enjoyed listening to him when discussing the topics at hand. Throughout the project, my third supervisor Jan-Erik Rosberg (LTH) gave me valuable tips which helped guide the project in the right direction. Jan-Eric also gave comments on the final manuscript before hand-in which helped to improve the overall quality of the text.

8 References

AGRCC. (2010a). *Australian Code for Reporting of Exploration Results, Geothermal Resources and Geothermal Reserves - The geothermal reporting code*. https://www.dmp.wa.gov.au/Documents/Geological-Survey/Geothermal_Lexicon_2010.pdf

AGRCC. (2010b). *Geothermal Lexicon For Resources and Reserves Definition and Reporting*. https://www.dmp.wa.gov.au/Documents/Geological-Survey/Geothermal_Lexicon_2010.pdf

Alm, P.-G., & Bjelm, L. (1995). *Geothermal energy in Scania : a summary of research activities and results within the national program for geothermal energy in sedimentary rocks 1977-1994 : NUTEK Project 656 090-3*. Lund Institute of Technology, Dept. of Engineering Geology. https://ludwig.lub.lu.se/login?url=https://search.ebscohost.com/login.aspx?direct=true&AuthType=ip,uid&db=cat07147a&AN=lub.990790&site=eds-live&scope=site

Anthonsen, K. L., Aagaard, P., Bergmo, P. E. S., Gislason, S. R., Lothe, A. E., Mortensen, G. M., & Snæbjörnsdóttir, S. Ó. (2014). Characterisation and Selection of the Most Prospective CO2 Storage Sites in the Nordic Region. *Energy Procedia*, *63*, 4884-4896. https://doi.org/10.1016/j.egypro.2014.11.519

Arkan, S., & Parlaktuna, M. (2005). *Resource Assessment of Balçova Geothermal Field* World Geothermal Congress 2005, Antalya Turkey. https://www.geothermal-energy.org/pdf/IGAstandard/WGC/2005/1130.pdf

Armstead, H. C. H. (1978). *Geothermal energy : its past, present and future contributions to the energy needs of man*. https://www.researchgate.net/publication/335136535_Creating_shallow_geothermal_potential_maps_for_Finland

Arola, T., Korhonen, K., Martinkauppi, A., Leppäharju, N., Hakala, P., Ahonen, L., & Pashkovskii, M. (2019). *Creating shallow geothermal potential maps for Finland*. https://www.researchgate.net/publication/335136535_Creating_shallow_geothermal_potential_maps_for_Finland

Balling, N., Major, M., Fuchs, S., Mathiesen, A., Møller Nielsen, C., Mejer Hansen, T., Kristensen, L., & Förster, A. (2019). *Geothermal reservoirs in the Danish area: temperatures, resources and models for long-term energy extraction*. https://dybgeotermi.geus.dk/wp-content/uploads/Final-report-M4.6_WP4.pdf

Banks, D. (2012). *An Introduction to Thermogeology: Ground Source Heating and Cooling*. Wiley. https://books.google.se/books?id=tVM8kL-w2jkC

Berthelsen, A. (1998). The Tornquist Zone northwest of the Carpathians: An intraplate pseudosuture. *Gff*, *120*(2), 223-230. https://doi.org/10.1080/11035899801202223

Bjelm, L. (1977). *Geotermisk energiutvinning i Skåne : slutrapport. Etapp 1, Förutsättningar för utvinning i Skåne*. Nämnden för energiproduktionsforskning. https://www.researchgate.net/publication/310288408_Geotermisk_energiutvinning_i_Skane_NE_Slutrapport_Etapp_1_Forutsattningarna_for_utvinning_i_Skane_Lund_University_of_Technology_Dept_of_Geology_and_Soil_Mechanics_Sweden

Bjelm, L., Hartlèn, J., Röshoff, K., Bennet, J., Bruch, H., & Persson, P. G. (1979). *Geotermisk energiutvinning i Skåne : slutrapport. Etapp 2 och 3 Förutsättningar för utvinning i Skåne* (Geotermisk energiutvinning i Skåne Slutrapport, Issue. https://www.scopus.com/inward/record.uri?eid=2-s2.0-85134315342&partnerID=40&md5=e2921a837fd67fc5cf331d637a6ae584

Bjelm, L., & Lindeberg, L. (1995). *Long term experience from a heat pump plant in Lund, Sweden, using a low-temperature geothermal aquifer*. https://www.geothermal-energy.org/pdf/IGAstandard/WGC/1995/3-bjelm.pdf

Bjelm, L., & Persson, P. G. (1981). *Geotermisk energiutvinning i Skåne : slutrapport. Etapp 4. D. 1, Förutsättningar för utvinning i Skåne. Lagring i geotermalformationer, D. 2, Provborrning vid Landskrona*. Nämnden för energiproduktionsforskning. https://www.researchgate.net/publication/310288999_Geotermisk_energiutvinning_i_Skane_NE_Forutsattningarna_for_utvinning_i_Skane_Lund_University_of_Technology_Etapp_2_3_Dept_of_Geology_and_Soil_Mechanics_Sweden

Brook, C., Mariner, R., Mabey, D., Swanson, J., Guffanti, M., & Muffler, L. (1979). Hydrothermal

convection systems with reservoir temperatures> 90 C. *Assessment of geothermal resources of the United States-1978: US Geological Survey Circular*, *790*, 18-85.

Brotzen, F. (1950). *De geologiska resultaten från borrningarna vid Höllviken*. https://ludwig.lub.lu.se/login?url=https://search.ebscohost.com/login.aspx?direct=true&AuthType=ip,uid&db=cat07147a&AN=lub.1789677&site=eds-live&scope=site

Bödvarsson, G. S., & Tsang, C. F. (1982). Injection and Thermal Breakthrough in Fractured Geothermal Reservoirs. *Journal of Geophysical Research: Solid Earth*, *87*(B2), 1031-1048. https://doi.org/https://doi.org/10.1029/JB087iB02p01031

Calcagno, P., Baujard, C., Guillou-Frottier, L., Dagallier, A., & Genter, A. (2014). Estimation of the deep geothermal potential within the Tertiary Limagne basin (French Massif Central): An integrated 3D geological and thermal approach. *Geothermics*, *51*, 496-508. https://doi.org/https://doi.org/10.1016/j.geothermics.2014.02.002

Christensen, W. K. (1984). The Albian to Masstrichtian of southern Sweden and Bornholm, Denmark; a review. *Cretaceous Research*, *5*(4), 313-327. https://ludwig.lub.lu.se/login?url=https://search.ebscohost.com/login.aspx?direct=true&AuthType=ip,uid&db=geh&AN=1985-048656&site=eds-live&scope=site

Christensen, W. K., & Schulz, M. G. (1997). Coniacian and Santonian belemnite faunas from Bornholm, Denmark. *Fossils and Strata*(44), 1-73-73. https://ludwig.lub.lu.se/login?url=https://search.ebscohost.com/login.aspx?direct=true&AuthType=ip,uid&db=edselc&AN=edselc.2-52.0-0031429047&site=eds-live&scope=site

Ciriaco, A. E., Zarrouk, S. J., & Zakeri, G. (2020). Geothermal resource and reserve assessment methodology: Overview, analysis and future directions. *Renewable and Sustainable Energy Reviews*, *119*. https://doi.org/10.1016/j.rser.2019.109515

Davies Jones, G. M. (2019). *A 3D Sub-Surface Characterisation of the Arnager Greensand, South-west Skåne* [Student thesis, DiVA. http://urn.kb.se/resolve?urn=urn:nbn:se:uu:diva-393263

de Bruijn, E. A. M., Bloemendal, M., ter Borgh, M. M., Godderij, R. R. G. G., & Vossepoel, F. C. (2021). Quantifying the contribution of heat recharge from confining layers to geothermal resources. *Geothermics*, *93*. https://doi.org/10.1016/j.geothermics.2021.102072

Deckers, J., & van der Voet, E. (2018). A review on the structural styles of deformation during Late Cretaceous and Paleocene tectonic phases in the southern North Sea area. *Journal of Geodynamics*, *115*, 1-9. https://doi.org/https://doi.org/10.1016/j.jog.2018.01.005

Dezayes, C., Genter, A., Thinon, I., Courrioux, G., & Tourliere, B. (2008). *Geothermal potential assessment of clastic triassic reservoirs (Upper Rhine Graben, France)*. https://www.researchgate.net/publication/236622991_Geothermal_potential_assessment_of_clastic_triassic_reservoirs_Upper_Rhine_Graben_France

Díaz, E., Prasad, M., Mavko, G., & Dvorkin, J. (2003). Effect of glauconite on the elastic properties, porosity, and permeability of reservoir rocks. *The Leading Edge*, *22*, 42-45. https://doi.org/10.1190/1.1542755

DiPippo, R. (2015). *Geothermal Power Plants: Principles, Applications, Case Studies and Environmental Impact: Fourth Edition*. https://www.researchgate.net/publication/303430711_Geothermal_Power_Plants_Principles_Applications_Case_Studies_and_Environmental_Impact_Fourth_Edition

Erlström, M. (1990). *Petrology and deposition of the Lund Sandstone, Upper Cretaceous, southwestern Scania*. SGU. https://ludwig.lub.lu.se/login?url=https://search.ebscohost.com/login.aspx?direct=true&AuthType=ip,uid&db=cat07147a&AN=lub.646229&site=eds-live&scope=site

Erlström, M. (1994). *Evolution of Cretaceous sedimentation in Scania* Dept. of Geology [Geologiska institutionen], Univ.]. https://ludwig.lub.lu.se/login?url=https://search.ebscohost.com/login.aspx?direct=true&AuthType=ip,uid&db=cat07147a&AN=lub.842759&site=eds-live&scope=site

Erlström, M. (2009). *Tectonic evolution and geological framework of Scania - A review of interpretations and geological models* (SGU-rapport 2009:10). https://resource.sgu.se/dokument/publikation/sgurapport/sgurapport200910rapport/s0910-rapport.pdf

Erlström, M. (2020). Carboniferous–Neogene tectonic evolution of the Fennoscandian transition zone, southern Sweden. *Geological Society, London, Memoirs*, *50*(1), 603-620. https://doi.org/doi:10.1144/M50-2016-25

Erlström, M., Bidstrup, T., Lindström, S., Nielsen, L. a. H., Kristensen, L., & Mathiesen, A. (2013). *Structural outline, depositional setting and assessment of Mesozoic low enthalpy geothermal reservoirs in the marginal eastern parts of the Danish Basin* European Geothermal Congress EGC 2013,

Erlström, M., Booldreel, L.-O., Lindström, S., Andersen, M. S., Kristensen, L., Mathiesen, A., Kamla, E., & Nielsen, L.-H. (2018). Stratigraphy and geothermal assessment of Mesozoic sandstone reservoirs in the Öresund Basin - exemplified by well data and seismic profiles.

Bulletin of the Geological Society of Denmark, *66*, 123-149. https://ludwig.lub.lu.se/login?url=https://search.ebscohost.com/login.aspx?direct=true&AuthType=ip,uid&db=edsswe&AN=edsswe.oai.lup.lub.lu.se.e6acde4a.baae.4448.95f7.38d03ffdeaeb&site=eds-live&scope=site

Erlström, M., Fredriksson, D., Juhojuntti, N., Sivhed, U., & Wickström, L. (2011). *Lagring av koldioxid i berggrunden : krav, förutsättningar och möjligheter* (9789174030983). (Rapporter och meddelanden / Sveriges geologiska undersökning: 131, Issue. https://ludwig.lub.lu.se/login?url=https://search.ebscohost.com/login.aspx?direct=true&AuthType=ip,uid&db=cat07147a&AN=lub.1976861&site=eds-live&scope=site

Erlström, M., & Guy-Ohlson, D. (1994). Campanian depositional settings in the Vomb Trough, Scania, Sweden. *Gff*, *116, Part 4*, 193-202. https://www.tandfonline.com/toc/sgff20/current

Erlström, M., Mellqvist, C., Schwarz, G., Gustafsson, M., & Dahlqvist, P. (2016). *Geologisk information för geoenergianläggningar – en översikt* (Geoenergi, Issue.

Erlström, M., & Rosberg, J.-E. (2022). Geothermal use and potential of the Lund Sandstone in SW Skåne, Sweden. *EGJ 54*, 5-11. https://doi.org/10.5281/zenodo.7882784

Erlström, M., & Sivhed, U. (2001). *Intra-cratonic dextral transtension and inversion of the southern Kattegatt on the southwest margin of Baltica : seismostratigraphy and structural development* [Book]. Sveriges geologiska undersökning (SGU). https://ludwig.lub.lu.se/login?url=https://search.ebscohost.com/login.aspx?direct=true&AuthType=ip,uid&db=cat07147a&AN=lub.1417744&site=eds-live&scope=site

Erlström, M., Sopher, D., & Dahlqvist, P. (2022). *Berggrunden på Sudret, Gotland Underlag för bedömning av grundvattentillgångar, geoenergipotential samt koldioxidlagring*. S. g. undersökning. https://resource.sgu.se/dokument/publikation/sgurapport/sgurapport202211rapport/s2211-rapport.pdf

Erlström, M., Thomas, S. A., Deeks, N., & Sivhed, U. (1997). Structure and tectonic evolution of the Tornquist Zone and adjacent sedimentary basins in Scania and the southern Baltic Sea area. *TECTONOPHYSICS*, *271*(3), 191-215. https://doi.org/https://doi.org/10.1016/S0040-1951(96)00247-8

ESRI. (2023a). *How Filter works*. ESRI. Retrieved 05-18 from https://pro.arcgis.com/en/pro-app/latest/tool-reference/spatial-analyst/how-filter-works.htm#:~:text=A%20low%20pass%20filter%20smooths,with%20the%20Mean%20statistic%20option.

ESRI. (2023b). *How Kriging works*. ESRI. Retrieved 05-18 from https://pro.arcgis.com/en/pro-app/latest/tool-reference/spatial-analyst/how-kriging-works.htm

ESRI. (2023c). *Understanding cokriging*. Retrieved 05-18 from https://pro.arcgis.com/en/pro-app/latest/help/analysis/geostatistical-analyst/understanding-cokriging.htm

ESRI. (2023d). *Using cross validation to assess interpolation results*. Retrieved 05 from https://pro.arcgis.com/en/pro-app/3.0/help/analysis/geostatistical-analyst/performing-cross-validation-and-validation.htm

European Commission. (2011). *Communication from the commission to the european parliament, the council, the european economic and social committee and the committee of the regions Energy Roadmap 2050*. https://eur-lex.europa.eu/legal-content/EN/TXT/PDF/?uri=CELEX:52011DC0885&from=EN

European Geothermal Energy Council. (2022). *EGEC Geothermal market report Key findings*.

Fetter, C. W. (2014). *Applied hydrogeology* (Fourth edition. ed.) [Book]. Pearson Education. https://ludwig.lub.lu.se/login?url=https://search.ebscohost.com/login.aspx?direct=true&AuthType=ip,uid&db=cat07147a&AN=lub.3480002&site=eds-live&scope=site

Frick, M., Kranz, S., Norden, B., Bruhn, D., & Fuchs, S. (2022). Geothermal Resources and ATES Potential of Mesozoic Reservoirs in the North German Basin. *Energies (19961073)*, *15*(6), 1980-1980. https://doi.org/10.3390/en15061980

Gando, A., Gando, Y., Ichimura, K., Ikeda, H., Inoue, K., Kibe, Y., Kishimoto, Y., Koga, M., Minekawa, Y., Mitsui, T., Morikawa, T., Nagai, N., Nakajima, K., Nakamura, K., Narita, K., Shimizu, I., Shimizu, Y., Shirai, J., Suekane, F., . . . The Kam, L. C. (2011). Partial radiogenic heat model for Earth revealed by geoneutrino measurements. *Nature Geoscience*, *4*(9), 647-651. https://doi.org/10.1038/ngeo1205

Garg, S. K. (2010). APPROPRIATE USE OF USGS VOLUMETRIC " HEAT IN PLACE " METHOD AND MONTE CARLO CALCULATIONS.

Garg, S. K. (2011). A REEXAMINATION OF USGS VOLUMETRIC " HEAT IN PLACE " METHOD.

Garg, S. K., & Combs, J. (2015). A reformulation of USGS volumetric "heat in place" resource estimation method. *Geothermics*, *55*, 150-158. https://doi.org/10.1016/j.geothermics.2015.02.004

Goldscheider, N., Mádl-Szőnyi, J., Erőss, A., & Schill, E. (2010). Review: Thermal water resources in carbonate rock aquifers. *Hydrogeology Journal*, *18*(6), 1303-1318. https://doi.org/10.1007/s10040-010-0611-3

Grant, M. A. (2015). Resource Assessment, a Review, with Reference to the Australian Code.

Grant, M. A., & Bixley, P. F. (2011). Chapter 3 - Simple Quantitative Models. In M. A. Grant & P. F. Bixley (Eds.), *Geothermal Reservoir Engineering (Second Edition)* (pp. 29-60). Academic Press. https://doi.org/https://doi.org/10.1016/B978-0-12-383880-3.10003-4

Gupta, H., & Roy, S. (2007). Chapter 4 - GEOTHERMAL SYSTEMS AND RESOURCES. In H. Gupta & S. Roy (Eds.), *Geothermal Energy* (pp. 49-59). Elsevier. https://doi.org/https://doi.org/10.1016/B978-044452875-9/50004-6

Hart, M. B. (1979). Biostratigraphy and palaeozoogeography of planktonic Foraminiferida from the Cenomanian of Bornholm, Denmark.

Hart, M. B., Bromley, R. G., & Packer, S. R. (2012). Anatomy of the stratigraphical boundary between the Arnager Greensand and Arnager Limestone (Upper Cretaceous) on Bornholm, Denmark. *Proceedings of the Geologists' Association*, *123*(3), 471-478. https://doi.org/https://doi.org/10.1016/j.pgeola.2011.11.006

Hurter, S., & Schellschmidt, R. (2003). Atlas of geothermal resources in Europe. *Geothermics*, *32*(4), 779-787. https://doi.org/https://doi.org/10.1016/S0375-6505(03)00070-1

International Energy Agency. (2011). *Technology Roadmap Geothermal Heat and Power*.

Jensen, J. B., & Hamann, N. E. (1989). Geological mapping of Mezozoic deposits along the eastern margin of the Ronne Graben, offshore Bornholm, Denmark. *Bulletin - Geological Society of Denmark*, *37*, 237-260. https://www.scopus.com/inward/record.uri?eid=2-s2.0-0024484175&partnerID=40&md5=b07c4bdc6bb0152a27100147542c1f6a

Juhlin, C., Ask, M., Bjelm, L., Elhami, E., Erlström, M., Joodak, S., Lazor, P., Lorenz, H., Niemi, A., Rosberg, J.-E., & Sopher, D. (2013). *Potential for CO2 storage in Swedish bedrock:SwedSTORECO2 - Phase 1*.

Juhlin, C., Erlström, M., Lund, B., & Rosberg, J.-E. (2022). Seismic reflectivity, fracturing and stress field data from the FFC-1 exploratory geothermal project in SW Skåne, Sweden. *Geothermics*, *105*, 102521. https://doi.org/https://doi.org/10.1016/j.geothermics.2022.102521

Karlqvist, L. (1982). *Hydrogeologisk karta över Gotlands län*. SGU. https://ludwig.lub.lu.se/login?url=https://search.ebscohost.com/login.aspx?direct=true&AuthType=ip,uid&db=cat07147a&AN=lub.101301&site=eds-live&scope=site

Kaya, E., Zarrouk, S. J., & O'Sullivan, M. J. (2011). Reinjection in geothermal fields: A review of worldwide experience. *Renewable and Sustainable Energy Reviews*, *15*(1), 47-68. https://doi.org/https://doi.org/10.1016/j.rser.2010.07.032

Kramers, L., Van Wees, J. D., Pluymaekers, M. P. D., Kronimus, A., & Boxem, T. (2012). Direct heat resource assessment and subsurface information systems for geothermal aquifers; The Dutch perspective. *Geologie en Mijnbouw/Netherlands Journal of Geosciences*, *91*(4), 637-649. https://doi.org/10.1017/S0016774600000421

Kunkel, C., Agemar, T., & Stober, I. (2019). Geothermal potential of the Buntsandstein and Keuper aquifers in NE Bavaria with a focus on deep thermal aquifer storage. *Grundwasser*, *24*(4), 251-267-267. https://doi.org/10.1007/s00767-019-00430-1

Larsson, K., Ahlberg, A., Guy-Ohlson, D., Arndorff, L., & Vajda, V. (1994). *The Subsurface Mesozoic geology of SW Scania, Southern Sweden : weII descriptions and annotations on stratigraphy, structural geology, depositional environments and diagenesis*. https://ludwig.lub.lu.se/login?url=https://search.ebscohost.com/login.aspx?direct=true&AuthType=ip,uid&db=edsswe&AN=edsswe.oai.lup.lub.lu.se.b8b17c0b.3d46.41a0.ac29.51ff21a35132&site=eds-live&scope=site

Larsson, K., Solakius, N., & Vajda, V. (2000). Foraminifera and palynomorphs from the Greensand -limestone sequences (Aptian-Coniacian) in southwestern Sweden. *Neues Jahrbuch fur Geologie und Palaontologie - Abhandlungen*, *216*, 277-312. https://doi.org/10.1127/njgpa/216/2000/277

Lavigne, J. (1977). LES RESSOURCES GÉOTHERMIQUES FRANÇAISES POSSIBILITÉS DE MISE EN VALEUR. http://infoterre.brgm.fr/rapports/77-SGN-433-GTH.pdf

Lawless, J., Ward, M., & Beardsmore, M. (2010). *The Australian Code for Geothermal Reserves and Resources Reporting: Practical Experience* https://www.geothermal-energy.org/pdf/IGAstandard/WGC/2010/0406.pdf

Lee, K. (2001). Classification of geothermal resources by exergy. *Geothermics*, *30*, 431-442. https://doi.org/10.1016/S0375-6505(00)00056-0

Liboriussen, J., Ashton, P., & Tygesen, T. (1987). The tectonic evolution of the Fennoscandian Border Zone in Denmark. *TECTONOPHYSICS*, *137*(1), 21-29. https://doi.org/https://doi.org/10.1016/0040-1951(87)90310-6

Lienau, P. J., Lunis, B. C., Center, O. I. o. T. G.-H. U., & Office, U. S. D. o. E. I. O. (1989). *Geothermal Direct Use Engineering and Design Guidebook*. Geo-Heat Center, Oregon Institute of Technology. https://books.google.se/books?id=YP1OAQAAIAAJ

Limberger, J., Boxem, T., Pluymaekers, M., Bruhn, D., Manzella, A., Calcagno, P., Beekman, F., Cloetingh, S., & van Wees, J.-D. (2018). Geothermal energy in deep aquifers: A global assessment of the resource base for direct heat utilization. *Renewable and Sustainable Energy Reviews*, *82*, 961-975. https://doi.org/https://doi.org/10.1016/j.rser.2017.09.084

Lopez, S., Hamm, V., Le Brun, M., Schaper, L., Boissier, F., Cotiche, C., & Giuglaris, E. (2010). 40 years of Dogger aquifer management in Ile-de-France, Paris Basin, France. *Geothermics*, *39*(4), 339-356. https://doi.org/https://doi.org/10.1016/j.geothermics.2010.09.005

Lund, J. (2009). Development and Utilization of Geothermal Resources. In (Vol. 1, pp. 87-95). https://doi.org/10.1007/978-3-540-75997-3_13

Lund, J. W., & Boyd, T. L. (2016). Direct utilization of geothermal energy 2015 worldwide review. *Geothermics*, *60*, 66-93. https://doi.org/https://doi.org/10.1016/j.geothermics.2015.11.004

Lund, J. W., Freeston, D. H., & Boyd, T. L. (2011). Direct utilization of geothermal energy 2010 worldwide review. *Geothermics*, *40*(3), 159-180. https://doi.org/https://doi.org/10.1016/j.geothermics.2011.07.004

Lund, J. W., & Toth, A. N. (2021). Direct utilization of geothermal energy 2020 worldwide review. *Geothermics*, *90*, 101915. https://doi.org/https://doi.org/10.1016/j.geothermics.2020.101915

Madsen, H. B., Stemmerik, L., & Surlyk, F. (2010). Diagenesis of silica-rich mound-bedded chalk, the Coniacian Arnager Limestone, Denmark. *Sedimentary Geology*, *223*(1), 51-60. https://doi.org/https://doi.org/10.1016/j.sedgeo.2009.10.002

Malcolm, A. G. (2018). STORED HEAT AND RECOVERY FACTOR REVIEWED.

Malmqvist, D., Eriksson, K. G., Ahlbom, K., Landström, O., Larson, S. Å., & Lind, G. (1978). Investigation for geothermal energy in Sweden. *Pure and Applied Geophysics PAGEOPH*, *117*(1-2), 196-204-204. https://doi.org/10.1007/BF00879746

Marrero-Diaz, R., Elsa, Ramalho, E., Costa, A., Ribeiro, L., Carvalho, J., Pinto, C., Rosa, D., & Correia, A. (2015). *Updated Geothermal Assessment of Lower Cretaceous Aquifer in Lisbon Region, Portugal* World Geothermal Congress Melbourne Australia. https://www.researchgate.net/publication/305899496_Updated_Geothermal_Assessment_of_Lower_Cretaceous_Aquifer_in_Lisbon_Region_Portugal

Moeck, I. S. (2014). Catalog of geothermal play types based on geologic controls. *Renewable and Sustainable Energy Reviews*, *37*, 867-882. https://doi.org/https://doi.org/10.1016/j.rser.2014.05.032

Mogensen, T. E. (1994). Palaeozoic structural development along the Tornquist Zone, Kattegat area, Denmark. *TECTONOPHYSICS*, *240*(1-4), 191-214-214. https://doi.org/10.1016/0040-1951(94)90272-0

Mortensen, G. M., Bergmo, P. E. S., & Emmel, B. U. (2016). Characterization and Estimation of CO2 Storage Capacity for the Most Prospective Aquifers in Sweden. *Energy Procedia*, *86*, 352-360. https://doi.org/10.1016/j.egypro.2016.01.036

Mortensen, G. M., & Sopher, D. (2021). *Geologisk lagring av koldioxid i Sverige och i grannländer – status och utveckling*. https://www.schweizerbart.de/papers/nos/detail/8/86849/Biostratigraphy_and_palaeozoogeography_of_planktonic_Foraminiferida_from_the_Cenomanian_of_Bornholm_Denmark

Muffler, L. J. P. (1978). *Assessment of geothermal resources of the United States: 1978* (790). U. S. G. Survey. http://pubs.er.usgs.gov/publication/cir790

Muffler, P., & Cataldi, R. (1978). Methods for regional assessment of geothermal resources. *Geothermics*, *7*(2-4), 53-89-89. https://doi.org/10.1016/0375-6505(78)90002-0

Nathenson, M. (1975a). *Physical factors determining the fraction of stored energy recoverable from hydrothermal convection systems and conduction-dominated areas* (75-525). U. S. G. Survey. http://pubs.er.usgs.gov/publication/ofr75525

Nathenson, M. (1975b). *Some reservoir engineering calculations for the vapor-dominated system at Larderello, Italy* (2331-1258). https://www.usgs.gov/publications/some-reservoir-engineering-calculations-vapor-dominated-system-larderello-italy

Norden, B. (2011). *Geothermal energy utilization in low-enthalpy sedimentary environments*. https://www.academia.edu/73949824/Geothermal_energy_utilization_in_low_enthalpy_sedimentary_environments

Norling, E. (1981). Upper Jurassic and Lower Cretaceous geology of Sweden. *Geologiska Föreningen i Stockholm Förhandlingar*, *103*(2), 253-269. https://doi.org/10.1080/11035898109454522

Norling, E., & Bergström, J. (1987). Mesozoic and Cenozoic tectonic evolution of Scania, southern Sweden. *TECTONOPHYSICS*, *137*(1), 7-19. https://doi.org/https://doi.org/10.1016/0040-1951(87)90309-X

O'Sullivan, M. J., & O'Sullivan, J. P. (2016). 7 - Reservoir modeling and simulation for geothermal resource characterization and evaluation. In R. DiPippo (Ed.), *Geothermal Power Generation* (pp. 165-199). Woodhead Publishing. https://doi.org/https://doi.org/10.1016/B978-0-08-100337-4.00007-3

Olaf, M., & Nielsen, L. H. (1991). *Well records on the Phanerozoic stratigraphy in the Fennoscandian border Zone, Denmark : Hans-1, Sæby-1, and Terne-1 wells*. Danmarks geologiske undersøgelse. https://ludwig.lub.lu.se/login?url=https://search.ebscohost.com/login.aspx?direct=true&AuthType=ip,uid&db=cat07147a&AN=lub.1671500&site=eds-live&scope=site

Packer, S. R., & Hart, M. B. (1994). Evidence for sea level change from the cretaceous of Bornholm, Denmark. *Gff*, *116*(3), 167-173. https://doi.org/10.1080/11035899409546180

Pahud, D. (2002). *Geothermal Energy and Heat Storage*. https://repository.supsi.ch/3651/1/82-Pahud-2002-Lecture-notes-GEO.pdf

Piris, G., Griera, A., Herms, I., Colomer, M., Arnó, G., & Gomez-rivas, E. (2021). 3DHIP-calculator—A new tool to stochastically assess deep geothermal potential using the heat-in-place method from voxel-based 3D geological models. *Energies*, *14*(21). https://doi.org/10.3390/en14217338

Pluymaekers, M. P. D., Kramers, L., van Wees, J. D., Kronimus, A., Nelskamp, S., Boxem, T., & Bonté, D. (2012). Reservoir characterisation of aquifers for direct heat production: Methodology and screening of the potential reservoirs for the Netherlands. *Netherlands Journal of Geosciences*, *91*(4), 621-636. https://doi.org/10.1017/S001677460000041X

Pocasangre, C., & Fujimitsu, Y. (2018). A Python-based stochastic library for assessing geothermal power potential using the volumetric method in a liquid-dominated reservoir. *Geothermics*, *76*, 164-176. https://doi.org/https://doi.org/10.1016/j.geothermics.2018.07.009

Poulsen, S. E., Balling, N., & Nielsen, S. B. (2015). A parametric study of the thermal recharge of low enthalpy geothermal reservoirs. *Geothermics*, *53*, 464-478. https://doi.org/https://doi.org/10.1016/j.geothermics.2014.08.003

Quinao, J., & Zarrouk, S. (2014). *A REVIEW OF THE VOLUMETRIC STORED-HEAT RESOURCE ASSESSMENT: ONE METHOD, DIFFERENT RESULTS*. https://www.researchgate.net/publication/269039552_A_REVIEW_OF_THE_VOLUMETRIC_STORED-HEAT_RESOURCE_ASSESSMENT_ONE_METHOD_DIFFERENT_RESULTS

Renewable Energy Policy Network. (2022). *Renewables 2022 global status report*. https://www.ren21.net/gsr-2022/

Rivera Diaz, A., Kaya, E., & Zarrouk, S. J. (2016). Reinjection in geothermal fields − A worldwide review update. *Renewable and Sustainable Energy Reviews*, *53*, 105-162. https://doi.org/https://doi.org/10.1016/j.rser.2015.07.151

Robertson, E. C. (1988). *Thermal properties of rocks* (88-441). U. S. G. Survey. http://pubs.er.usgs.gov/publication/ofr88441

Rosberg, J.-E., & Erlström, M. (2019). Evaluation of the Lund deep geothermal exploration project in the Romeleåsen Fault Zone, South Sweden: a case study. *Geothermal Energy*, *7*(1), N.PAG-N.PAG. https://doi.org/10.1186/s40517-019-0126-7

Rosberg, J.-E., & Erlström, M. (2021). Evaluation of deep geothermal exploration drillings in the crystalline basement of the Fennoscandian Shield Border Zone in south Sweden. *Geothermal Energy*, *9*(1), 20. https://doi.org/10.1186/s40517-021-00203-1

Sadiq, Z., & Florida, S. (2013). A REVIEW OF GEOTHERMAL RESOURCE ESTIMATION METHODOLOGY. https://www.geothermal-energy.org/pdf/IGAstandard/NZGW/2013/Zarrouk_Simiyu_Final.pdf

Sanyal, S. K., Klein, C. W., Lovekin, J. W., & Henneberger, R. C. (2004). National assessment of U.S Geotherma resources - A perspective. http://repository.usgin.org/sites/default/files/dlio/files/2011/u19/national_assessment_of_u.s._geothermal_resources_-_a_perspective_-_by_subir_sanyal_-_christopher_klein_-_james_lovekin_and_roger_henneberger.pdf

Sivhed, U., Wikman, H., & Erlström, M. (1999). *Berggrundskartan. [Kartografiskt material]*. SGU. https://ludwig.lub.lu.se/login?url=https://search.ebscohost.com/login.aspx?direct=true&AuthType=ip,uid&db=cat07147a&AN=lub.1234644&site=eds-live&scope=site

SMHI. (2023). *Månads-, årstids- och årskartor*. SMHI. Retrieved 05-26 from https://www.smhi.se/data/meteorologi/kartor/normal/arsmedeltemperatur-normal

Solakius, N. (1989). Foraminifera from the Arnager Limestone-Bavnodde Greensand boundary on Bornholm, Denmark. *Geologiska Föreningen i Stockholm Förhandlingar*, *111*(2), 101-104. https://doi.org/10.1080/11035898909453780

Stober, I., & Bucher, K. (2021a). Geothermal Energy Resources. In I. Stober & K. Bucher (Eds.), *Geothermal Energy: From Theoretical Models to Exploration and Development* (pp. 33-42). Springer International Publishing. https://doi.org/10.1007/978-3-030-71685-1_3

Stober, I., & Bucher, K. (2021b). Geothermal Probes. In I. Stober & K. Bucher (Eds.), *Geothermal Energy: From Theoretical Models to Exploration and Development* (pp. 85-144). Springer International Publishing. https://doi.org/10.1007/978-3-030-71685-1_6

Stober, I., & Bucher, K. (2021c). Thermal Structure of the Earth. In I. Stober & K. Bucher (Eds.), *Geothermal Energy: From Theoretical Models to Exploration and Development* (pp. 1-19). Springer International Publishing. https://doi.org/10.1007/978-3-030-71685-1_1

Stober, I., & Bucher, K. (2021d). Uses of Geothermal Energy. In I. Stober & K. Bucher (Eds.), *Geothermal Energy: From Theoretical Models to Exploration and Development* (pp. 43-79). Springer International Publishing. https://doi.org/10.1007/978-3-030-71685-1_4

Thomas, S. A., Sivhed, U., Erlström, M., & Seifert, M. (1993). Seismostratigraphy and structural framework of the SW Baltic Sea. *Terra Nova*, *5*(4), 364-374. https://doi.org/10.1111/j.1365-3121.1993.tb00270.x

Tiab, D., & Donaldson, E. C. (2012). Chapter 2 - Introduction to Petroleum Geology. In D. Tiab

& E. C. Donaldson (Eds.), *Petrophysics (Third Edition)* (pp. 27-83). Gulf Professional Publishing. https://doi.org/https://doi.org/10.1016/B978-0-12-383848-3.00002-5

Toth, A., & Bobok, E. (2017). Chapter 1 - What Is Geothermal Energy? In A. Toth & E. Bobok (Eds.), *Flow and Heat Transfer in Geothermal Systems* (pp. 1-19). Elsevier. https://doi.org/https://doi.org/10.1016/B978-0-12-800277-3.00001-3

Trumpy, E., Botteghi, S., Caiozzi, F., Donato, A., Gola, G., Montanari, D., Pluymaekers, M. P. D., Santilano, A., van Wees, J. D., & Manzella, A. (2016). Geothermal potential assessment for a low carbon strategy: A new systematic approach applied in southern Italy. *Energy*, *103*, 167-181. https://doi.org/https://doi.org/10.1016/j.energy.2016.02.144

Tröger, K.-A., & Kegel Christensen, W. (1991). *Upper Cretaceous (Cenomanian-Santonian) inoceramid bivalve faunas from the island of Bornholm, Denmark : with a review of the Cenomanian-Santonian lithostratigraphic formations and locality details*. Danmarks geologiske undersøgelse. https://ludwig.lub.lu.se/login?url=https://search.ebscohost.com/login.aspx?direct=true&AuthType=ip,uid&db=cat07147a&AN=lub.1671474&site=eds-live&scope=site

Tyson, R. V., & Funnell, B. M. (1987). European cretaceous shorelines, stage by stage. *Palaeogeography, Palaeoclimatology, Palaeoecology*, *59*, 69-91. https://doi.org/https://doi.org/10.1016/0031-0182(87)90075-7

Vajda-Santivanez, V., & Solakius, N. (1999). Palynomorphs, foraminifera, and calcispheres from the greensand-limestone transition at Arnager, Bornholm: Evidence of transgression during the late Cenomanian to early Coniacian. *Gff*, *121*(4), 281-286. https://doi.org/10.1080/11035899901214281

Van Schmus, W. R. (1995). Natural Radioactivity of the Crust and Mantle. In *Global Earth Physics* (pp. 283-291). https://doi.org/https://doi.org/10.1029/RF001p0283

Vejbaek, O. (1997). Dybe strukturer i danske sedimentære bassiner. *Geologisk Tidsskrift*, *4*, 1-31. https://2dgf.dk/xpdf/gt1997-4-1-31.pdf

Wang, Y., Voskov, D., Khait, M., Saeid, S., & Bruhn, D. (2021). Influential factors on the development of a low-enthalpy geothermal reservoir: A sensitivity study of a realistic field. *Renewable Energy*, *179*, 641-651. https://doi.org/https://doi.org/10.1016/j.renene.2021.07.017

Watanabe, K., & Takahashi, H. A. (1995). Fractal geometry characterization of geothermal reservoir fracture networks. *Journal of Geophysical Research*, *100*, 521-528. https://agupubs.onlinelibrary.wiley.com/doi/abs/10.1029/94JB02167

White, D. E. (1966). Geothermal energy. *Bulletin Volcanologique*, *29*(1), 481-483. https://doi.org/10.1007/BF02597170

White, D. E., & Williams, D. L. (1975). *Assessment of geothermal resources of the United States, 1975* (726). G. S. U.S. Dept. of the Interior. http://pubs.er.usgs.gov/publication/cir726

Willems, C. J. L., Nick, H. M., Goense, T., & Bruhn, D. F. (2017). The impact of reduction of doublet well spacing on the Net Present Value and the life time of fluvial Hot Sedimentary Aquifer doublets. *Geothermics*, *68*, 54-66. https://doi.org/https://doi.org/10.1016/j.geothermics.2017.02.008

Williams, C. F. (2004). DEVELOPMENT OF REVISED TECHNIQUES FOR ASSESSING GEOTHERMAL RESOURCES. https://pangea.stanford.edu/ERE/pdf/IGAstandard/SGW/2004/Williams.pdf

Williams, C. F. (2007). UPDATED METHODS FOR ESTIMATING RECOVERY FACTORS FOR GEOTHERMAL RESOURCES.

Williams, C. F. (2014). Evaluating the volume method in the assessment of identified geothermal resources. *Geotherm. Resour. Counc. Trans.*, *38*, 967-974. https://www.researchgate.net/publication/284585969_Evaluating_the_volume_method_in_the_assessment_of_identified_geothermal_resources

Williams, C. F., Reed, M. J., & Mariner, R. H. (2008). *A Review of Methods Applied by the U.S. Geological Survey in the Assessment of Identified Geothermal Resources*. (Open-File Report, Issue. U. S. G. Survey. http://pubs.er.usgs.gov/publication/ofr20081296

Winterer, E. L. (2012). 19 - Pelagic realms. In D. G. Roberts & A. W. Bally (Eds.), *Regional Geology and Tectonics: Principles of Geologic Analysis* (pp. 538-551). Elsevier. https://doi.org/https://doi.org/10.1016/B978-0-444-53042-4.00019-4

Zarrouk, S. J., & McLean, K. (2019a). Chapter 1 - Introduction. In S. J. Zarrouk & K. McLean (Eds.), *Geothermal Well Test Analysis* (pp. 1-11). Academic Press. https://doi.org/https://doi.org/10.1016/B978-0-12-814946-1.00001-3

Zarrouk, S. J., & McLean, K. (2019b). Chapter 2 - Geothermal systems. In S. J. Zarrouk & K. McLean (Eds.), *Geothermal Well Test Analysis* (pp. 13-38). Academic Press. https://doi.org/https://doi.org/10.1016/B978-0-12-814946-1.00002-5

Zobin, V. M. (2017). Chapter 20 - The Seismic Signals Associated With the Natural Seismicity of Geothermal Structures Within Volcanic Environment. In V. M. Zobin (Ed.), *Introduction to Volcanic Seismology (Third Edition)* (pp. 497-517). Elsevier. https://doi.org/https://doi.org/10.1016/B978-0-444-63631-7.00020-0

7 Appendix

Appendix 1

Additional borehole data related to the depth reference values for each borehole. This includes the ground height above mean sea level and the rotary table height (Kelly bushing height) above mean sea level.

Borehole	Ground level (a.m.s.l)	Rotary table (a.m.s.l)
Norrevång-1	12.25	17.2
Barsebäck-1	3.3	8.1
Mossheddinge-1	33.36	36.06
FFC-1	3.1	10.1
Magreteholm-1	9.2	NoData
Svedala-1	NoData	47
Eskilstorp-1	25.21	30.06
Håslöv-1	13.3	18.2
Kungstorp-1	1.1	3.8
Höllviken-1	NoData	4
Granvik-1	NoData	NoData
Maglarp-1	13.5	17.91
Hammarlöv-1	3.7	8.2
Trelleborg-1	NoData	5
Höllviksnäs-1	2.8	7.8
Höllviken-2	NoData	4
Ljunghusen-1	3	5
Smygehuk-1	-29	22.6

Appendix 2

The interpolation settings for the TWT raster surface, velocity raster surface, and the thickness raster surface.

Interpolation settings	**TWT Interpolation**	**Velocity Interpolation**		**Thickness interpolation**	
Method	Kriging	Cokriging		Cokriging	
Type	Ordinary	Ordinary		Ordinary	
Output type	Prediction	Prediction		Prediction	
Dataset	1	1	2	1	2
Trend type	First	First	First	First	First
Trend removal	Local Polynomial Interpolation	Local Polynomial Interpolation	Local Polynomial Interpolation	Local Polynomial Interpolation	Local Polynomial Interpolation
Power	1	1	1	1	1
Output type	Prediction	Prediction	Prediction	Prediction	Prediction
Exploratory trend surface analysis	0	0	0	0	0
Searching neighbourhood	Standard	Standard	Standard	Standard	Standard
Neighbours to include	5	5	5	5	5
Include at last	2	2	2	2	2
Sector type	Four and 45 degree	Four and 45 degree	Four and 45 degree	Four and 45 degree	Four and 45 degree
Major semiaxis	1 163.07834454738	15099.03504	15099.03504	10088.75554	10088,7555363633
Minor semiaxis	1521.244536	22648.55257	22648.55257	15133.1333	15 133,133304545
Angle	4763671875	44.47265625	44.47265625	69.78515625	69,78515625
Variogram	Semivariogram	Semivariogram	Semivariogram	Semivariogram	Semivariogram
Number of lags	12	12		12	
Lag size	126.770378	1 887.37938049622		1261.094442	
Nugget	0.162933858	677.5536466	289.3420482	0	0
Measurement error %	100	100	100	100	100
Shift		0;0	0;0	0;0	0;0
Model type	Stable	Stable		Stable	
Parameter	2	1.854101563		1.305664063	
Range	1 014.1630239356	15099.03504		10088.75554	
Anisotropy	Yes	Yes		Yes	
Minor range	1 521.2445359034	22648.55257		15133.1333	
Direction	47.63671875	44.47265625		69.78515625	
Partial Sill	162.9338577	5 093.4665194489; -622.810147463735	-622.810147463735; 1 054.03332655853	0.027831730706; -1.710405901336	1.710405901336; 1 081.95712181537

Appendix 3

The cross-validation statistics for the TWT raster surface, the velocity raster surface, and the thickness raster surface. The table presents statistical measures such as mean values, mean standardised, root-mean-square, root-mean-squared standardised, and average standard errors on the degree of fit between hidden and known points using a leave-one-out resampling technique.

Cross validation statistics	TWT Interpolation	Velocity Interpolation	Thickness interpolation
Count	12203	18	18
Mean	0.000232863	0.282201137	1.660822607
Root-mean-square	0.228028074	60.55453221	7.641738937
Mean standardised	0.000579764	0.006418304	0.005009696
Root-mean-square Standardised	0.348788336	0.943640367	1.672159256
Average standard error	0.630602084	56.70763667	5.260797794

Appendix 4

The table compares the raw depth and thickness data with the modelled results for the same parameters. The table also include the modelled reservoir temperature at the top boundary of the Arnager Greensand. The cross plot displays the correlation between the interpolated TWT values and the thickness of the Arnager Greensand in each borehole.

Borehole	Top Arnager Greensand (b.m.s.l)	Depth model (b.m.s.l)	Thickness (m)	Thickness model (m)	TWT (Two-way-time) (ms)	Velocity (m/s)	Reservoir temperature (°C)
NV	1768	1769.1	24	23.3	1141	3098.2	56.1
Ba	1743	1744.0	17	17.2	1127	3092.4	55.7
Mo	1675	1671.1	11	11.3	1087	3081.6	53.5
FFC-1	1605	1606.3	27	26.8	1045	3071.3	51.6
Mah-1	1601	Out of bounds	28	Out of Bounds	994	3222.5	Out of Bounds
Sv	1435	1440.2	24	23.8	971	2956.9	47.4
Es	1353	1349.5	28	28.6	873	3098.4	45.0
Hå	1306	1308.5	36	35.8	851	3069.9	43.9
Ku	1274	1259.6	47	46.7	829	3072.7	42.6
Hö-1	1226	1232.9	55	54.5	818	2998.3	41.9
Gr	1245	1234.1	55	54.2	813	3061.4	41.9
Ma	1232	1227.5	47	45.5	809	3045.9	41.7
Ha	1204	1212.2	38	38.9	802	3004.3	41.3
Tr	1200	1201.9	38	37.2	788	3043.8	40.8
Hn	1190	1196.6	52	53.3	803	2963.5	40.9
Hö-2	1187	1183.9	54	53.1	798	2973.2	40.6
Lj	1182	1180.4	48	48.6	802	2949.3	40.5
Sm	1071	Out of bounds	46	Out of Bounds	756	2833.8	Out of Bounds

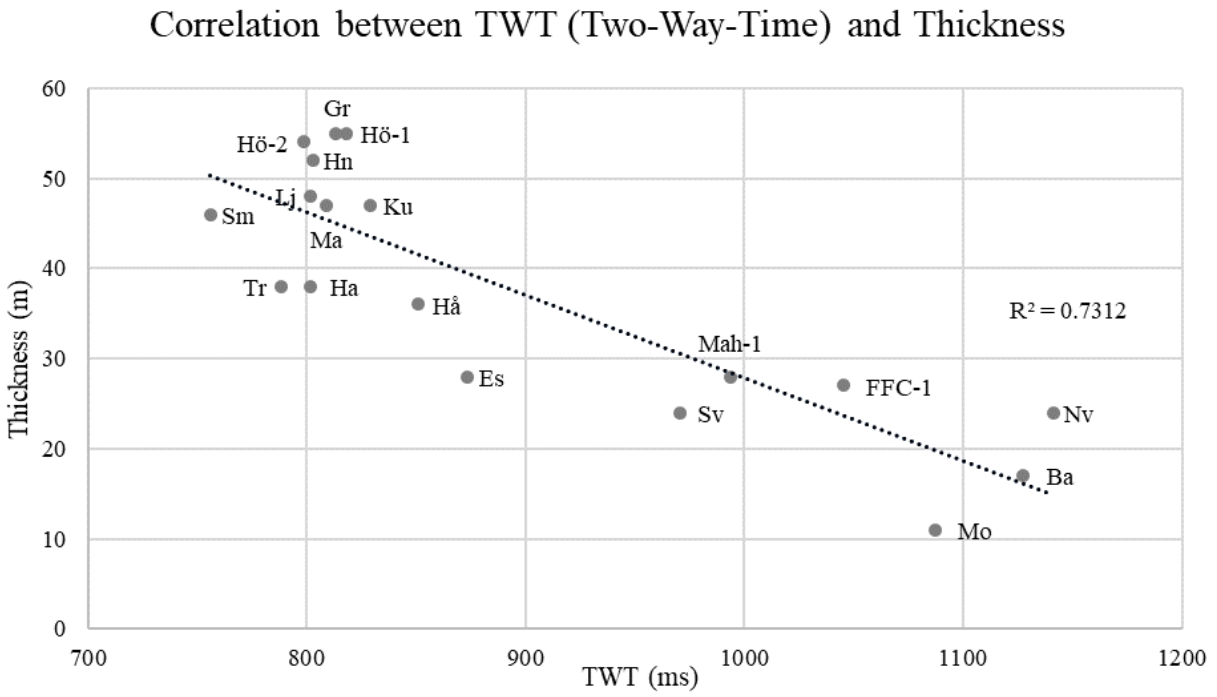

Appendix 5.

Histograms for the presented stored heat maps which shows the cell distribution over SW Scania. The first histogram corresponds to Figure (13) and the second histogram corresponds to Figure (14). The impact of the thickness interpolation becomes apparent in the 5 – 7 brackets. The low thickness in the Mosshedinge-1 borehole and Svedala -1 borehole extends over the Skurup Platform and results in relatively low stored heat values.

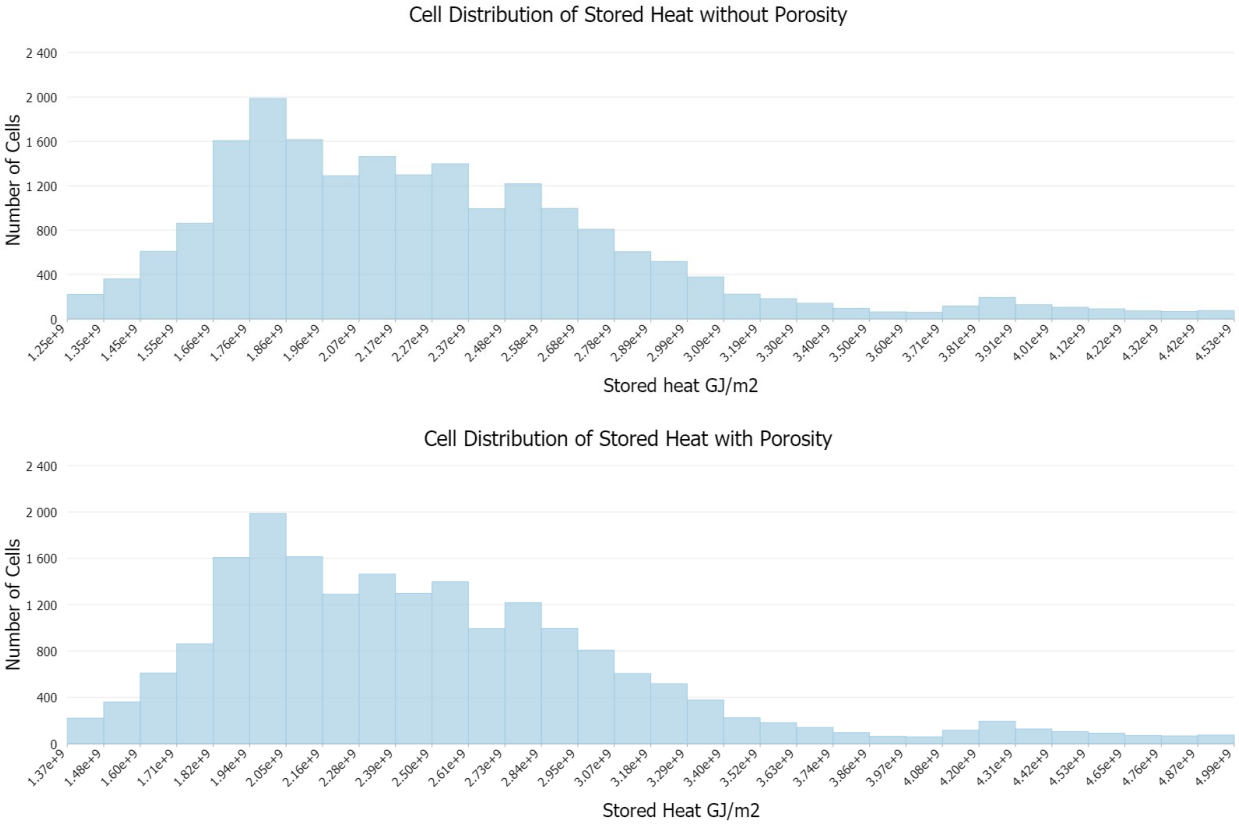

Appendix 6.

The modelled stored heat results based on different values for the porosity and reference temperature. The tables consider the stored heat in the rock matrix and the reservoir fluids separately, as well as using the reference value for the volumetric heat capacity of water-saturated rocks. The table presents both the stored heat value as Q (J/ m^2) and Q (Joules).

Stored Heat (HIP)	**Q (J/m^2)**			**Q (J)**		
Porosity (%)	Mean	Min	Max	Rock matrix	Fluid	Total Stored Heat
Volumetric heat capacity of water-saturated rocks	2.27E+09	1.25E+09	4.53E+09	Nodata	Nodata	3.27E+18
0	1.95E+09	1.07E+09	3.89E+09	2.82E+18	0	2.82E+18
8	2.13E+09	1.17E+09	4.26E+09	2.59E+18	4.89E+17	3.08E+18
16	2.32E+09	1.27E+09	4.62E+09	2.37E+18	9.78E+17	3.34E+18
24	2.50E+09	1.37E+09	4.99E+09	2.14E+18	1.47E+18	3.61E+18
32	2.68E+09	1.47E+09	5.35E+09	1.92E+18	1.96E+18	3.87E+18

Stored Heat (HIP)	**Q (J/m^2)**			**Q (J)**		
Porosity (%)	Mean	Min	Max	Rock matrix	Fluid	Total Stored Heat
Volumetric heat capacity of water-saturated rocks	2.27E+09	1.25E+09	4.53E+09	Nodata	Nodata	3.27E+18
0	1.95E+09	1.07E+09	3.89E+09	2.82E+18	0	2.82E+18
8	2.13E+09	1.17E+09	4.26E+09	2.59E+18	4.89E+17	3.08E+18
16	2.32E+09	1.27E+09	4.62E+09	2.37E+18	9.78E+17	3.34E+18
24	2.50E+09	1.37E+09	4.99E+09	2.14E+18	1.47E+18	3.61E+18
32	2.68E+09	1.47E+09	5.35E+09	1.92E+18	1.96E+18	3.87E+18

Tidigare skrifter i serien ”Examensarbeten i Geologi vid Lunds universitet”:

616. Greiff, Johannes, 2021: Oolites from the Arabian platform: Archives for the aftermath of the end-Triassic mass extinction. (45 hp)
617. Ekström, Christian, 2021: Rödfärgade utfällningar i dammanläggningar orsakade av *G. ferruginea* och *L. ochracea* - Problemstatistik och mikrobiella levnadsförutsättningar. (15 hp)
618. Östsjö, Martina, 2021: Geologins betydelse i samhället och ett första steg mot en geopark på Gotland. (15 hp)
619. Westberg, Märta, 2021: The preservation of cells in biomineralized vertebrate tissues of Mesozoic age – examples from a Cretaceous mosasaur (Reptilia, Mosasauridae). (45 hp)
620. Gleisner, Lovisa, 2021: En detaljerad undersökning av kalkstenslager i den mellanordoviciska gullhögenformationen på Billingen i Västergötland. (15 hp)
621. Bonnevier Wallstedt, Ida, 2021: Origin and early evolution of isopods - exploring morphology, ecology and systematics. (15 hp)
622. Selezeneva, Natalia, 2021: Indications for solar storms during the Last Glacial Maximum in the NGRIP ice core. (45 hp)
623. Bakker, Aron, 2021: Geological characterisation of geophysical lineaments as part of the expanded site descriptive model around the planned repository site for high-level nuclear waste, Forsmark, Sweden. (45 hp)
624. Sundberg, Oskar, 2021: Jordlagerföljden i Höjeådalen utifrån nya borrningar. (15 hp)
625. Sartell, Anna, 2021: The igneous complex of Ekmanfjorden, Svalbard: an integrated field, petrological and geochemical study. (45 hp)
626. Juliusson, Oscar, 2021: Implications of ice-bedrock dynamics at Ullstorp, Scania, southern Sweden. (45 hp)
627. Eng, Simon, 2021: Rödslam i svenska kraftdammar - Problematik och potentiella lösningar. (15 hp)
628. Kervall, Hanna, 2021: Feasibility of Enhanced Geothermal Systems in the Precambrian crystalline basement in SW Scania, Sweden. (45 hp)
629. Smith, Thomas, 2022: Assessing the relationship between hypoxia and life on Earth, and implications for the search for habitable exoplanets. (45 hp)
630. Neumann, Daniel, 2022: En mosasaurie (Reptilia, Mosasauridae) av paleocensk ålder? (15 hp)
631. Svensson, David, 2022: Geofysisk och geologisk tolkning av kritskollors utbredning i Ystadsområdet. (15 hp)
632. Allison, Edward, 2022: Avsättning av Black Carbon i sediment från Odensjön, södra Sverige. (15 hp)
633. Jirdén, Elin, 2022: OSL dating of the Mesolithic site Nilsvikdalen 7, Bjorøy, Norway. (45 hp)
634. Wong, Danny, 2022: GIS-analys av effekten vid stormflod/havsnivåhöjning, Morupstrakten, Halland. (15 hp)
635. Lycke, Björn, 2022: Mikroplast i vattenavsatta sediment. (15 hp)
636. Schönherr, Lara, 2022: Grön fältspat i Varbergskomplexet. (15 hp)
637. Funck, Pontus, 2022: Granens ankomst och etablering i Skandinavien under postglacial tid. (15 hp)
638. Brotzen, Olga M., 2022: Geologiska besöksmål och geoparker som plattform för popularisering av geovetenskap. (15 hp)
639. Lodi, Giulia, 2022: A study of carbon, nitrogen, and biogenic silica concentrations in *Cyperus papyrus*, the sedge dominating the permanent swamp of the Okavango Delta, Botswana, Africa. (45 hp)
640. Nilsson, Sebastian, 2022: PFAS- En sammanfattning av ny forskning, med ett fokus på föroreningskällor, provtagning, analysmetoder och saneringsmetoder. (15 hp)
641. Jägfeldt, Hans, 2022: Molnens påverkan på jordens strålningsbalans och klimatsystem. (15 hp)
642. Sundberg, Melissa, 2022: Paleontologiska egenskaper och syreisotopsutveckling i borrkärnan Limhamn-2018: Kopplingar till klimatförändringar under yngre krita. (15 hp)
643. Bjermo, Tim, 2022: A re-investigation of hummocky moraine formed from ice sheet decay using geomorphological and sedimentological evidence in the Vomb area, southern Sweden. (45 hp)
644. Halvarsson, Ellinor, 2022: Structural investigation of ductile deformations across the Frontal Wedge south of Lake Vättern, southern Sweden. (45 hp)
645. Brakebusch, Linus, 2022: Record of the end-Triassic mass extinction in shallow marine carbonates: the Lorüns section (Austria). (45 hp)
646. Wahlquist, Per, 2023: Stratigraphy and palaeoenvironment of the early Jurassic volcaniclastic strata at Djupadalsmölla, central Skåne, Sweden. (45 hp)
647. Gebremedhin, G. Gebreselassie, 2023: U-Pb geochronology of brittle deformation

using LA-ICP-MS imaging on calcite veins. (45 hp)

648. Mroczek, Robert, 2023: Petrography of impactites from the Dellen impact structure, Sweden. (45 hp)
649. Gunnarsson, Niklas, 2023: Upper Ordovician stratigraphy of the Stora Sutarve core (Gotland, Sweden) and an assessment of the Hirnantian Isotope Carbon Excursion (HICE) in high-resolution. (45 hp)
650. Cordes, Beatrix, 2023: Vilken ny kunskap ger aDNA-analyser om vegetationsutvecklingen i Nordeuropa under och efter Weichsel-istiden? (15 hp)
651. Bonnevier Wallstedt, Ida, 2023: Palaeocolour, skin anatomy and taphonomy of a soft-tissue ichthyosaur (Reptilia, Ichthyopterygia) from the Toarcian (Lower Jurassic) of Luxembourg. (45 hp)
652. Kryffin, Isidora, 2023: Exceptionally preserved fish eyes from the Eocene Fur Formation of Denmark – implications for palaeobiology, palaeoecology and taphonomy. (45 hp)
653. Andersson, Jacob, 2023: Nedslagskratrars inverkan på Mars yt-datering. En undersökning av Mars främsta yt-dateringsmetod ”Crater Counting". (15 hp)
654. Sundberg, Melissa, 2023: A study in ink – the morphology, taphonomy and phylogeny of squid-like cephalopods from the Jurassic Posidonia Shale of Germany and the first record of a loligosepiid gill. (45 hp)
655. Häggblom, Joanna, 2023: En patologisk sjölilja från silur på Gotland, Sverige. (15 hp)
656. Bergström, Tim, 2023: Hur gammal är jordens inre kärna? (15 hp)
657. Bollmark, Viveka, 2023: Ca isotope, oceanic anoxic events and the calcareous nannoplankton. (15 hp)
658. Madsen, Ariella, 2023: Polycykliska aromatiska kolväten i Hanöbuktens kustnära sediment - En sedimentologisk undersökning av vikar i närhet av pappersbruk. (15 hp)
659. Wangritthikraikul, Kannika, 2023: Holocene Environmental History of Warming Land, Northern Greenland: a study based on lake sediments. (45 hp)
660. Kurop, Anna, 2023: Reconstruction of the glacier dynamics and Holocene chronology of retreat of Helagsglaciären in Central Sweden. (45 hp)
661. Frisendahl, Kajsa, 2023: Holocene environmental history of Washington Land, NW Greenland: a study based on lake sediments. (45 hp)
662. Ryan, Cathal, 2023: Luminescence dating of the late Quaternary loess-palaeosol sequence at Velika Vrbica, Serbia. (45 hp)
663. Lindow, Wilma, 2023: U-Pb datering av zirkon i metasediment tillhörande Stora Le-Marstrand, SV Sverige. (15 hp)
664. Bengtsson, Kaisa, 2023: Geologisk karaktärisering av den kambriska Faluddensandstenen i Östersjön och dess lämplighet för koldioxidlagring. (15 hp)
665. Granbom, Johanna, 2023: Insights into simple crater formation: The Hummeln impact structure (Småland, Sweden). (45 hp)
666. Jonsson, Axel, 2023: Datering av vulkanen Rangitoto, Nya Zeeland, genom paleomagnetiska analysmetoder. (15 hp)
667. Muller, Elsa, 2023: Response of foraminifera *Ammonia confertitesta* (T6) to ocean acidification, warming, and Deoxygenation An experimental approach. (45 hp)
668. Struzynska, Patrycja, 2023: Petrography, geochemistry, and origin of deep magmatic cumulates in the Canary Islands – the xenolith record. (45 hp)
669. Krätzer, Tobias, 2023: Artificiella torskrev i Hanöbukten: Förstudie. (15 hp)
670. Khorshidian, Farid, 2023: 3D modelling and resistivity measurements for hydrogeological assessments in the northern part of Vombsänkan. (45 hp)
671. Sundberg, Oskar: 2023: Methodology for Stored Heat “Heat In Place” (HIP) assessment of geothermal aquifers – Exemplified by a study of the Arnager Greensand in SW Scania. (45 hp)

LUNDS UNIVERSITET

Geologiska institutionen
Lunds universitet
Sölvegatan 12, 223 62 Lund